Analytical Techniques for Acoustic Scattering by Arrays of Cylinders

by

Nikolaos Tymis

A Doctoral Thesis

Submitted in partial fulfilment of the requirements for the award of degree of Philosophy of Loughborough University

CERTIFICATE OF ORIGINALITY

This is to certify that I am responsible for the work submitted in this thesis, that the original work is my own except as specified in acknowledgments or in footnotes, and that neither the thesis nor the original work contained therein has been submitted to this or any other institution for a degree.

..... (Signed)

..... (Date)

To Ioanna

Abstract

The problem of two-dimensional acoustic scattering of an incident plane wave by a semi-infinite lattice is solved. The problem is first considered for sound-soft cylinders whose size is small compared to the wavelength of the incident field. In this case the formulation leads to a scalar Wiener–Hopf equation, and this in turn is solved via the discrete Wiener–Hopf technique. We then deal with a more complex case which arises either by imposing Neumann boundary condition on the cylinders' surface or by increasing their radii. This gives rise to a matrix Wiener–Hopf equation, and we present a method of solution that does not require the explicit factorisation of the kernel. In both situations, a complete description of the far field is given and a conservation of energy condition is obtained. For certain sets of parameters ('pass bands'), a portion of the incident energy propagates through the lattice in the form of a Bloch wave. For other parameters ('stop bands' or 'band gaps'), no such transmission is possible, and all of the incident field energy is reflected away from the lattice.

Acknowledgements

I am extremely grateful to Dr. Ian Thompson and Professor Chris M. Linton for their assistance and support during this project. I would like to thank Loughborough University for providing me with the necessary funding and equipment to carry out my research. I would also like to thank Assistant Professor Dimitrios Betsakos for teaching me analysis and for encouraging me to pursue an advanced degree. Last by no means least, I would like to thank my family for their unconditional support, understanding and belief throughout my studies.

'I am a weak, ephemeral creature made of mud and dream. But I feel all the powers of the universe whirling within me.

Before they crush me, I want to open my eyes for a moment and to see them. I set my life no other purpose.'

Nikos Kazantzakis

Contents

Introduction **1**

1 Acoustic scattering by cylinders **3**

1.1 The Helmholtz equation 3

1.2 Scattering by a single cylinder 4

1.3 Multiple Scattering 9

1.4 Scattering by an infinite grating of small cylinders 15

1.5 Bloch waves 20

2 The Wiener–Hopf technique **26**

2.1 The Wiener–Hopf equation and its solution 27

2.2 The bilateral $\mathcal{Z}$-transform 31

2.3 The discrete Wiener–Hopf method 34

2.4 Scattering by a semi-infinite grating of small cylinders 36

2.5 Literature 42

3 Scattering by a semi-infinite lattice of small cylinders **45**

3.1 Formulation 46

3.2 The discrete Wiener-Hopf method 50

3.3 The kernel and its approximate factorisation 52
3.4 Explicit solution 58
3.5 The far field pattern 62
3.6 Conservation of energy 71

4 The general case **75**

4.1 Formulation 76
4.2 The matrix Wiener–Hopf equation 78
4.3 Symmetry 81
4.4 The method of solution 84
4.5 The far field pattern 92
4.6 Conservation of energy 96
4.7 Numerical Results 98

5 Conclusions **104**

5.1 Future work 106

A Miscellaneous functions **108**

A.1 Multiple valued functions 108
A.2 Bessel functions 109
A.3 Integral representations of multipoles 111
A.4 Polynomial matrices 111

B Arrays of singularities **114**

B.1 Quasi-periodic arrays of singularities 115
B.2 Lattice sums 120

Bibliography **123**

Introduction

When a propagating wave encounters an obstacle in its path a scattered field is produced. The problem of determining the scattered field, given the parameters that describe the obstacle(s) and the incident field, is known as a 'direct scattering problem'. Research on this subject is of considerable interest in many physical contexts, including acoustics, electromagnetism and hydrodynamics. Cases where a periodic array of bodies plays the role of the scattering structure are of particular interest in developing the theoretical framework needed to model metamaterials [18], large offshore structures [28], and antenna arrays [9, 51].

In mathematical terms, the problem of two-dimensional acoustic wave scattering by arrays of cylinders, using linear theory under time-harmonic conditions, is reduced to a boundary value problem governed by the Helmholtz equation. A variety of techniques have been developed over the years for its solution [34, 37], with the multipole expansion method being the most suitable mainly due to the ease of applying the boundary condition on the surface of the cylinders. It was devised by Záviška [66] in 1913 and has been used widely ever since in different physical and geometrical settings (see [37, §4.2.1]). A multipole expansion is essentially a linear combination of separable solutions of the Helmholtz equation. The field scattered by each cylinder is expressed in terms of a multipole expansion, and an appropriate addition theorem is used to reduce the initial boundary value problem into a rapidly convergent infinite system of algebraic equations. This is an effective approach to tackle a scattering problem by an array with a small number of cylinders, but as this number increases so does the computational cost, thus making the solution impractical.

Wave scattering by a long one-dimensional array of cylinders can be studied by decomposing it into a set of canonical problems formulated on infinite and semi-infinite arrays [53]. An infinite row of cylinders, or a grating, presents a geometrical periodicity that can be exploited to simplify the analysis. In scattering theory this is a subject of considerable importance that has resulted in a large number of scientific publications [62]. On the other hand the semi-infinite grating problem presents a more challenging proposition. On this subject, the pioneering work by Hills & Karp [16] and the modern approach by Linton & Martin [33] are of most relevance here. The Wiener–Hopf technique is used in these articles, and the advantages of employing this analytical approach are highlighted.

The scattering effect of two-dimensional arrays and in particular those consisting of multiple parallel rows, has been consider in several articles, notably [4], [28], and [33]. In contrast, the case of the semi-infinite lattice has received far less attention. A brief consideration in the water-wave context is given in [27]. Also, the overall structure of the field generated when a plane electromagnetic wave strikes the edge of a photonic crystal discussed in [18, pp. 221–225], but no actual calculations are given. The purpose of this thesis is to begin filling in this gap by studying acoustic wave scattering by a semi-infinite lattice of cylinders.

The structure of the thesis is as follows. In the first chapter we introduce the mathematical framework that will be required in subsequent chapters. Chapter 2 contains a review of the discrete Wiener–Hopf technique, which is the analytical tool employed to solve the problem under consideration. The last two chapters present the solution of the problem, first for small sound-soft cylinders (chapter 3) and then for the general case (chapter 4). A detailed analysis of the scattered field is given, and a conservation of energy condition is obtained. Some concluding remarks follow in the last chapter. Finally, two appendices are included, containing various definitions and formulae that will be useful throughout.

Chapter 1

Acoustic scattering by cylinders

In this chapter, we present the mathematical theory that underlies acoustic scattering by cylinders in two dimensions, and a method of solution based on separation of variables.

1.1 The Helmholtz equation

In physics, the wave equation governs the propagation of acoustic waves through a homogeneous, compressible fluid. The form of the equation is:

$$\nabla^2 U(\mathbf{r}, t) = \frac{1}{c^2} \frac{\partial^2 U(\mathbf{r}, t)}{\partial t^2}, \tag{1.1.1}$$

where ∇^2 is the Laplacian, c is the speed of sound and U is the acoustic pressure (or the velocity potential), which depends on the spatial position $\mathbf{r}$ and the time t. We shall limit ourselves to time harmonic motion with angular frequency ω, in which case the acoustic pressure is given by

$$U(\mathbf{r}, t) = Re[u(\mathbf{r})e^{-i\omega t}]. \tag{1.1.2}$$

In view of (1.1.1) and (1.1.2), the complex-valued function u must satisfy the Helmholtz equation

$$(\nabla^2 + k^2)u(\mathbf{r}) = 0, \tag{1.1.3}$$

where $k = \omega/c$ is the wavenumber.

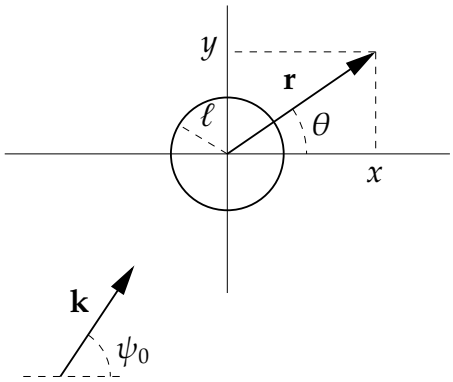

Figure 1.1: *Schematic diagram showing the cylinder and the notation in use*

To illustrate the mathematical framework used in describing these physical phenomena, we begin by considering a relatively simple case, namely the scattering of a plane wave by a single cylinder.

1.2 Scattering by a single cylinder

Consider a cylinder of radius ℓ. We choose a two dimensional Cartesian coordinate system (x, y), the origin of which coincides with the cylinder's centre. In polar coordinates the position vector is given by $\mathbf{r} = (r\cos\theta, r\sin\theta)$. Here we have introduced the convention that $|\mathbf{v}| = \mathrm{v}$ for any vector $\mathbf{v}$, which will be used throughout. Let the plane wave

$$u_{inc}(\mathbf{r}) = e^{i\mathbf{k}\cdot\mathbf{r}}, \tag{1.2.1}$$

be incident upon the cylinder at an angle ψ_0 with respect to the x-axis, so that the wavenumber vector $\mathbf{k}$ is given by

$$\mathbf{k} = (k\cos\psi_0, k\sin\psi_0). \tag{1.2.2}$$

Note that the incident field (1.2.1) satisfies the Helmholtz equation (1.1.3) and it is the only field that would exist if there was no cylinder present.

The interaction of the incident wave with the cylinder, will produce a scattered response $u_{sc}(\mathbf{r})$ and it is this field that we seek to determine. We can then

construct the total field $u(\mathbf{r})$, by linear superposition; that is

$$u(\mathbf{r}) = u_{inc}(\mathbf{r}) + u_{sc}(\mathbf{r}). \tag{1.2.3}$$

1.2.1 Boundary conditions

We will express the boundary condition in terms of polar coordinates, because the cylinder's boundary coincides with the circle $r = \ell$. The three most common conditions are

- **Dirichlet** condition (*sound-soft cylinder*),

$$u(\ell, \theta) = 0, \qquad 0 \leqslant \theta < 2\pi. \tag{1.2.4}$$

- **Neumann** condition (*sound-hard cylinder*),

$$\left.\frac{\partial u(r,\theta)}{\partial r}\right|_{r=\ell} = 0, \qquad 0 \leqslant \theta < 2\pi. \tag{1.2.5}$$

- **Robin** condition,

$$f(\theta)u(\ell,\theta) + \left.\frac{\partial u(r,\theta)}{\partial r}\right|_{r=\ell} = 0, \qquad 0 \leqslant \theta < 2\pi. \tag{1.2.6}$$

  Note that $f(\theta)$ may be a constant.

1.2.2 The radiation condition

In order to completely state a scattering problem in an unbounded domain, we must impose a constraint on the behaviour of the field as $r \to \infty$. This is known as the Sommerfeld radiation condition, and in two dimensions it is given by

$$\lim_{r\to\infty} r^{1/2}\left(\frac{\partial u_{sc}(r,\theta)}{\partial r} - iku_{sc}(r,\theta)\right) = 0, \tag{1.2.7}$$

converging uniformly in θ. The physical interpretation of (1.2.7) is that the scattered field behaves like an outgoing wave in the far field. In other words, the radiation condition in scattering problems ensures that the scattered wave propagates away from the obstacle (in our case the cylinder).

The Helmholtz equation, subject to appropriate boundary and radiation conditions defines a well-posed boundary value problem, and therefore uniqueness theorems can be proved in some cases. For the case of scattering by one cylinder, a proof can be found in [10]. In the trivial situation where we have no incident wave propagating, the unique solution is $u(\mathbf{r}) = 0$.

1.2.3 Solution based on separation of variables

The method of separation of variables is one of the oldest [11] and most important for finding explicit solutions of the Helmholtz and related partial differential equations. It is widely used because of its simplicity and numerical effectiveness. The Helmholtz equation (1.1.3) separates in polar coordinates, which is ideal in our case, since the boundary of the cylinder coincides with a coordinate line. It is an easy mater to check that the separated solutions are

$$u(r,\theta) = J_q(kr)e^{iq\theta} \qquad \text{and} \qquad u(r,\theta) = Y_q(kr)e^{iq\theta}, \qquad q \in \mathbb{Z}, \tag{1.2.8}$$

where $J_q(\cdot)$, $Y_q(\cdot)$ are Bessel functions of the first and second kind, respectively (see appendix A.2). Alternatively, we can write the solutions in terms of the cylindrical wavefunctions

$$\mathcal{J}_q(\mathbf{r}) = J_q(kr)e^{iq\theta} \qquad \text{and} \qquad \mathcal{H}_q(\mathbf{r}) = H_q(kr)e^{iq\theta}, \qquad q \in \mathbb{Z}, \tag{1.2.9}$$

where $H_q(\cdot) \equiv H_q^{(1)}(\cdot) = J_q(\cdot) + iY_q(\cdot)$ is the Hankel function of the first kind. We call $\mathcal{J}_q(\mathbf{r})$ a regular wavefunction, since it is free of singularities and we call $\mathcal{H}_q(\mathbf{r})$ an outgoing wavefunction because it behaves like an outgoing wave at infinity, i.e. it satisfies the radiation condition (1.2.7) (see (A.2.11)). The functions $\mathcal{H}_q(\mathbf{r})$ are also known as multipoles and all of them have a singularity at $\mathbf{r} = \mathbf{0}$.

With the above notation, the boundary value problem in hand can be tackled by expressing the scattered field in terms of a multipole expansion series

$$u_{sc}(\mathbf{r}) = \sum_{q=-\infty}^{\infty} A^q \mathcal{H}_q(\mathbf{r}). \tag{1.2.10}$$

This series satisfies the Helmholtz equation (1.1.3) and the radiation condition (1.2.7), as long as it converges. The unknown amplitude coefficients A^q can be determined by applying the boundary condition on the cylinder's surface. To proceed in this direction, we use the generating function of the Bessel functions (see [60, §2.1] or [26, §5.2-5.3])

$$\exp\left[\frac{z}{2}\left(t-\frac{1}{t}\right)\right]=\sum_{n=-\infty}^{\infty}J_n(z)t^n, \tag{1.2.11}$$

with the substitution $z = kr$ and $t = ie^{i(\theta-\psi_0)}$ to obtain the Jacobi expansion

$$e^{ikr\cos(\theta-\psi_0)}=\sum_{n=-\infty}^{\infty}e^{in(\pi/2+\theta-\psi_0)}J_n(kr). \tag{1.2.12}$$

Equation (1.2.12) shows that any plane wave can be expanded in terms of regular wavefunctions. Thus, the total field in polar coordinates can be written

$$u(\mathbf{r})=\sum_{q=-\infty}^{\infty}\Big(A^qH_q(kr)+e^{iq(\pi/2-\psi_0)}J_q(kr)\Big)e^{iq\theta}. \tag{1.2.13}$$

Now, we can apply the boundary condition on the cylinder's surface and make use of the orthogonality of the trigonometric functions $e^{iq\theta}$, to obtain

$$A^q=-e^{iq(\pi/2-\psi_0)}Z_q,\qquad q\in\mathbb{Z}, \tag{1.2.14}$$

where

$$Z_q=\begin{cases}J_q(k\ell)/H_q(k\ell), & \text{for Dirichlet boundary conditions,}\\ J_q'(k\ell)/H_q'(k\ell), & \text{for Neumann boundary conditions.}\end{cases} \tag{1.2.15}$$

Hence, the scattered field is given by

$$u_{sc}(\mathbf{r})=-\sum_{q=-\infty}^{\infty}e^{iq(\pi/2-\psi_0)}Z_q\mathcal{H}_q(\mathbf{r}). \tag{1.2.16}$$

We see that the method of multipole expansion, based on separation of variables, leads to an exact solution (1.2.16). Our ultimate goal is to extend this method to account for more complicated cases where the incident wave interacts with semi-infinite lattices of cylinders.

1.2.4 Low frequency approximations

Consider a sound-soft cylinder, the radius of which is small compared to the wavelength of the incident field, that is

$$0 < k\ell \ll 1. \tag{1.2.17}$$

In this case the leading order contribution to the scattered field comes from the term with $q = 0$ in (1.2.10) [1]; that is

$$u_{sc}(\mathbf{r}) \sim A^0 H_0(kr), \qquad \text{as} \qquad k\ell \to 0. \tag{1.2.18}$$

Note that there is no dependence on θ here, meaning that sound-soft cylinders scatter waves isotropically in the low frequency limit. Also note that (1.2.18) is a constant multiple of the free-space Green's function for the two dimensional Helmholtz equation. See [37, §8.3]

For sound-hard cylinders, at low frequency additional terms are required; it turns out that the scattered field can be approximated by (see [37, §8.2.6 and 8.3.3])

$$u_{sc}(\mathbf{r}) \sim \sum_{q=-1}^{1} A^q \mathcal{H}_q(\mathbf{r}), \qquad \text{as} \qquad k\ell \to 0. \tag{1.2.19}$$

These approximations are justified rigorously by the work of Kleinmann and Vainberg [21]. In their paper, one can find low-frequency asymptotic expansions of solutions of a large class of boundary value problems involving second-order elliptic equations in two dimensions. For the special case of scattering by a small sound-soft cylinder, Kleinmann–Vainberg theory gives (see [37, §8.2.3-8.2.5])

$$u_{sc}(\mathbf{r}) \approx f_0 u_{inc}(\mathbf{0}) H_0(kr), \tag{1.2.20}$$

where

$$f_0 = -\left(1 + \frac{2i}{\pi}\Big(\mathfrak{c} + \ln(k\ell) - \ln 2\Big)\right)^{-1}, \tag{1.2.21}$$

in which $\mathfrak{c} = 0.55721...$ is Euler's constant (see [2, eq. 6.1.3]). Note that f_0 is an approximation of $-Z_0 = -J_0(k\ell)/H_0(k\ell)$, with an error of order $(k\ell)^2$; see (A.2.9).

[1] Note that for $q \neq 0$, $Z_q \to 0$ as $k\ell \to 0$; see (A.2.10). Hence, for $q \neq 0$, $A^q \to 0$ as $k\ell \to 0$.

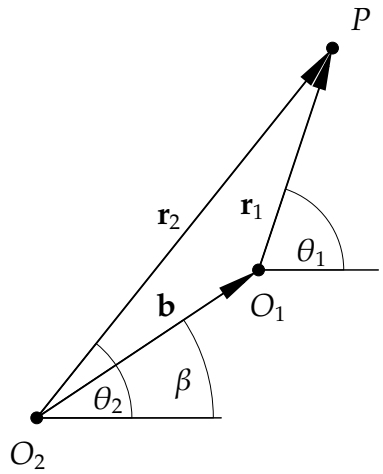

Figure 1.2: *Geometry for Graf's addition theorem*

1.3 Multiple Scattering

We can extend the mathematical theory described so far to account for multiple scattering, where the incident wave interacts with two or more cylinders. The method we use to solve these problems is based on multipole expansions and Graf's addition theorem.

1.3.1 Graf's addition theorem

Consider two origins O_j, $j = 1, 2$, and let $\mathbf{r_j}$ be the position vector of a given point P with respect to O_j. If $\mathbf{b}$ is the position vector of O_1 with respect to O_2, then

$$H_q(kr_2)e^{iq\theta_2} = \sum_{n=-\infty}^{\infty} H_{q-n}(kb)e^{i(q-n)\beta}J_n(kr_1)e^{in\theta_1} \quad \text{for} \quad r_1 < b, \tag{1.3.1}$$

and

$$H_q(kr_2)e^{iq\theta_2} = \sum_{n=-\infty}^{\infty} J_{q-n}(kb)e^{i(q-n)\beta}H_n(kr_1)e^{in\theta_1} \quad \text{for} \quad r_1 > b, \tag{1.3.2}$$

where θ_1, θ_2 and β are the angles of $\mathbf{r_1}$, $\mathbf{r_2}$ and $\mathbf{b}$ with the x-axis respectively; see figure 1.2. The formulae (1.3.1) and (1.3.2) are due to Graf and they are used to transform an outgoing wavefunction about a point O_2 in space in terms of an expansion of wavefunctions about a different point O_1. These types of expansion are commonly described as addition theorems and they are of crucial

importance in multiple scattering problems. Further discussion on addition theorems and their proofs can be found in [37, Ch. 2] and [60, Ch. 11].

1.3.2 Scattering by multiple cylinders

We are now ready to tackle the problem of acoustic scattering by N (> 1) cylinders of radius ℓ. First we introduce a two dimensional Cartesian system (x, y), whose origin is O and as before the position vector in polar coordinates is given by $\mathbf{r} = (r\cos\theta, r\sin\theta)$. Let O_n, $n = 1, 2, \ldots N$ denote the cylinders' centres and let $\mathbf{P}_n$ be the position vector of the point O_n; see figure 1.3. A plane wave is incident upon the structure at an angle ψ_0; that is

$$u_{inc}(\mathbf{r}) = e^{i\mathbf{k}\cdot\mathbf{r}}, \quad \text{where} \quad \mathbf{k} = (k\cos\psi_0, k\sin\psi_0) \tag{1.3.3}$$

and we seek to determine the scattered field. A good description of the interaction effect is given in [31, p. 551]

> *'The effect of a given cylinder on the incident wave will be to produce a scattered wave which will in turn be scattered by adjacent cylinders and so on. A description of all the possible interactions that take place is provided by associating with each cylinder a general wave potential describing waves radiating away from that cylinder, which, together with the incident wave potential, describes the total wave field.'*

Thus, setting $u^n_{sc}(\mathbf{r})$ to be the radiating wave emanating from the n^{th} cylinder, the total potential can be written

$$u(\mathbf{r}) = u_{inc}(\mathbf{r}) + \sum_{n=1}^{N} u^n_{sc}(\mathbf{r}), \tag{1.3.4}$$

where the sum represents the total scattered field.

In §1.2.3 where we had only one cylinder, the scattered field was written as a linear combination of multipoles (1.2.10) centred at the origin (the cylinder's

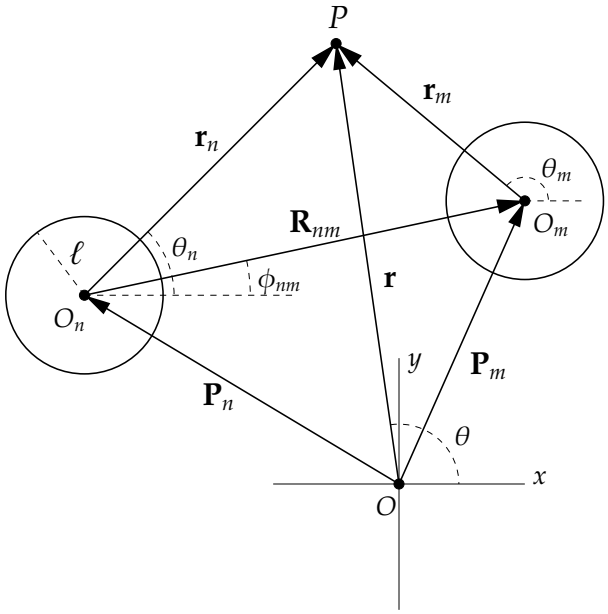

Figure 1.3: *Schematic diagram showing the n^{th} and m^{th} cylinder and the notation in use.*

centre). Similar representations for the fields u_{sc}^n can be given, with the expansions centred at O_n. For this reason we introduce N polar coordinates systems (r_n, θ_n), $n = 1, 2, \ldots, N$, each one centred on O_n. The position vector with respect to O_n is $\mathbf{r}_n = \mathbf{r} - \mathbf{P}_n$, and in the associated polar coordinate system, it is given by $\mathbf{r}_n = (r_n \cos\theta_n, r_n \sin\theta_n)$; see figure 1.3. With this notation we write

$$u_{sc}^n(\mathbf{r}_n) = \sum_{q=-\infty}^{\infty} A_n^q \mathcal{H}_q(\mathbf{r}_n), \qquad n = 1, \ldots, N, \tag{1.3.5}$$

so that these fields satisfy the Helmholtz equation and the radiation condition (1.2.7).

The unknown amplitude coefficients A_n^q can be determined by applying the boundary conditions. This can be accomplished by writing the total potential (1.3.4) solely in terms of the coordinates (r_m, θ_m), for an arbitrary natural number $m \leqslant N$. For the incident wave, we write

$$u_{inc}(\mathbf{r}) = e^{i\mathbf{k}\cdot\mathbf{r}} = e^{i\mathbf{k}\cdot(\mathbf{P}_m + \mathbf{r}_m)},$$

and use Jacobi's expansion (1.2.12) to obtain

$$u_{inc}(\mathbf{r}_m) = e^{i\mathbf{k}\cdot\mathbf{P}_m} \sum_{j=-\infty}^{\infty} e^{ij(\pi/2-\psi_0)} \mathcal{J}_j(\mathbf{r}_m). \tag{1.3.6}$$

For the fields u_{sc}^n, $n \neq m$, we introduce the vector $\mathbf{R}_{nm} = \mathbf{P}_m - \mathbf{P}_n$, which in polar coordinates with respect to O_n is given by $\mathbf{R}_{nm} = R_{nm}(\cos\phi_{nm}, \sin\phi_{nm})$ (see figure 1.3). Assuming that $r_m < R_{nm}$, Graf's addition theorem (1.3.1) can be applied, and the outcome is

$$u_{sc}^n(\mathbf{r}_n) = \sum_{q=-\infty}^{\infty} A_n^q \sum_{j=-\infty}^{\infty} H_{q-j}(kR_{nm}) e^{i(q-j)\phi_{nm}} \mathcal{J}_j(\mathbf{r}_m), \quad n \neq m. \tag{1.3.7}$$

Substitution of (1.3.6), (1.3.7) for $n \neq m$, and (1.3.5) for $n = m$, in (1.3.4) yields

$$u(\mathbf{r}_m) = \sum_{j=-\infty}^{\infty} \left(e^{i\mathbf{k}\cdot\mathbf{P}_m} e^{ij(\pi/2-\psi_0)} \mathcal{J}_j(\mathbf{r}_m) + A_j^m \mathcal{H}_j(\mathbf{r}_m) \right) + \sum_{\substack{n=1 \\ n\neq m}}^{N} \sum_{q=-\infty}^{\infty} A_n^q \sum_{j=-\infty}^{\infty} H_{q-j}(kR_{nm}) e^{i(q-j)\phi_{nm}} \mathcal{J}_j(\mathbf{r}_m). \tag{1.3.8}$$

Now we can apply the boundary conditions (Dirichlet or Neumann) on the surface of the m^{th} cylinder by writing the wavefunctions in full form and taking into account the orthogonality of the trigonometric functions $e^{ij\theta_m}$. This yields

$$A_m^p + Z_p \sum_{\substack{n=1 \\ n\neq m}}^{N} \sum_{q=-\infty}^{\infty} A_n^q H_{q-p}(kR_{nm}) e^{i(q-p)\phi_{nm}} = -Z_p e^{i\mathbf{k}\cdot\mathbf{P}_m} e^{ip(\pi/2-\psi_0)}, \quad m = 1, \ldots, N, \;\; p = 0, \pm 1, \ldots \tag{1.3.9}$$

where Z_p is defined in (1.2.15).

The infinite system of algebraic equations for the unknown amplitudes A_m^p (1.3.9), can be solved numerically by truncating the inner sum at $|q| = Q$ for some nonnegative integer Q. That is, the solution of (1.3.9) is approximated as the solution of the finite system

$$A_m^p + Z_p \sum_{\substack{n=1 \\ n\neq m}}^{N} \sum_{q=-Q}^{Q} A_n^q H_{q-p}(kR_{nm}) e^{i(q-p)\phi_{nm}} = -Z_p e^{i\mathbf{k}\cdot\mathbf{P}_m} e^{ip(\pi/2-\psi_0)}, \quad m = 1, \ldots, N, \;\; p = 0, \pm 1, \ldots, \pm Q, \tag{1.3.10}$$

and experience shows that this is effective because $|A_m^p| \to 0$ very rapidly as $|p| \to \infty$ (see figure 1.4).

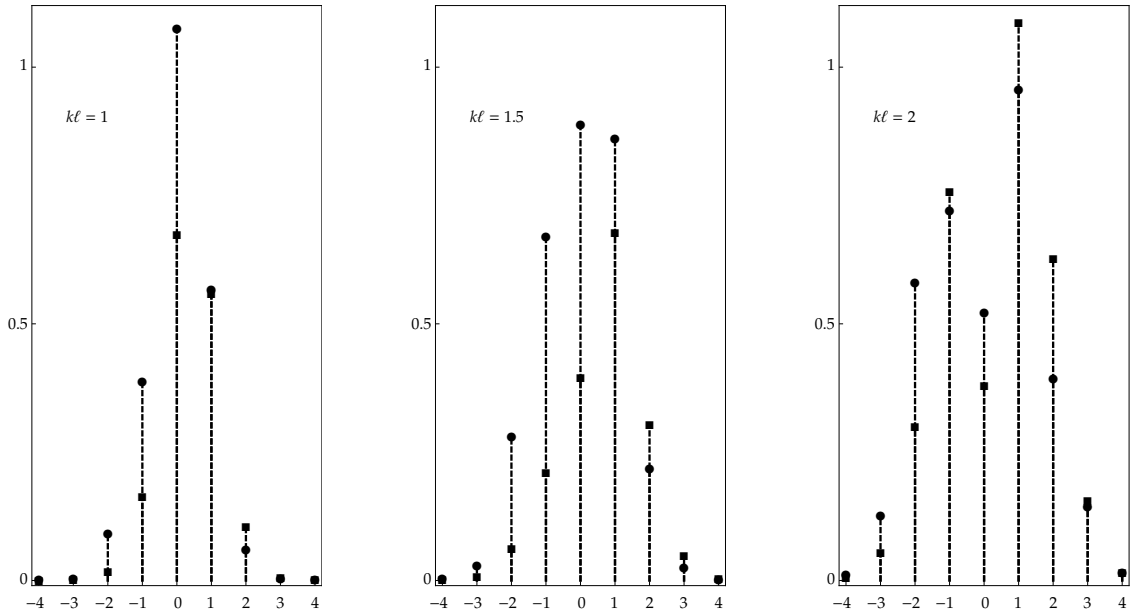

Figure 1.4: *Plot displaying the decay rate of the amplitudes. The results have been obtained by solving the system* (1.3.10) *for* $Q = 6$ *and* $N = 2$*. For* $q = -4, \ldots, 4$*, the value* $|A_m^q|$ *is marked with a disc for* $m = 1$ *and a square for* $m = 2$*. The other parameters in use are* $\ell = 1$*,* $\psi_0 = \pi/4$*, and* $R_{12} = 4$ *(spacing).*

Systems of the form (1.3.9) arise also in other physical contexts and a solution based on truncation again leads to accurate results. Row [49] considered electromagnetic scattering by two identical conducting cylinders. The incident field was generated by a line source, and the formulation (using integral equations methods) led to a system of equations similar to (1.3.9). Truncating this system at $Q = 6$ gave results that were in excellent agreement with experiments. Linton & Evans [31] considered the scattering of water waves by N bottom-mounted vertical cylinders. Similarly, truncation at order $Q = 6$ gave results to four significant figures as long as the cylinders are not very close together. Note that [31, fig. 2] is incorrect; a corrected version is given in [34, fig. 6.2].

To illustrate the effectiveness of the method we solved the truncated system (1.3.10) for two sound-soft cylinders and $Q = 6$. Figure 1.5 shows the total field $Re[u(\mathbf{r})]$ on the boundary of each cylinder. It is clear that the accuracy of the method deteriorates as we increase the frequency, and the same phenomenon is observed when the spacing is decreased. The accuracy can be improved by

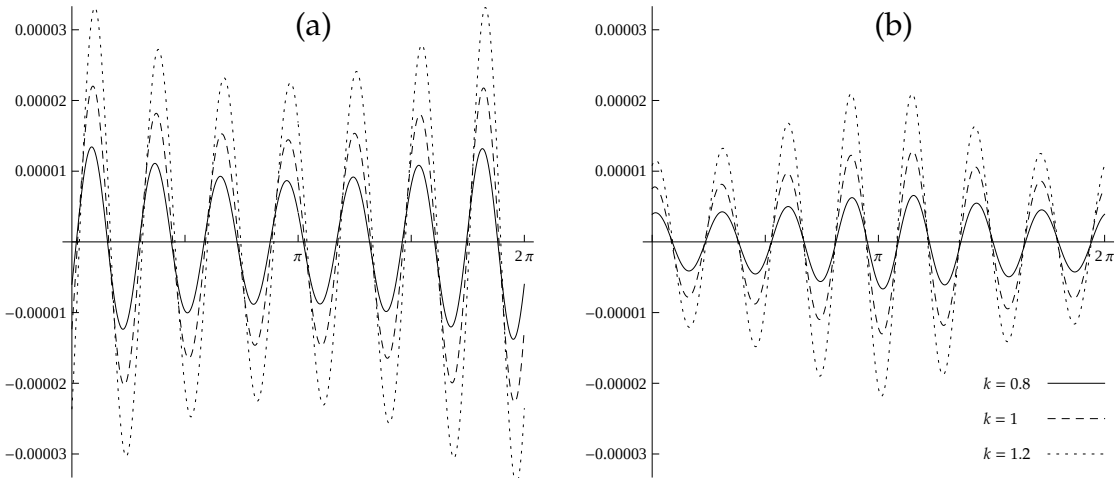

Figure 1.5: *Plots of the total field on the boundary of the two cylinders, illustrating the accuracy of the multipole method. The parameters in use are* $\ell = 1$, $\psi_0 = \pi/4$, *and* $R_{12} = 4$ *(spacing). In particular, the plots are for the functions (a)* $Re[u(\ell e^{it})]$ *and (b)* $Re[u(R_{12} + \ell e^{it})]$.

increasing the order of truncation Q.

1.3.3 Literature

The literature on multiple scattering is vast. For the most comprehensive review see the book by Martin [37] and in particular for references regarding scattering by cylinders see §4.5.1. There is also the book by Linton & McIver [34], which draws together a number of mathematical techniques for wave/structure interactions within the water wave context, which is closely related to acoustics.

The multipole expansion method employed to solve the problem of acoustic scattering by multiple cylinders was devised by Záviška [66]. This method will be used throughout the thesis. There are other ways to approach multiple scattering problems. For example, a solution based on integral equation methods for acoustic scattering by two cylinders can be found in [36]. In this paper one can find a brief survey regarding the methods mentioned above as well as Twersky's pioneering work on the subject [55] (see also [37, §6.13]).

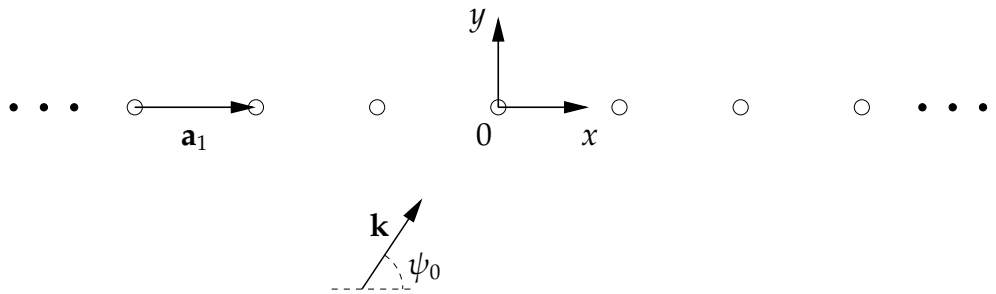

Figure 1.6: *Schematic diagram showing a section of the grating and the notation in use.*

1.4 Scattering by an infinite grating of small cylinders

Having developed the multipole expansion method for more than one cylinder, we can proceed and apply the technique to study acoustic scattering by an infinite row of equally-spaced cylinders. Such a structure is often referred to as a diffraction grating (or simply a grating). Useful discussions on the subject, as well as an extensive bibliography, can be found in the book by Wilcox [62]. Multipole expansions have been used in the study of diffraction gratings by numerous authors; for example see [32], [33, §3], [51], and [57] and references therein.

Here, we solve the problem of acoustic scattering by an infinite grating consisting of small sound-soft cylinders. The periodicity of the geometry plays a crucial role in this kind of problem, as it leads to considerable simplifications. In addition, it enables us to determine the behaviour of the scattered field far away from the grating in a straightforward manner.

1.4.1 Formulation

Consider an infinite grating of cylinders, in which the position vector of the n^{th} cylinder is $n\mathbf{a}_1$, where $n \in \mathbb{Z}$. We choose a coordinate system (x, y) so that its origin coincides with the centre of one of the cylinders and the x-axis is parallel to the vector $\mathbf{a}_1$, i.e. $\mathbf{a}_1 = (a_1, 0)$ (see figure 1.5). Let the plane wave

$$u_{inc}(\mathbf{r}) = e^{i\mathbf{k}\cdot\mathbf{r}}, \quad \text{where} \quad \mathbf{k} = (k\cos\psi_0, k\sin\psi_0)$$

be incident upon the grating at an angle ψ_0, with $0 < \psi_0 < \pi$. Let us assume that the cylinders are sound-soft and their radius ℓ is small compared to the wavelength of the incident field. This means that (see §1.2.4) the radiating field u_{sc}^n emanating from the n^{th} cylinder will behave like

$$u_{sc}^n(\mathbf{r}) = A_n H_0(k|\mathbf{r} - n\mathbf{a}_1|), \tag{1.4.1}$$

where A_n is an unknown amplitude, and by linear superposition the total field is given by

$$u(\mathbf{r}) = u_{inc}(\mathbf{r}) + \sum_{j=-\infty}^{\infty} A_j H_0(k|\mathbf{r} - j\mathbf{a}_1|). \tag{1.4.2}$$

To apply the boundary conditions we will work in the vicinity of the n^{th} cylinder, wherein an observer can distinguish an incoming and an outgoing wave. The former consists of the incident plane wave plus the contributions radiating from all the other scatterers, i.e.

$$u_{inc}^n(\mathbf{r}) = u_{inc}(\mathbf{r}) + \sum_{\substack{j=-\infty \\ j\neq n}}^{\infty} A_j H_0(k|\mathbf{r} - j\mathbf{a}_1|), \tag{1.4.3}$$

and the latter is the scattered response

$$u_{sc}^n(\mathbf{r}) = A_n H_0(k|\mathbf{r} - n\mathbf{a}_1|). \tag{1.4.4}$$

Now, bearing in mind that u_{inc}^n is the field incident upon the n^{th} cylinder, we can use the the asymptotic approximation (1.2.20) to obtain

$$u_{sc}^n(\mathbf{r}) \approx f_0 u_{inc}^n(n\mathbf{a}_1) H_0(k|\mathbf{r} - n\mathbf{a}_1|), \tag{1.4.5}$$

where f_0 is given by (1.2.21). Hence,

$$A_n = f_0 u_{inc}^n(n\mathbf{a}_1), \tag{1.4.6}$$

which upon substitution of (1.4.3) for $\mathbf{r} = n\mathbf{a}_1$, yields the infinite system of algebraic equations

$$A_n - f_0 \sum_{\substack{j=-\infty \\ j\neq n}}^{\infty} A_j H_0(ka_1|n-j|) = f_0 e^{in\mathbf{k}\cdot\mathbf{a}_1}, \qquad n \in \mathbb{Z}. \tag{1.4.7}$$

1.4.2 The solution

Gratings are structures that are repetitive in one direction. This means that they have a discrete translational symmetry dependent on the step vector $\mathbf{a}_1$, or in other words their geometry is invariant under the translation $T : \mathbf{v} \mapsto \mathbf{v} + m\mathbf{a}_1$. Also it is evident that the incident field is quasi-periodic (see Definition 2, in Appendix B) since

$$u_{inc}(\mathbf{r} + m\mathbf{a}_1) = e^{im\mathbf{k}\cdot\mathbf{a}_1} u_{inc}(\mathbf{r}), \quad \forall m \in \mathbb{Z}. \tag{1.4.8}$$

Since the problem is linear we expect the total field to exhibit the same behaviour, that is

$$u(\mathbf{r} + m\mathbf{a}_1) = e^{im\mathbf{k}\cdot\mathbf{a}_1} u(\mathbf{r}), \quad \forall m \in \mathbb{Z}. \tag{1.4.9}$$

Hence, we seek for a solution with the property that

$$A_m = e^{im\mathbf{k}\cdot\mathbf{a}_1} A_0. \tag{1.4.10}$$

Using this in the system (1.4.7), yields

$$A_0 - f_0 A_0 \sum_{\substack{j=-\infty \\ j\neq n}}^{\infty} e^{i(j-n)\mathbf{k}\cdot\mathbf{a}_1} H_0(ka_1|n-j|) = f_0, \tag{1.4.11}$$

and therefore

$$A_0 = \frac{f_0}{1 - f_0 \mathcal{S}_0}, \tag{1.4.12}$$

where

$$\mathcal{S}_0 = \sum_{\substack{j=-\infty \\ j\neq 0}}^{\infty} e^{ijka_1 \cos\psi_0} H_0(ka_1|j|). \tag{1.4.13}$$

The last series converges slowly, but we can use the alternative representation (B.2.5) in order to evaluate it efficiently. Further discussion of sums of this type, which are called Schlömilch series, or one-dimensional lattice sums, can be found in Appendix B.2.

To summarise, since A_0 can be calculated from (1.4.12) and all the other amplitudes are given in terms of A_0 from (1.4.10), we have an explicit formula

for the total field

$$u(\mathbf{r}) = u_{inc}(\mathbf{r}) + A_0 \sum_{j=-\infty}^{\infty} e^{ij\mathbf{k}\cdot\mathbf{a}_1} H_0(k|\mathbf{r} - j\mathbf{a}_1|). \tag{1.4.14}$$

1.4.3 The far field pattern

We will now examine the behavior of the scattered field far away from the grating. To do this we first note that

$$u_{sc}(\mathbf{r}) = A_0 G_0^{(1)}(\mathbf{r}, k\cos\psi_0), \tag{1.4.15}$$

where $G_0^{(1)}$ denotes the 1D quasi-periodic Green's function given in (B.1.19). Substituting the spectral form of this function (B.1.23) in (1.4.15), yields

$$u_{sc}(x, y) = \frac{2A_0}{ka_1} \sum_{j=-\infty}^{\infty} \frac{e^{ik(\cos\psi_j x + \sin\psi_j |y|)}}{\sin\psi_j}. \tag{1.4.16}$$

where the quantities ψ_j are the so-called scattering angles and they are defined in (B.1.12). Observe that (see §B.1.1) $\cos\psi_j$ is always real, whereas $\sin\psi_j$ is real for $j \in \mathcal{M}$ and positive imaginary for $j \in \mathcal{N}$, where $\mathcal{M}$ and $\mathcal{N}$ are sets of indexes defined in (B.1.13) and (B.1.14), respectively.

Returning to the representation (1.4.16), we can derive two important conclusions. The first one is that the scattered field is symmetric about the x-axis, which is clearly necessary because the scatterers are isotropic. The second is that all but a finite number of the terms decay exponentially as $|y|$ is increased. Thus, only the terms for which $\sin\psi_j$ is real (i.e. $j \in \mathcal{M}$) contribute to the far-field and so

$$u_{sc}(x, y) \sim \frac{2A_0}{ka_1} \sum_{j\in\mathcal{M}} \frac{e^{ik(\cos\psi_j x + \sin\psi_j |y|)}}{\sin\psi_j}, \qquad \text{as} \quad |y| \to \infty, \tag{1.4.17}$$

which means that the scattered field far away from the grating consists of a finite number of plane waves which make angles ψ_j with the positive x-axis for $y > 0$ (and $-\psi_j$ for $y < 0$). For $ka_1 < \pi$, the far field expansion consists of a single plane wave, corresponding to the term with $j = 0$ in (1.4.17).

1.4.4 Resonance

In the analysis we used so far we implicitly excluded the case in which

$$\cos\psi_0 + \frac{2\pi n}{ka_1} = \pm 1, \quad \text{for some} \quad n \in \mathbb{Z}. \tag{1.4.18}$$

The reason was that if for example

$$ka_1 + ka_1\cos\psi_0 = -2\pi n, \quad \text{for some} \quad n \in \mathbb{N}, \tag{1.4.19}$$

then, using the asymptotic formula (A.2.11) for $H_0(kja_1)$ we have

$$e^{ijka_1\cos\psi_0}H_0(kja_1) \sim e^{-i\pi/4}\sqrt{\frac{2}{\pi kja_1}}, \qquad \text{as} \quad j \to \infty, \tag{1.4.20}$$

which means that the series $\mathcal{S}_0$ in (1.4.13) fails to converge. In addition, equation (1.4.18) means that the scattering angles are not well-defined (see §B.1.1), and therefore, the representation (1.4.16) is not valid.

In order to study the case (1.4.19) we will examine what happens as $\cos\psi_0 + 2\pi n/ka_1$ approaches -1, for some $n \in \mathbb{Z}$, or equivalently what happens as ψ_n approaches π. The alternative representation for $\mathcal{S}_0$ given in (B.2.5), shows that as ψ_n approaches π,

$$\mathcal{S}_0 = \frac{2}{ka_1\sin\psi_n} + \hat{\mathcal{S}}_0, \tag{1.4.21}$$

where $\hat{\mathcal{S}}_0$ remains bounded as $\psi_n \to \pi$. From (1.4.12) and (1.4.10) we see that all the coefficients A_n tend to zero in this limit. Nevertheless, the scattered field is not zero, since

$$\frac{A_0}{\sin\psi_n} = -\frac{ka_1}{2} \qquad \text{as} \quad \psi_n \to \pi, \tag{1.4.22}$$

and therefore from (1.4.16) we have

$$u_{sc} = -e^{-ikx} \qquad \text{as} \quad \psi_n \to \pi. \tag{1.4.23}$$

Thus, the scattered field reduces to a wave propagating parallel to the grating, towards $x = -\infty$, and this phenomenon is called resonance. Similar conclusions can be drawn for the case where $\cos\psi_0 + 2\pi n/ka_1$ approaches 1 (ψ_n approaches 0), only this time the wave will propagate towards $x = +\infty$.

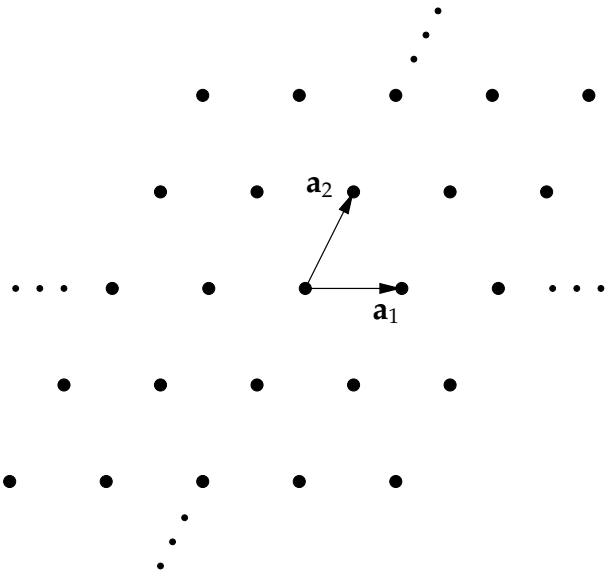

Figure 1.7: *A lattice of cylinders defined by two linear independent vectors* $\mathbf{a}_1$ *and* $\mathbf{a}_2$.

1.5 Bloch waves

A homogeneous medium is characterised by a continuous translational symmetry, i.e. its geometry is invariant under any translation. As pointed out in §1.2 a plane wave propagating through free-space is a solution of the Helmholtz equation (1.1.3) in a homogeneous medium. Here, we discuss wave propagation through a medium with discrete translational symmetry. Consider the lattice of points

$$\Lambda = \{\mathbf{R}_{jm} = j\mathbf{a}_1 + m\mathbf{a}_2, \quad j, m \in \mathbb{Z}\} \tag{1.5.1}$$

defined by the two linearly independent vectors $\mathbf{a}_1$ and $\mathbf{a}_2$, and suppose that cylinders of radius ℓ are centred at $\mathbf{R}_{jm}$; see figure (1.7). This doubly periodic structure has a discrete translational symmetry since its geometry is invariant under the translation

$$T : \mathbf{v} \mapsto \mathbf{v} + \mathbf{R}_{jm}. \tag{1.5.2}$$

A wave u_b propagating through the lattice is called a Bloch wave, after the German physicist Felix Bloch (1905–1983). This field must satisfy the Helmholtz equation, and as Bloch's theorem [6] (see also [18, pp. 32–35]) dictates, the quasi-

periodicity condition

$$u_b(\mathbf{r} + \mathbf{R}_{jm}) = e^{i\boldsymbol{\beta}\cdot\mathbf{R}_{jm}} u_b(\mathbf{r}), \tag{1.5.3}$$

where $\boldsymbol{\beta}$ is called the Bloch wave vector.

The problem of wave propagation through a periodic medium can be formulated as an eigenvalue problem. The procedure originates from the classic paper of Lord Rayleigh [47], and since then it has been refined and generalised (see for example [43]). A comprehensive review on the subject can be found in the book by A. B. Movhan et al. [41, Ch. 3]. Here, a slightly different approach will be used to formulate the problem, but the main principle, which is to express the field u_b around the central cylinder into regular and singular parts, remains the same. We begin by expressing the Bloch wave in terms of the functions $G_q^{(2)}(\mathbf{r}, \boldsymbol{\beta})$, defined in (B.1.5). These are singular at the centre of each cylinder, and they satisfy the Helmholtz equation and the quasi-periodicity condition (1.5.3). Hence, the expansion

$$u_b(\mathbf{r}) = \sum_{q=-\infty}^{\infty} \mathcal{B}_q G_q^{(2)}(\mathbf{r}, \boldsymbol{\beta}), \tag{1.5.4}$$

has all the characteristics of a Bloch wave. In order to apply the boundary condition, we need to restrict ourselves to the vicinity of a particular cylinder. Without loss of generality, we can work on a disc D, centred at the origin, and with its radius chosen so that it does not includes any other lattice points. In this region, $G_q^{(2)}(\mathbf{r}, \boldsymbol{\beta})$ can be split into a singular and a regular part; that is

$$G_q^{(2)}(\mathbf{r}, \boldsymbol{\beta}) = \mathcal{H}_q(\mathbf{r}) + \sum_{m=-\infty}^{\infty} {\sum_{j=-\infty}^{\infty}}' e^{i\mathbf{R}_{jm}\cdot\boldsymbol{\beta}} \mathcal{H}_q(\mathbf{r} - \mathbf{R}_{jm}), \tag{1.5.5}$$

where the prime on the summation symbol indicates that term $(j, m) = (0, 0)$ is to be omitted from the series. Each term in the double sum is regular in D, and hence we can use Graf's addition theorem (1.3.1), to write

$$G_q^{(2)}(\mathbf{r}, \boldsymbol{\beta}) = \mathcal{H}_q(\mathbf{r}) + \sum_{n=-\infty}^{\infty} (-1)^{q-n} \sigma_{q-n}^{(2)}(\boldsymbol{\beta}) \mathcal{J}_n(\mathbf{r}), \qquad \mathbf{r} \in D, \tag{1.5.6}$$

where the two-dimensional lattice sum $\sigma_q^{(2)}(\boldsymbol{\beta})$ is defined in (B.2.9). Now we can substitute (1.5.6) into (1.5.4) and then apply the boundary condition to obtain

the so-called Rayleigh idenity

$$\mathcal{B}_n Z_n^{-1} + \sum_{q=-\infty}^{\infty} (-1)^{q-n} \sigma_{q-n}^{(2)}(\boldsymbol{\beta}) \mathcal{B}_q = 0, \qquad n \in \mathbb{Z}, \tag{1.5.7}$$

where Z_n is defined in (1.2.15). The homogeneous system (1.5.7) can be truncated and solved for the coefficients $\mathcal{B}_n$. A nontrivial solution exists in cases where the determinant of the truncated system is zero, and this implicitly defines a dispersion relation, which is a relation between the Bloch wave vector $\boldsymbol{\beta}$ and the wavenumber k of the propagating wave.

At this point it is convenient to introduce the reciprocal lattice

$$\Lambda^* = \{\mathbf{K}_{jm} = 2\pi j \mathbf{b}_1 + 2\pi m \mathbf{b}_2, \quad j, m \in \mathbb{Z}\}, \tag{1.5.8}$$

where the vectors $\mathbf{b}_1$ and $\mathbf{b}_2$, are chosen so that

$$\mathbf{a}_i \cdot \mathbf{b}_j = \delta_{ij}, \quad i, j = 1, 2. \tag{1.5.9}$$

The significance of the reciprocal lattice vectors is encapsulated in the identity

$$e^{i\mathbf{R}_{nm} \cdot \mathbf{K}_{jp}} = 1, \tag{1.5.10}$$

which implies that

$$G_q^{(2)}(\mathbf{r}, \boldsymbol{\beta}) = G_q^{(2)}(\mathbf{r}, \boldsymbol{\beta} + \mathbf{K}_{jm}), \qquad \forall j, m \in \mathbb{Z}. \tag{1.5.11}$$

From the last equation it appears that different values of $\boldsymbol{\beta}$ do not necessarily lead to different Bloch waves, and in order to ensure unique correspondence between Bloch vectors and modes, we restrict our attention to an area of the reciprocal space called the 'Brillouin zone'. Around a point of the reciprocal lattice, say the point Γ_0 with position vector $\mathbf{K}_{00}$, the Brillouin zone is defined as the locus of points in the reciprocal space that are closer to Γ_0 than to any of the other lattice points. Geometrically, the zone is constructed by drawing perpendicular bisectors between the point Γ_0 and each neighbouring lattice point (see figure 1.8). In addition, if we take into account symmetries of the lattice like rotations and reflections, the area of interest for the vector $\boldsymbol{\beta}$ reduces

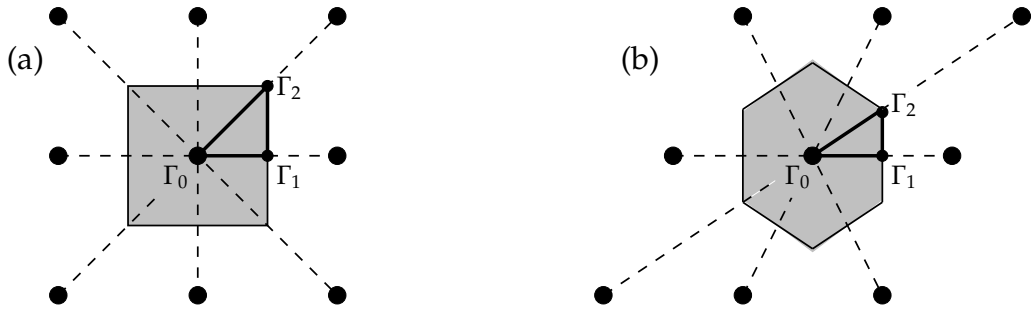

Figure 1.8: *The Brillouin zone (shaded region) for a square (a) and a hexagonal lattice (b). The irreducible Brillouin zone is the triangle* $\Gamma_0\Gamma_1\Gamma_2$.

further to the 'irreducible Brillouin zone' (the triangle $\Gamma_0\Gamma_1\Gamma_2$ in figure 1.8). A detailed discussion on the Brillouin zone can be found in [18, Appendix B].

Another important feature of the reciprocal lattice is that we can express the lattice sums $\sigma_q^{(2)}(\boldsymbol{\beta})$ in terms of the reciprocal vectors. Such representations are suitable for calculations since the convergence rate is fast. Details on the derivations can be found [30, §3.2]. Here, we use [30, eq. 3.15] and [30, eq 3.18] to express the lattice sums in the form

$$\sigma_n^{(2)}(\boldsymbol{\beta}) = \frac{4i^{n+1}}{A}\sum_{j=-\infty}^{\infty}\sum_{m=-\infty}^{\infty}\left(\frac{k}{B_{jm}}\right)^L \frac{J_{n+L}(B_{jm}\xi)}{J_{n+L}(k\xi)(k^2-B_{jm}^2)}e^{in\phi_{jm}} - \delta_{0n}\left[1+\frac{i}{J_L(k\xi)}\left(Y_L(k\xi)+\frac{1}{\pi}\sum_{l=1}^{L}\left(\frac{k\xi}{2}\right)^{L-2l}\frac{(l-1)!}{(L-l)!}\right)\right] \qquad n\geq 0. \quad (1.5.12)$$

where $A = |\mathbf{a}_1 \times \mathbf{a}_2|$,

$$\mathbf{B}_{jm} = \boldsymbol{\beta} + \mathbf{K}_{jm} = B_{jm}(\cos\phi_{jm}, \sin\phi_{jm}),$$

and

$$\xi \leq \min_{\substack{(j,m)\in\mathbb{Z}^2 \\ (j,m)\neq(0.0)}} R_{jm}.$$

The free parameter L is associated with the convergence rate of the double sum in (1.5.12). Note that each term in this sum decays like $m^{-L-5/2}$, and for numerical calculations it is recommended [41, p. 147] that L should be set in the range $5-7$. Finally, if we insert the full form of the wavefunctions in the definition of

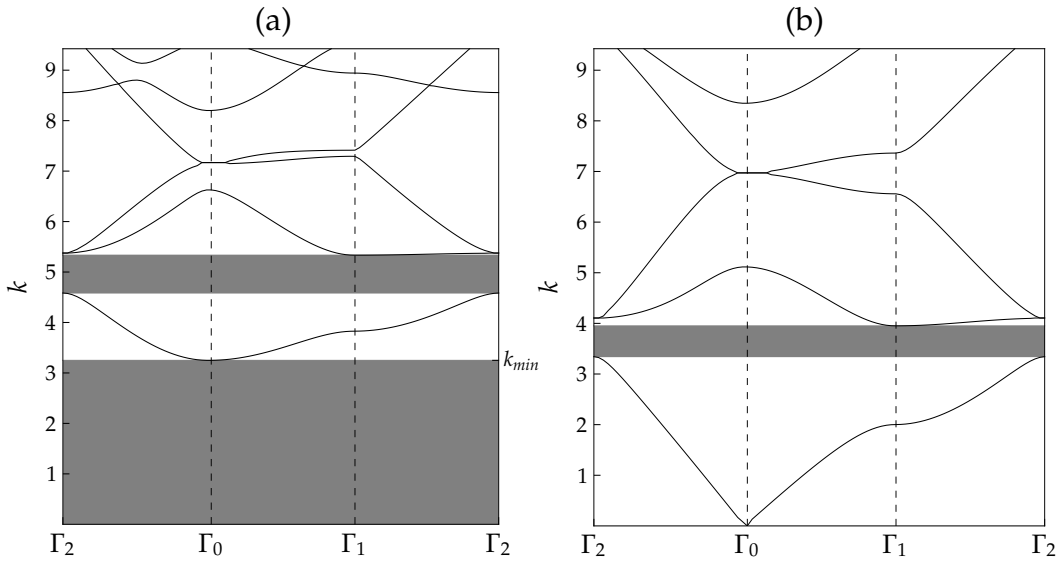

Figure 1.9: *The band structure of a square lattice ($a_1 = a_2 = 1$) for sound-soft cylinders of radius $\ell = 0.187$ (a), and for sound-hard cylinders of radius $\ell = 0.375$ (b).*

the lattice sums (B.2.9), then it is trivial to check that

$$\sigma^{(2)}_{-q}(\boldsymbol{\beta}) = -\left(\sigma^{(2)}_{q}(\boldsymbol{\beta})\right)^{*}, \qquad q \neq 0, \tag{1.5.13}$$

where the asterisk denotes complex conjugation. From the identity (1.5.13) and the representation (1.5.12) we can calculate lattice sums of negative order.

The band structure of a lattice with a specific geometry is usually obtained by letting $\boldsymbol{\beta}$ vary on the edge of the irreducible Brillouin zone and searching for values of k for which the determinant in (1.5.7) vanishes. The curves formed by this procedure are called dispersion curves (or band diagrams), and the slope at any point on these defines the group velocity of the wave. In figure 1.9 we plot the band diagrams for a square lattice of sound-soft cylinders of radius $\ell = 0.187$ (a) and sound-hard cylinders of radius $\ell = 0.375$ (b). We can see that the lattice can prohibit wave propagation for certain domains of frequency. The shaded regions in figure 1.9 indicate such domains which are known as band-gaps. It is worth remarking that for the case of sound-soft cylinders, the minimum value of k in the first dispersion curve is always positive, and tends slowly to zero as $\ell \to 0$ (see [43, fig. 9]). In other words if $k_{min} > 0$ denotes that value, then a first

band gap always exists in the region $0 < k < k_{min}$. In contrast, for the case of sound-hard cylinders we have that $k_{min} = 0$.

The phenomenon of Bloch wave propagation through a periodic medium has been studied extensively in a number of physical contexts, including composite materials [65], perforated thin elastic plates [40] and photonic crystals [18, 43]. In almost all these texts band diagrams are generated by essentially the same procedure presented in this section. The problem is first formulated in terms of a homogeneous system of equations of the form (1.5.7), and values for $\boldsymbol{\beta}$ and k such that the determinant of the truncated system is zero are sought numerically. However for certain limiting cases, an approximation of the dispersion relation can be obtain analytically. For small scatterers, such approximation has been obtained in [45] by analysing the effect of perturbation to plane wave solutions. In a similar fashion, coupled with a scheme of matched asymptotic expansion, analytical results are given in [38] and [22].

Chapter 2

The Wiener–Hopf technique

In 1931 the mathematicians Norbert Wiener (1894–1964) and Eberhard Hopf (1902–1983) published a paper [61], wherein a novel analytical procedure is presented for the solution of an integral equation. Their method, now called the Wiener–Hopf technique, has been used widely ever since to solve problems arising in physics, engineering and applied mathematics [24]. An abstract framework of the method will be given in §2.1.

In wave diffraction theory, the Wiener–Hopf technique was adopted to solve problems involving scattering by semi-infinite structures. Initially, these problems were formulated in terms of a semi-infinite integral equation, but later on, Jones [19] demonstrated that one can bypass this formulation by applying Laplace (or other) transforms directly to the boundary-value problem. In this way, the technique was simplified considerably and this led to further acknowledgement of its utility. The book by Noble [44] contains a number of examples of the refined method.

Less well-known is the fact that the Wiener–Hopf technique can also be used to solve problems involving scattering by semi-infinite arrays of discrete bodies. The formulation of this type of problem leads to an infinite system of algebraic equations, and its solution requires the use of the $\mathcal{Z}$-transform (§2.2). An outline sketch of this 'discrete Wiener–Hopf method' is given in §2.3 and in

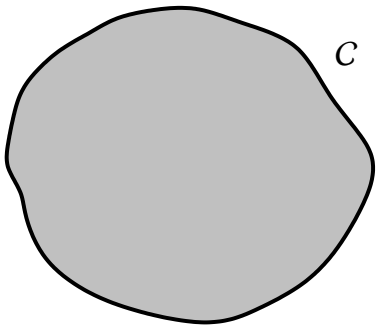

Figure 2.1: *The closed curve C, where the Wiener–Hopf equation holds and C^+ (C^-) is the (un)shaded region.*

§2.4 we present a concrete example.

2.1 The Wiener–Hopf equation and its solution

In this section we shall be concerned with the solution of the Wiener–Hopf equation, expressed in the following form

$$K(z)A^+(z) = T^+(z) + T^-(z), \tag{2.1.1}$$

and defined on a closed curve C of the complex plane [1]. In essence, the Wiener–Hopf equation defines a relation between two known functions $K(z)$ and $T^+(z)$ and two functions $A^+(z)$ and $T^-(z)$ which we seek to determine, along with significant information about the domains of analyticity of all its terms. To denote these domains, we introduce the set C^+ consisting of all the points that lie inside or on C and the set C^- consisting of all the points that lie outside or on C; see figure 2.1 and note that $\infty \in C^-$. The common characteristic of all the functions in (2.1.1) is that they are analytic on C and the superscript plus and minus indicate functions that are analytic on C^+ and C^-, respectively.

[1] In general, C is a closed curve on the Riemann sphere, which means that it could also be a line or a curve passing through infinity. The exact form of C depends on the transform we use to obtain the Wiener–Hopf equation, and since in this text we will use the $\mathcal{Z}$-transform, C will always be a closed curve of the complex plane.

The Wiener–Hopf technique is essentially a three-step procedure to solve equation (2.1.1). The first step is to factorise the function $K(z)$ known as the kernel, into a product of two functions

$$K(z) = K^+(z)K^-(z), \tag{2.1.2}$$

where $K^+(z)$ and $K^-(z)$ are analytic and zero-free on C^+ and C^-, respectively. On implementing this factorisation in (2.1.1), yields

$$A^+(z)K^+(z) = \frac{T^+(z)}{K^-(z)} + \frac{T^-(z)}{K^-(z)}. \tag{2.1.3}$$

The next step is to construct two functions $D^+(z)$ and $D^-(z)$, which are analytic on C^+ and C^-, respectively, and satisfy the relation

$$\frac{T^+(z)}{K^-(z)} = D^+(z) + D^-(z). \tag{2.1.4}$$

Substituting (2.1.4) into (2.1.3) we obtain

$$A^+(z)K^+(z) - D^+(z) = D^-(z) + \frac{T^-(z)}{K^-(z)}, \tag{2.1.5}$$

where the left hand side of the equation represents a function analytic on C^+ and the right hand side represents a function analytic on C^-. Since $C = C^+ \cap C^-$, there exists an entire function $J(z)$, which is the analytic continuation of both sides into the entire complex plane. The last step is to prove that the right hand side of (2.1.5) tends to zero as $z \to \infty$. This will mean that $J(z)$ is a bounded entire function and Liouville's theorem dictates that it must be a constant. In fact $J(z) = 0$, for all z, in order to have the correct behaviour at infinity, and therefore the solution of the Wiener–Hopf equation is given by

$$A^+(z) = \frac{D^+(z)}{K^+(z)} \qquad \text{and} \qquad T^-(z) = -D^-(z)K^-(z). \tag{2.1.6}$$

It is clear that a successful execution of the Wiener–Hopf technique depends on our ability to decompose complex functions into either a sum or a product of two functions one of which is analytic in C^+ and the other in C^-. In the case of a product factorisation, the factors must also be zero-free in their domain of analyticity. We shall use the term 'plus-minus' factorisation or sum-split

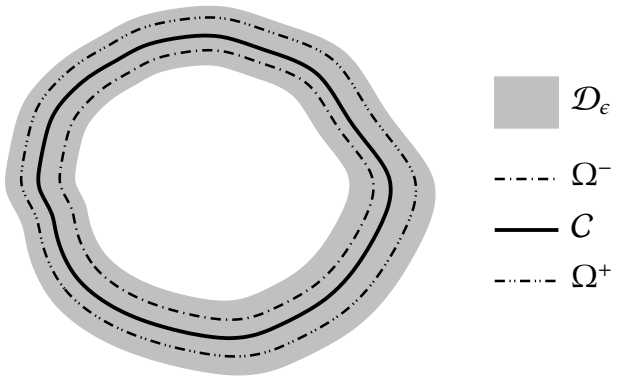

Figure 2.2: *Schematic diagram for Cauchy's integral formula.*

accordingly, to name such decompositions and we note that in general these can be constructed by inspection in an ad hoc manner. However, in some cases, it may be possible to apply standard methods to derive them.

2.1.1 Cauchy's integral formula

The most common way to construct Wiener–Hopf decompositions is by using Cauchy's integral formula . Let $\Omega : [a, b] \to \mathbb{C}$ be a piecewise smooth curve, and let $f(z)$ be analytic on Ω. The Cauchy integral of $f(z)$ over Ω is the function $g(z)$ defined by

$$g(z) = \int_\Omega \frac{f(\zeta)}{\zeta - z}\, d\zeta, \quad z \in \mathbb{C} - \Omega. \tag{2.1.7}$$

Note that $g(z)$ is analytic in $\mathbb{C} - \Omega$ (see [54, 2.83]).

Consider a function $f(z)$ which is analytic on a closed curve C. Analyticity is a property defined over open sets and this means that there exists $\epsilon > 0$ such that the function $f(z)$ is analytic in

$$\mathcal{D}_\epsilon = \bigcup_{w \in C} \{z : |z - w| < \epsilon\}. \tag{2.1.8}$$

Now we set Ω^- and Ω^+ to be the inner and outer boundary of $\mathcal{D}_{\epsilon/2}$, respectively (see figure 2.2), and define the Cauchy integrals of $f(z)$ over Ω^+ and Ω^- by

$$f^\pm(z) = \pm \frac{1}{2\pi i} \oint_{\Omega^\pm} \frac{f(\zeta)}{\zeta - z}\, d\zeta, \quad z \in \mathbb{C} - \Omega^\pm. \tag{2.1.9}$$

It is not difficult to see that

$$f(z) = f^+(z) + f^-(z), \qquad z \in C, \tag{2.1.10}$$

and since $f^\pm(z)$ is analytic in $C^\pm$, we can conclude that the equation (2.1.10) defines the sum-split required in applications of the Wiener–Hopf technique.

We can construct a product decomposition in a similar manner. Suppose that the singularity structure of $f(z)$ is such that a continuous branch of the logarithm exists on the closed curve C. Then, we can use the Cauchy integral of $\log f(z)$ over $\Omega^\pm$ to obtain the factorisation

$$f(z) = f^+(z)f^-(z), \qquad z \in C, \tag{2.1.11}$$

where $f^\pm(z)$ is analytic in $C^\pm$, and given by

$$f^\pm(z) = \exp\left(\pm\frac{1}{2\pi i}\oint_{\Omega^\pm} \frac{\log f(\zeta)}{\zeta - z}\, d\zeta\right). \tag{2.1.12}$$

2.1.2 Decompositions of meromorphic functions

We say that a function is meromorphic in a region $\mathcal{D}$ if it is analytic in $\mathcal{D}$ except possibly at isolated singularities, each of which is a pole. Consider a meromorphic function $f(z)$ which has a finite number of poles in $\mathbb{C}$ and is analytic on the closed curve C. If $f(z)$ is also zero free on C, then the 'plus-minus' product decomposition of this function is trivial. On the other hand a sum decomposition can be constructed easily if the poles are simple. Let

$$f^+(z) = \sum_{j=1}^{n} \frac{a_j}{z - p_j}, \tag{2.1.13}$$

and

$$f^-(z) = f(z) - f^+(z), \tag{2.1.14}$$

where $p_j,\ j = 1, \ldots, n$, are all the poles of $f(z)$ which are situated in C^-, and $a_j,\ j = 1, \ldots, n$, denote the residues of $f(z)$ at p_j. It is evident that $f^\pm(z)$ is analytic in $C^\pm$, with

$$f(z) = f^+(z) + f^-(z). \tag{2.1.15}$$

In cases where $f(z)$ has infinitely many poles, product and sum decompositions can be constructed with the aid of the Weierstrass product theorem and the Mittag-Leffler theorem, respectively (see [13, Ch. 13]). The former can be applied to express $f(z)$ in terms of an infinite product of linear factors, whereas the latter provides the means to decompose $f(z)$ into an infinite sum of partial fractions. The required 'plus-minus' decompositions follow, and details can be found in [48, §3.1 and §3.3] and [54, §3.2].

2.2 The bilateral $\mathcal{Z}$-transform

The bilateral $\mathcal{Z}$-transform is generally used to convert a two-sided sequence $X_n : \mathbb{Z} \to \mathbb{C}$, into an analytic function $X(z)$. We shall use the definition

$$X(z) = \mathcal{Z}(X_n) = \sum_{n=-\infty}^{\infty} X_n z^n, \tag{2.2.1}$$

and focus our interest on sequences whose $\mathcal{Z}$-transform is analytic on an open set $\mathcal{D}$. In addition, we assume that there exists a closed curve $C \subset \mathcal{D}$ that encircles the origin, so that the inverse $\mathcal{Z}$-transform is well-defined by

$$X_n = \mathcal{Z}_C^{-1}\big(X(z)\big) = \frac{1}{2\pi i} \oint_C X(z) z^{-n-1} dz, \tag{2.2.2}$$

where the integration is performed counterclockwise.

In some cases the region of analyticity $\mathcal{D}$ of the forward transform and the contour of integration C of its inverse can be determined explicitly. For example, consider a sequence $X_n : \mathbb{Z} \to \mathbb{C}$, which has the property

$$\sum_{n=-\infty}^{\infty} |X_n| < \infty. \tag{2.2.3}$$

Then, it is evident that the series in (2.2.1) converges on the unit circle. In fact there exists $R^+ > 1$ and $R^- < 1$, such that the tail of the series with positive powers of z

$$\sum_{n=1}^{\infty} X_n z^n, \tag{2.2.4}$$

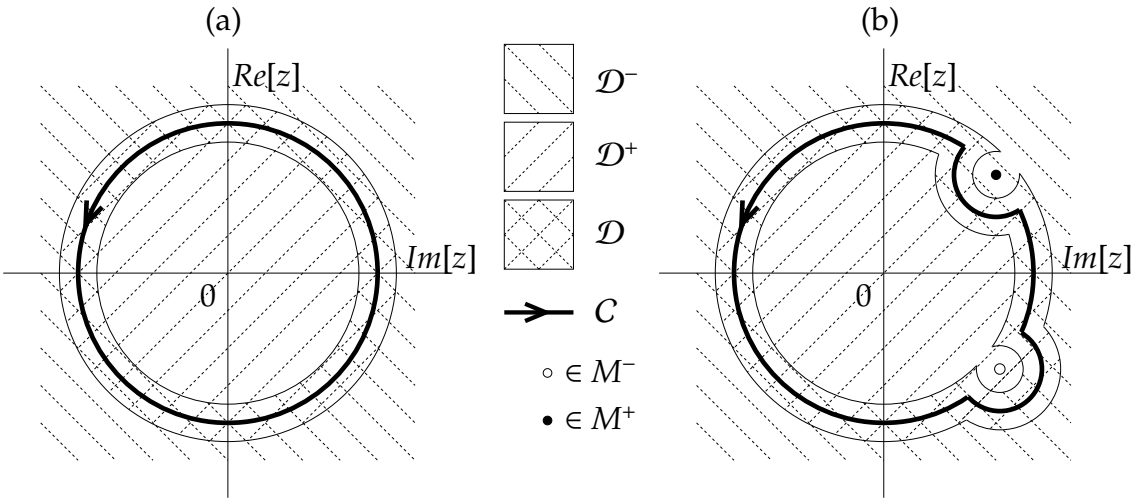

Figure 2.3: *The region of analyticity $\mathcal{D}$ of the forward $\mathcal{Z}$-transform and the contour of integration C of its inverse for two cases: (a) The $\mathcal{Z}$-transform is analytic on the unit circle. (b) The $\mathcal{Z}$-transform is analytic almost everywhere on the unit circle except of finite isolated singularities.*

converges and is analytic on the open disc $\mathcal{D}^+ = \{z : z < R^+\}$, while the tail with negative powers of z

$$\sum_{n=1}^{\infty} X_{-n} z^{-n}, \tag{2.2.5}$$

converges and is analytic on $\mathcal{D}^- = \{z : z > R^-\}$. Hence, it is clear that the $X(z) = \mathcal{Z}(X_n)$ is analytic on the annulus $\mathcal{D} = \{z : R^- < |z| < R^+\}$, and the inverse $X_n = \mathcal{Z}_C^{-1}\big(X(z)\big)$ is well-defined on the contour $C = \{z : |z| = 1\}$. See figure 2.3 (a). In other words the property (2.2.3) suggests that X_n are the coefficients of the Laurent expansion of a function $X(z)$ which is analytic on an annulus.

In practice, more often than not we need to $\mathcal{Z}$-transform a bounded sequence $X_n : \mathbb{Z} \to \mathbb{C}$, which does not necessarily satisfy the condition (2.2.3). In such cases the series (2.2.4) and (2.2.5) converge and are analytic on $\{z : |z| < 1\}$ and $\{z : |z| > 1\}$ respectively, but their behaviour on the unit circle is unknown. Note that in order for the forward $\mathcal{Z}$-transform to be meaningful, the series (2.2.4) and (2.2.5) must have common points of convergence. In addition, the inverse $\mathcal{Z}$-transform is well-defined if a subset of these points forms a closed curve in the complex plane that encircles the origin. In this respect consider the finite

sets M^+ and M^-, containing points of the unit circle, so that

$$M^+ \cap M^- = \varnothing. \tag{2.2.6}$$

Also let $\mathcal{D}^+$ ($\mathcal{D}^-$) be an open set that contains $\{z : |z| \leqslant 1\}$ $\Big(\{z : |z| \geqslant 1\}\Big)$, except the points M^+ (M^-); see figure 2.3 (b). If we can find functions $X^+(z)$ and $X^-(z)$ analytic in $\mathcal{D}^+$ and $\mathcal{D}^-$, respectively, so that

$$X^+(z) = \sum_{n=1}^{\infty} X_n z^n, \quad \text{for} \quad |z| < 1, \tag{2.2.7}$$

and

$$X^-(z) = \sum_{n=1}^{\infty} X_{-n} z^{-n}, \quad \text{for} \quad |z| > 1, \tag{2.2.8}$$

then, the forward $\mathcal{Z}$-transform of $X_n : \mathbb{Z} \to \mathbb{C}$, can be defined by

$$X(z) = \mathcal{Z}(X_n) = X_0 + X^+(z) + X^-(z), \tag{2.2.9}$$

and it is obvious that it is analytic on $\mathcal{D} = \mathcal{D}^+ \cap \mathcal{D}^-$. In addition, (2.2.6) ensures the existence of a closed curve $\mathcal{C} \subset \mathcal{D}$ on which the inverse $\mathcal{Z}$-transform is well-defined; see figure 2.3 (b).

The analysis presented above in an abstract manner, will be used throughout the thesis in specific situations, where the definition of the forward $\mathcal{Z}$-transform (2.2.1) of a bounded sequence $X_n : \mathbb{Z} \to \mathbb{C}$ is ambiguous. In such cases, analytic continuation arguments are required in order to express $\mathcal{Z}(X_n)$ in the form (2.2.9). To see a simple example, we consider the sequence

$$X_n = p^{|n|}, \quad n \in \mathbb{Z}, \tag{2.2.10}$$

with $|p| = 1$. It is evident that

$$\frac{zp}{1 - zp} = \sum_{n=1}^{\infty} p^n z^n, \quad \text{for} \quad |z| < 1, \tag{2.2.11}$$

and

$$\frac{p}{z - p} = \sum_{n=1}^{\infty} p^n z^{-n}, \quad \text{for} \quad |z| > 1. \tag{2.2.12}$$

The functions on the left hand side of (2.2.11) and (2.2.12) represent the analytic continuation of the right hand side into $\mathcal{D}^+ = \mathbb{C} - \{p^{-1}\}$ and $\mathcal{D}^- = \mathbb{C} - \{p\}$, respectively. Thus, the $\mathcal{Z}$-transform is given by

$$X(z) = \mathcal{Z}(X_n) = \frac{1}{1-zp} + \frac{p}{z-p}, \tag{2.2.13}$$

and it is analytic on $\mathcal{D} = \mathbb{C} - \{p^{-1}, p\}$. Also, its inverse (2.2.2) can be defined on any contour that encircles the origin and p, and excludes p^{-1}.

2.2.1 The class $\mathscr{Z}(C)$

It is worth remarking that we cannot explicitly define the largest class of double-sided sequences, on which both the forward and the inverse $\mathcal{Z}$-transform are well-defined. Nevertheless , we can implicitly form this class:

Definition 1. *Let $X_n : \mathbb{Z} \to \mathbb{C}$ be a two-sided sequence and C be a closed curve in the complex plane that encircles the origin. We will say that X_n is a member of the class $\mathscr{Z}(C)$ if and only if there exists a function $X(z)$ analytic on C such that*

$$X_n = \frac{1}{2\pi i} \oint_C X(z) z^{-n-1} dz, \qquad n \in \mathbb{Z}. \tag{2.2.14}$$

2.3 The discrete Wiener–Hopf method

Consider the infinite system of algebraic equations

$$\sum_{j=0}^{\infty} K_{n-j} A_j = T_n, \quad n = 0, 1, \ldots, \tag{2.3.1}$$

where A_j are the unknowns. Here we shall show how this system can be $\mathcal{Z}$-transformed into a Wiener–Hopf equation of the form (2.1.1). Note that $\left[K_{n-j}\right]_{n,j=0,1\ldots}$ defines a Toeplitz matrix, and this is a necessary requirement for a successful transformation. First we need to extend the validity of (2.3.1) to negative indices n. This can be accomplished by rewriting it in the equivalent form

$$\sum_{j=-\infty}^{\infty} K_{n-j} A_j^+ = T_n^+ + T_n^-, \quad n \in \mathbb{Z}, \tag{2.3.2}$$

where A_n^+, T_n^+ are the two-sided extensions of A_n and T_n respectively with

$$A_n^+ = T_n^+ = 0, \quad \text{for} \quad n = -1, -2, \ldots, \tag{2.3.3}$$

T_n^- is an unknown, with

$$T_n^- = \sum_{j=0}^{\infty} K_{n-j} A_j, \quad \text{for} \quad n = -1, -2, \ldots, \tag{2.3.4}$$

and

$$T_n^- = 0, \quad \text{for} \quad n = 0, 1, \ldots. \tag{2.3.5}$$

Next, we assume that all the terms in (2.3.2) are members of the class $\mathscr{L}(C)$, i.e. they have a representation of the form (2.2.14). Using this integral representation for A_j^+, T_n^+ and T_n^- in the system (2.3.2) yields

$$\sum_{j=-\infty}^{\infty} K_{n-j} \oint_C A^+(z) z^{-j-1} dz = \oint_C \Big(T^+(z) + T^-(z) \Big) z^{-n-1} dz. \tag{2.3.6}$$

Now, if we re-index the sum by replacing j with $n - j$, and interchange the order of integration and summation in the left hand side of (2.3.6) we obtain the functional equation

$$K(z)A^+(z) = T^+(z) + T^-(z), \tag{2.3.7}$$

where the functions $K(z)$ and $T^+(z)$ are known and given by the $\mathcal{Z}$-transformation of K_n and T_n^+, respectively, and we seek to obtain the two unknown functions $A^+(z)$ and $T^-(z)$. It is not difficult to see that (2.3.7) has all the characteristics of a Wiener–Hopf equation. By assumption, all of its terms are functions analytic on C, and subsequently on this curve the equation holds. In particular, the superscript '+' indicates functions that are analytic in C^+, so that the condition (2.3.3) is satisfied. Likewise, the condition (2.3.5) dictates that the function $T^-(z)$ is analytic in C^-, with

$$T^-(z) \to 0 \qquad \text{as} \qquad z \to \infty. \,^{2} \tag{2.3.8}$$

[2] We will see in later sections that this is a necessary condition for carrying out the third step of the Wiener–Hopf technique. One must keep in mind that this is an immediate consequence of the fact that $T^-(z) = \mathcal{Z}(T_n^-)$ and (2.3.5).

The system (2.3.1) may be regarded as the discrete analogue of the Wiener–Hopf equation (2.3.7) and therefore an analytical solution is feasible. First we need to specify the closed curve C on which both the forward transforms $K(z) = \mathcal{Z}(K_n)$ and $T^+(z) = \mathcal{Z}(T_n^+)$ converge and are analytic, and also to substantiate the assumption (2.2.14) regarding their inverse. Second, we need to solve the corresponding Wiener–Hopf equation by following the procedure described in §2.1. Once we have determine $A^+(z)$ then the solution of the system (2.3.1) is given by

$$A_n = A_n^+ = \frac{1}{2\pi i} \oint_C A^+(z) z^{-n-1} dz, \quad n = 0, 1, \ldots. \tag{2.3.9}$$

This method of solution is often referred as the discrete Wiener–Hopf technique and sufficient conditions for a successful execution can be found in [8] (wherein the authors used the Fourier-transform).

2.4 Scattering by a semi-infinite grating of small cylinders

As an example on the application of the discrete Wiener–Hopf technique, we consider the problem of acoustic scattering by a semi-infinite grating of cylinders. The position vector of the j^{th} cylinder is $j\mathbf{a}_1$, $j = 0, 1, \ldots$, where without loss of generality we can assume that $\mathbf{a}_1 = (a_1, 0)$. Let the plane wave

$$u_{inc}(\mathbf{r}) = e^{i\mathbf{k}\cdot\mathbf{r}}, \quad \text{where} \quad \mathbf{k} = (k\cos\psi_0, k\sin\psi_0),$$

be incident upon the grating at an angle ψ_0, with $0 < \psi_0 < \pi$. We will assume that the cylinders are sound-soft and their radius ℓ is small compared to wavelength of the incident field. Hence, the total is given by

$$u(\mathbf{r}) = u_{inc}(\mathbf{r}) + \sum_{j=0}^{\infty} A_j H_0(k|\mathbf{r} - j\mathbf{a}_1|), \tag{2.4.1}$$

where A_j are the unknown amplitudes.

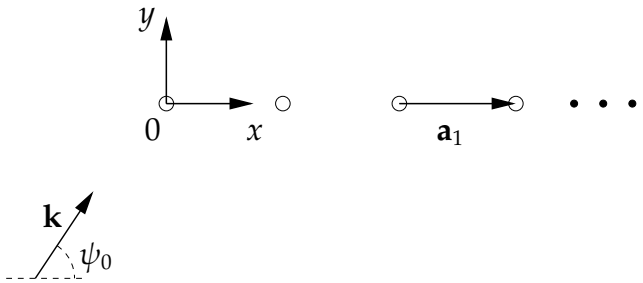

Figure 2.4: *Schematic diagram showing a section of the grating and the notation in use.*

2.4.1 Wiener–Hopf formulation

If we apply the boundary condition on the n^{th} cylinder by following the same formulation as for the infinite grating considered in §1.4.1, then the unknowns A_n are found to satisfy

$$A_n - f_0 \sum_{\substack{j=0 \\ j\neq n}}^{\infty} A_j H_0(ka_1|n-j|) = f_0 e^{in\mathbf{k}\cdot\mathbf{a}_1}, \quad n = 0, 1, \ldots. \tag{2.4.2}$$

This time there is no simple relation between the amplitudes A_n, and therefore a solution of the system (2.4.2) is required. This can be accomplished via the discrete Wiener–Hopf method. Note that (2.4.2) is of the form

$$\sum_{j=0}^{\infty} K_{n-j} A_j = T_n, \quad n = 0, 1, \ldots, \tag{2.4.3}$$

where $T_n = f_0 e^{in\mathbf{k}\cdot\mathbf{a}_1}$, and

$$K_j = \begin{cases} 1, & j = 0, \\ -f_0 H_0(ka_1|j|), & j \neq 0. \end{cases}$$

Next, we rewrite (2.4.3) as

$$\sum_{j=-\infty}^{\infty} K_{n-j} A_j^+ = T_n^+ + T_n^-, \quad n \in \mathbb{Z}, \tag{2.4.4}$$

where A_n^+, T_n^+ are the two-sided extensions of A_n and T_n respectively with $A_n^+ = T_n^+ = 0$, for $n = -1, -2, \ldots$, and T_n^- is equal to the left hand side of (2.4.3) for negative integers and zero otherwise. Now assuming that all the terms of the

system (2.4.4) are members of the class $\mathscr{Z}(C)$, we can transform it into the Wiener–Hopf equation

$$K(z)A^+(z) = T^+(z) + T^-(z), \quad z \in C, \tag{2.4.5}$$

where

$$K(z) = 1 - f_0 \sum_{\substack{j=-\infty \\ j\neq 0}}^{\infty} H_0(ka_1|j|)z^j, \tag{2.4.6}$$

and

$$T^+(z) = -\frac{f_0 p_0}{z - p_0}, \quad \text{with} \quad p_0 = e^{-ika_1\cos\psi_0}, \tag{2.4.7}$$

The '+' and '−' signs in (2.4.5) indicate analyticity in C^+ and C^-, respectively and this information will be used to obtain $A^+(z)$ and subsequently the unknown amplitudes from the integral

$$A_n = \frac{1}{2\pi i}\oint_C A^+(z)z^{-n-1}dz, \quad n = 0, 1, \ldots. \tag{2.4.8}$$

At this stage the only information we have about the closed curve C, where all the functions in (2.4.5) are assumed to be analytic, is that

$$0 \in C^+ - C, \quad \text{and} \quad p_0 \in C^- - C, \tag{2.4.9}$$

where the second condition is immediate consequence of the fact that $T^+(z)$ is analytic in C^+. In order to get a clearer picture of C we must examine where the sum in (2.4.6) converges. To simplify the procedure we let the wavenumber have a positive imaginary part $k = Re[k] + i\epsilon$, which is equivalent to allowing the medium surrounding the grating to have small loses. It is not difficult to see using (A.2.11), that this assumption ensures the convergence and analyticity of the kernel in the annulus

$$\mathcal{D} = \{z : \ e^{-\epsilon a_1} < |z| < e^{\epsilon a_1}\}. \tag{2.4.10}$$

Therefore, if we choose C to be a circle of radius r with $e^{-\epsilon a_1} < r < e^{\epsilon a_1\cos\psi_0}$, then both $K(z)$ and $T^+(z)$ are analytic on C and in addition the condition (2.4.9) is satisfied. We can also determine a neighbourhood of the origin in which

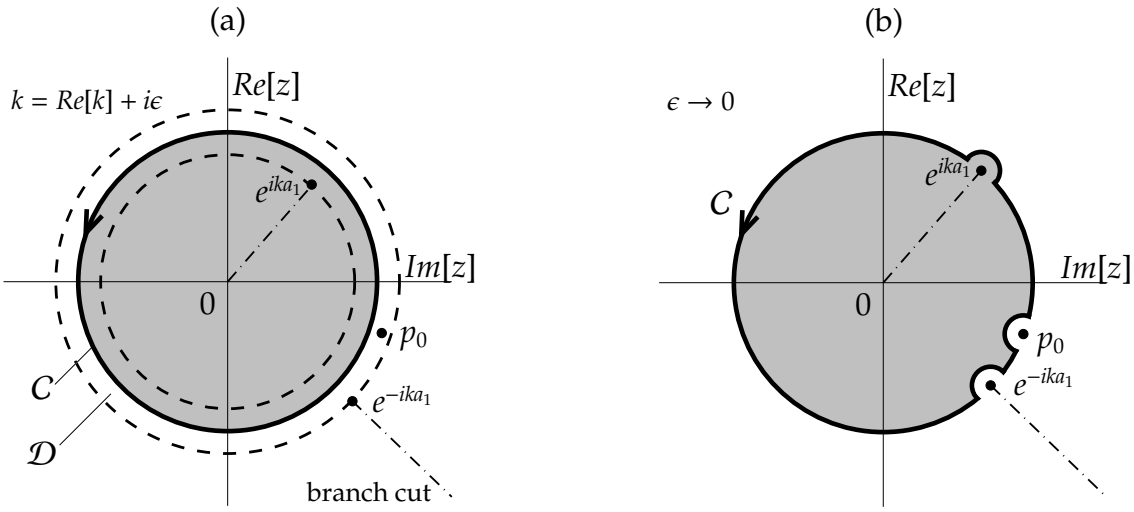

Figure 2.5: *The singularities of the kernel and $T^+(z)$ and the common curve of analyticity C for the case (a) where $k = Re[k] + i\epsilon$, and (b) taking the limit $\epsilon \to 0$. The shaded region represents C^+.*

$A^+(z)$ is analytic, by considering the behaviour of A_n as $n \to \infty$ using (2.4.8). If $0 < \psi_0 \leqslant \pi/2$, then the amplitude of the incident wave does not grow as the observer moves from left to right, and there must be no contributions to A_n from singularities of $A^+(z)$ in the region $|z| \leqslant 1$, because the magnitude of such contributions would grow as $n \to \infty$. On the other hand, if $\psi_0 > \pi/2$ then the incident field propagates to the left, and the overall field strength grows as the observer moves from left to right. Consequently, $|A_n| \to \infty$ as $n \to \infty$, but the growth rate can be no faster than that of the incident wave. In general,

$$\left|A_n e^{-inka_1 \cos\psi_0}\right| = \left|A_n e^{n\epsilon a_1 \cos\psi_0}\right|, \tag{2.4.11}$$

must remain bounded as $n \to \infty$, meaning that $A^+(z)$ is analytic in the region where $|z| < e^{\epsilon a_1 \cos\psi_0}$.

Allowing the wavenumber to have a small imaginary part is a standard mechanism that is used in scattering problems in order to ensure the absolute convergence of series of the form (2.4.6). At the end of the calculations we must take the limit $\epsilon \to 0$. To see how the kernel behaves in this limit note that

$$K(e^{ia_1 x}) = 1 - f_0\, \sigma_0^{(1)}(x), \tag{2.4.12}$$

where $\sigma_0^{(1)}(x)$ represents the 1D lattice sum given in (B.2.2). More generally, for $x = -i \log z/a_1$ we have

$$K(z) = 1 - f_0 \sigma_0^{(1)}(-i \log z/a_1). \tag{2.4.13}$$

The alternative representation (B.2.4) of $\sigma_0^{(1)}(\cdot)$ reveals that the kernel has branch points at $e^{\pm ika_1}$, 0 and ∞, and if we take branch cuts along $(0, e^{ika_1})$ and (e^{-ika_1}, ∞), as illustrated in figure 2.5 (a), then we can extend the analyticity of the kernel from $\mathcal{D}$ to the cut plane. We are now in the position to take the limit $\epsilon \to 0$, and to identify how C is deformed in this limit; see figure 2.5 (b).

2.4.2 The solution

The first fundamental step in order to apply the Wiener–Hopf technique is to find a factorisation

$$K(z) = K^+(z)K^-(z), \tag{2.4.14}$$

where $K^+(z)$ and $K^-(z)$ are analytic and zero free in C^+ and C^-, respectively. Assuming that it is possible to choose a branch of $\log K(z)$ that is continuous on C (see [7, §3.2]), the required factors can be obtained from Cauchy's integral formula (2.1.12)

$$K^\pm(z) = \exp\Big(\pm \frac{1}{2\pi i} \oint_C \frac{\log K(\zeta)}{\zeta - z} d\zeta \Big), \quad z \in C^\pm - C. \tag{2.4.15}$$

Although these representations are not valid on C, we can deform the contour of integration slightly (outwards or inwards) to make them analytic in the corresponding sets C^+ and C^-; see §2.2.1.

With this factorisation and in view of (2.4.7), the Wiener–Hopf equation (2.4.5) becomes

$$A^+(z)K^+(z) = -\frac{f_0 p_0}{K^-(z)(z - p_0)} + \frac{T^-(z)}{K^-(z)}. \tag{2.4.16}$$

It clear that the right-hand side of (2.4.16), is analytic in C^-, except at the point p_0, corresponding to a simple pole. We can move this pole to the other side by

adding the term $f_0 p_0/K^-(p_0)(z-p_0)$ to both sides, and this yields

$$A^+(z)K^+(z) + \frac{f_0 p_0}{K^-(p_0)(z-p_0)} = -\frac{f_0 p_0}{z-p_0}\Big(\frac{1}{K^-(z)} - \frac{1}{K^-(p_0)}\Big) + \frac{T^-(z)}{K^-(z)}. \tag{2.4.17}$$

Now the left-hand side of (2.4.17) is a function analytic in C^+, whereas the right-hand side is a function analytic in C^-. Using the customary Wiener–Hopf argument that there exists an entire function $J(z)$, which is the analytic continuation of both sides into the entire complex plane, and the fact that $J(z) \to 0$, as $z \to \infty$ (since from (2.3.8), the right-hand side of (2.4.17) tends to zero in this limit), we can conclude by Liouville's theorem that $J(z) = 0$, and consequently

$$A^+(z) = \frac{-f_0 p_0}{K^+(z)K^-(p_0)(z-p_0)}. \tag{2.4.18}$$

Hence,

$$A_n = -\frac{f_0 p_0}{2\pi i K^-(p_0)} \oint_C \frac{z^{-n-1}}{K^+(z)(z-p_0)} dz, \quad n = 0, 1, 2, \ldots. \tag{2.4.19}$$

Now, to calculate the amplitudes A_n, we expand the function $1/K^+(z)$ as a Taylor series

$$\frac{1}{K^+(z)} = \sum_{m=0}^{\infty} \lambda_m z^m, \quad z \in C^+. \tag{2.4.20}$$

The coefficients λ_m can be found with the aid of the integral representation (2.4.15). For example

$$\lambda_0 = \exp\Big(-\frac{1}{2\pi i}\oint_C \frac{\log K(z)}{z}\, dz\Big), \tag{2.4.21}$$

where, in order to compute $K(z)$ on the unit circle we use (2.4.12) and (B.2.4). For the others coefficients λ_m, $m = 1, 2, \ldots$, we set

$$\nu_m = -\frac{m!}{2\pi i}\oint_C \frac{\log K(z)}{z^{m+1}}\, dz, \quad \text{for} \quad m = 1, 2, \ldots, \tag{2.4.22}$$

and note that

$$\begin{aligned}
\lambda_1 &= \lambda_0 \nu_1 \\
\lambda_2 &= \frac{\lambda_0}{2!}(\nu_1^2 + \nu_2) \\
\lambda_3 &= \frac{\lambda_0}{3!}(\nu_1^3 + 3\nu_1\nu_2 + \nu_3) \\
\lambda_4 &= \frac{\lambda_0}{4!}(\nu_1^4 + 6\nu_1^2\nu_2 + 3\nu_2^2 + 4\nu_1\nu_3 + \nu_4) \\
&\ldots
\end{aligned}$$

Inserting the Taylor expansion (2.4.20) in (2.4.19), we obtain

$$A_n = -\frac{f_0 p_0}{K^-(p_0)} \sum_{m=0}^{\infty} \lambda_m \frac{1}{2\pi i} \oint_C \frac{z^{m-n-1}}{z - p_0} dz, \quad n = 0, 1, 2, \ldots. \tag{2.4.23}$$

The last integral is zero for $m > n$, whereas

$$\frac{1}{2\pi i} \oint_C \frac{z^{m-n-1}}{z - p_0} dz = -p_0^{m-n-1}, \quad \text{for} \quad m \leqslant n. \tag{2.4.24}$$

Hence,

$$A_n = \frac{f_0}{K^-(p_0)} \sum_{m=0}^{n} \lambda_m p_0^{m-n}, \quad n = 0, 1, 2, \ldots. \tag{2.4.25}$$

2.5 Literature

The problem of acoustic scattering by a semi-infinite grating of 'small' cylinders considered in the previous section was solved by Hills & Karp [16]. A more modern approach that can also be used to treat the semi-infinite strip grating is presented in [33], and much of the preceding analysis has been based on this text. In these papers one can find details regarding the analysis of the far field pattern and the resonance case. The ability to obtain the unknowns of an infinite system of equations in closed-form (see (2.4.25)), is crucial for studying the underlying physical problem in its entirety, and this highlights the advantages of employing the discrete Wiener–Hopf technique, against a numerical solution by truncation. The technique has been also used to study diffraction of electromagnetic waves by semi-infinite gratings; see for example [9], which contains a short review on the literature.

A number of boundary value problems involving structures with semi-infinite geometry have been solved via the Wiener–Hopf technique; see references in [24]. The classic example in the context of acoustic scattering theory is Sommerfeld's half-plane problem which can be found in several texts, notably [19, §1], [34, §5.1.1], [44, Ch. 2] and [63, Ch. 5]. In particular, the book by Noble [44] contains further examples (Ch. 3) and also a discussion regarding technical issues that might arise in applications of the Wiener–Hopf technique (Ch. 4, see

also [48, Ch. 3 & 4]). It is worth remarking that it is not always possible to find exact factorisations, which is a necessary step for the successful execution of the method. To overcome such difficulties approximation techniques are required. A discussion on this topic and examples of the use of Padé approximants for Wiener–Hopf factorisations is given in [1].

2.5.1 Matrix Wiener–Hopf equation

So far we have discussed about the solution of a single Wiener–Hopf equation (2.1.1). However, in some cases we need to deal with n functional equations with $2n$ unknown functions which can be written in terms of a matrix Wiener–Hopf equation

$$\mathbf{K}(z)\mathbf{A}^{+}(z) = \mathbf{T}^{+}(z) + \mathbf{T}^{-}(z). \tag{2.5.1}$$

Assuming that this equation holds on a closed curve C, the kernel $\mathbf{K}(z)$ is an $n \times n$ matrix containing functions analytic on C. The other terms represent $n \times 1$ matrices and as before the '+' and '−' signs indicate that they contain functions analytic in C^{+} and C^{-}, respectively.

The procedure for the solution of (2.5.1) is as described in §2.1, but this time the factorisation of the kernel

$$\mathbf{K}(z) = \mathbf{K}^{-}(z)\mathbf{K}^{+}(z), \tag{2.5.2}$$

is performed so that the determinant of each matrix $\mathbf{K}^{\pm}(z)$, must be zero free in the respective region of analyticity $C^{\pm}$. Gohberg & Krein [14] proved the existence of the factorisation (2.5.2) for an arbitary matrix $\mathbf{K}(z)$, but no general method has yet been developed for constructing such decompositions Nevertheless, for certain classes of matrices standard procedures have been devised, see for example [3] (for rational matrices), [20], and [59]. The latter also contains a discussion on the strengths and weaknesses of various methods that have been used so far.

We also remark that one of the main advantages of the Wiener–Hopf tech-

nique is its flexibility. The systematic procedure described in §2.1 may be subjected to modifications so that it can been adjusted to solve a variety of different problems. For example, in Chapter 4 where we need to deal with a matrix Wiener–Hopf equation we will present a solution which does not require the explicit factorisation of the kernel.

Chapter 3

Scattering by a semi-infinite lattice of small cylinders

In this chapter we consider the problem of acoustic scattering by a semi-infinite lattice of sound-soft cylinders [1]. We restrict ourselves to cases where the radius of the cylinders is small compared to the wavelength of the incident field. This assumption simplifies the representation of the scattered field, and in §3.1 we present the details of how the formulation leads to an infinite system of algebraic equations. The system is then transformed into a Wiener–Hopf equation and an outlined sketch of its solution is given in §3.2.

In §3.3 we examine the physical and mathematical nature of the kernel. It turns out that it can be written as an infinite sum of partial fractions and it has an infinite number of poles, with associated nonisolated essential singularities at the origin and at infinity. One way to factorise such a function is to represent it as an infinite product; see e.g. [25]. A different approach will be considered here which relies on the truncation of the infinite sum. In physical terms, such an approximation can be justified on the grounds of disregarding interaction effects due to strongly damped modes. The kernel is thereby replaced by a ra-

[1] The material of this chapter has been published in the Quarterly Journal of Mechanics and Applied Mathematics; see [58].

tional function, which is easily factorised. The explicit solution to the scattering problem is then given in §3.4.

The structure of the scattered field is examined in §3.5. Initially we consider the situation in which the problem parameters reside in a band gap so that no waves can propagate through the lattice. We then consider the more physically interesting case in which some of the incident field energy propagates through the lattice in the form of a Bloch wave. Plots of the reflected coefficient are presented which implicitly illustrate pass band and band gap phenomena.

Finally, a useful check on our numerical results is provided by the principle of conservation of energy, and this is considered in §3.6. For cases where no Bloch waves are excited, we obtain a simple identity, and show that this is always satisfied. The presence of Bloch waves in the solution leads to a more complicated identity, which involves terms that must be computed numerically. Our calculations indicate that this is always satisfied to a high degree of accuracy.

3.1 Formulation

Let $\mathbf{a}_1$ and $\mathbf{a}_2$ be a linearly independent pair of vectors in the (x, y) plane. Suppose that sound-soft cylinders of radius ℓ are centred at the points with position vectors

$$\mathbf{R}_{jp} = j\mathbf{a}_1 + p\mathbf{a}_2, \tag{3.1.1}$$

where $j \in \mathbb{Z}$ and $p = 0, 1, \ldots$, thus forming a semi-infinite lattice (see figure 3.1). Without loss of generality, we can assume that

$$\mathbf{a}_1 = (a_1, 0) \quad \text{and} \quad \mathbf{a}_2 = (\eta_1, \eta_2), \tag{3.1.2}$$

where $\eta_2 > 0$. Let the plane wave

$$u_{inc}(\mathbf{r}) = e^{i\mathbf{k}\cdot\mathbf{r}} \tag{3.1.3}$$

be incident upon the lattice, where the wavenumber vector is given by

$$\mathbf{k} = (k\cos\psi_0,\, k\sin\psi_0), \quad \psi_0 \in (0, \pi). \tag{3.1.4}$$

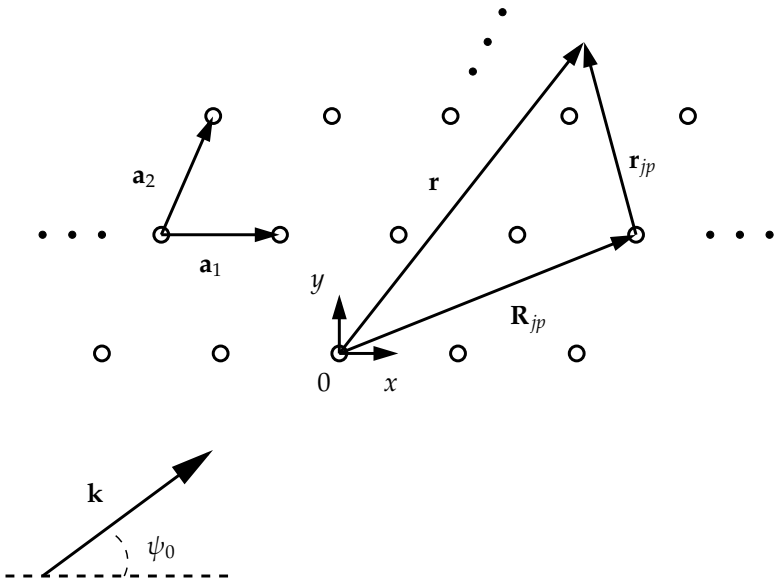

Figure 3.1: *Schematic diagram showing a section of the lattice, and illustrating the notation in use.*

We consider the case where the wavelength of the incident field is assumed to be greater than the cylinders' radii; in particular

$$k\ell \ll 1. \tag{3.1.5}$$

In this regime, the elements of the lattice may be considered to be isotropic point scatterers (see §1.2.4), and so the total field can be represented in the form

$$u(\mathbf{r}) = u_{inc}(\mathbf{r}) + \sum_{p=0}^{\infty}\sum_{j=-\infty}^{\infty} A_{jp}H_0(k|\mathbf{r}_{jp}|), \tag{3.1.6}$$

where $\mathbf{r}_{jp}$ is a position vector relative to the centre of scatterer (j,p), i.e.

$$\mathbf{r}_{jp} = \mathbf{r} - \mathbf{R}_{jp}. \tag{3.1.7}$$

Our ultimate goal is to obtain the scattered field by determining the unknown amplitude coefficients A_{jp}. To begin this process, we must apply the boundary condition on the scatterers' surfaces. Now the field that is incident on a particular cylinder, centred at $\mathbf{r} = \mathbf{R}_{mn}$, say, consists of the incident wave, plus the contributions radiating from all of the other scatterers. That is

$$u^{mn}_{inc}(\mathbf{r}) = u_{inc}(\mathbf{r}) + \sum_{p=0}^{\infty}\sum_{j=-\infty}^{\infty} (1-\delta_{jm}\delta_{pn})A_{jp}H_0(kr_{jp}), \tag{3.1.8}$$

where δ_{jp} represents Kronecker's delta, i.e. 1 when $j = p$ and 0 otherwise. On the other hand, the scattered response from this cylinder is simply given by

$$u_{sc}^{mn}(\mathbf{r}) = A_{mn} H_0 \left(k r_{mn}\right). \tag{3.1.9}$$

Now, bearing in mind that u_{inc}^{mn} is the field incident upon the cylinder (m, n) we can use the the asymptotic approximation (1.2.20) to obtain

$$u_{sc}^{mn}(\mathbf{r}) \simeq f_0 u_{inc}^{mn}\left(\mathbf{R}_{mn}\right) H_0(k|\mathbf{r}_{mn}|), \tag{3.1.10}$$

where f_0 is given in (1.2.21). Hence,

$$A_{mn} = f_0 u_{inc}^{mn}\left(\mathbf{R}_{mn}\right), \tag{3.1.11}$$

and by using (3.1.8) for $\mathbf{r} = \mathbf{R}_{mn}$, we obtain the infinite system of algebraic equations

$$A_{mn} - f_0 \sum_{p=0}^{\infty} {\sum_{j=-\infty}^{\infty}}' A_{jp} H_0(k R_{j-m,p-n}) = f_0 e^{i\mathbf{k}\cdot\mathbf{R}_{mn}}, \quad m \in \mathbb{Z},\ n = 0, 1, \ldots. \tag{3.1.12}$$

Here, and henceforth, the prime on the summation symbol is used to indicate that the term in which the argument of the Hankel function vanishes (in this case $(j, p) = (m, n)$) is to be omitted from the series.

Due to the periodicity of the geometry, the only difference between the total field at the point $\mathbf{r}$ and that at $\mathbf{r} + m\mathbf{a}_1$ for integer m is the phase shift due to the incident wave, i.e.

$$u(\mathbf{r} + m\mathbf{a}_1) = e^{im\mathbf{k}\cdot\mathbf{a}_1} u(\mathbf{r}) = e^{imka_1 \cos\psi_0} u(\mathbf{r}). \tag{3.1.13}$$

Hence, we seek a solution with the property that

$$A_{mn} = \mathrm{e}^{\mathrm{i}mka_1 \cos\psi_0} A_{0n}, \quad m \in \mathbb{Z}. \tag{3.1.14}$$

Using this in (3.1.12), and then replacing j with $j + m$, we obtain the reduced system

$$A_{0n} - f_0 \sum_{p=0}^{\infty} {\sum_{j=-\infty}^{\infty}}' A_{0p} e^{ijka_1 \cos\psi_0} H_0(k R_{j,p-n}) = f_0 e^{in\mathbf{k}\cdot\mathbf{a}_2}, \quad n = 0, 1, \ldots \tag{3.1.15}$$

Note that it may turn out that the double series in (3.1.15) does not converge absolutely and therefore we need to specify how this sum should be interpreted. This is addressed in appendix B.1.3. For later convenience we multiply the system (3.1.15) with if_0^{-1} and rewrite it in the form

$$-if_0^{-1}A_{0n} + i\sum_{p=0}^{\infty} A_{0p}\mathcal{S}_{n-p} = -ie^{in\mathbf{k}\cdot\mathbf{a}_2}, \quad n = 0, 1, \ldots. \tag{3.1.16}$$

where

$$\mathcal{S}_0 = \sum_{\substack{j=-\infty \\ j\neq 0}}^{\infty} e^{ijka_1\cos\psi_0} H_0(kR_{j,0}), \tag{3.1.17}$$

and

$$\mathcal{S}_n = \sum_{j=-\infty}^{\infty} e^{ijka_1\cos\psi_0} H_0(kR_{j,-n}), \qquad n \in \mathbb{Z} - \{0\}. \tag{3.1.18}$$

The series $\mathcal{S}_n$ can be converted into a more practically useful form in terms of the scattering angles ψ_j, which are defined in (B.1.12). First note that (see appendix B.2.1)

$$\mathcal{S}_0 = \sigma_0^{(1)}(k\cos\psi_0), \tag{3.1.19}$$

where $\sigma_0^{(1)}$ is a 1D lattice sum, and its spectral representation is given in (B.2.5). On the other hand,

$$\mathcal{S}_n = G_0^{(1)}(n\mathbf{a}_2, k\cos\psi_0), \quad \text{for} \quad n \neq 0, \tag{3.1.20}$$

where $G_0^{(1)}$ is the 1D quasi-periodic Green's function defined in (B.1.19). An alternative representation for this function is given in (B.1.23), which yields

$$\mathcal{S}_n = \frac{2}{ka_1}\sum_{j=-\infty}^{\infty} \frac{1}{\sin\psi_j} e^{ik(n\eta_1\cos\psi_j + |n|\eta_2\sin\psi_j)}, \quad n \neq 0. \tag{3.1.21}$$

Equivalently,

$$\mathcal{S}_n = \frac{2}{ka_1}\sum_{j=-\infty}^{\infty} \frac{p_j^{-n}}{\sin\psi_j}, \quad \text{for} \quad n > 0, \tag{3.1.22}$$

and

$$\mathcal{S}_n = \frac{2}{ka_1}\sum_{j=-\infty}^{\infty} \frac{\tau_j^{n}}{\sin\psi_j}, \quad \text{for} \quad n < 0. \tag{3.1.23}$$

where the points p_j and τ_j are defined in (B.1.16). For future convenience we assume that

$$ka_1 < \pi, \tag{3.1.24}$$

in order to have that (see (B.1.17), and (B.1.18)),

$$|p_0| = |\tau_0| = 1, \tag{3.1.25}$$

and

$$p_j^* = \tau_j, \quad \text{for} \quad j \neq 0. \tag{3.1.26}$$

3.2 The discrete Wiener-Hopf method

We now look to solve the system (3.1.16) analytically, via the discrete Wiener–Hopf technique as in §2.3. We begin by setting

$$A_{0n} = 0, \quad \text{for} \quad n < 0 \tag{3.2.1}$$

so that the system of equations can be written in the form

$$\sum_{p=-\infty}^{\infty} K_{n-p} A_{0p} = T_n^+ + T_n^-, \quad n \in \mathbb{Z}, \tag{3.2.2}$$

where

$$T_n^+ = \begin{cases} -ip_0^{-n}, & n \geqslant 0, \\ 0, & n < 0, \end{cases} \qquad T_n^- = \begin{cases} 0, & n \geqslant 0, \\ \sum_{p=0}^{\infty} K_{n-p} A_{0p}, & n < 0, \end{cases} \tag{3.2.3}$$

and

$$K_n = \begin{cases} -if_0^{-1} + i\mathcal{S}_0, & n = 0, \\ i\mathcal{S}_n, & n \neq 0. \end{cases} \tag{3.2.4}$$

Assuming that all the double-sided sequences in (3.2.2) are members of the class $\mathscr{Z}(C)$, we can transform (3.2.2) into the Wiener–Hopf equation

$$K(z)A^+(z) = T^+(z) + T^-(z), \quad z \in C, \tag{3.2.5}$$

where C is a closed curve that encircles the origin. In this equation the kernel and the function $T^+(z)$ are given by $\mathcal{Z}(K_n)$ and $\mathcal{Z}(T_n^+)$, respectively and we seek

to determine the functions $A^+(z)$ and $T^-(z)$. As is customary in this text, the '+' and '−' signs indicate analyticity in the corresponding sets C^+ and C^-, where C^+ consists of all the points that lie inside and on C, and C^- consists of all the points that lie outside and on C.

Before we set out to solve the Wiener–Hopf equation, a few remarks are in order regarding the shape of the closed curve C. We could proceed by letting the wave number have a small imaginary part as in §2.4, and then look for a circle of radius r where all the terms in (3.2.5) are analytic. However, this method is not well suited to this problem, because it turns out that r is dependent on the angle of incidence ψ_0 and the geometry of the lattice, and this makes the argumentation more complex. In addition the important symmetry relation (3.3.7) breaks down if k is not real. For these reasons, we will instead specify C by determining the positions of singularities of the functions $K(z)$ and $T^+(z)$ relative to C. For the function $T^+(z)$, it is an easy matter to check that for $|z| < 1$

$$T^+(z) = \frac{ip_0}{z - p_0}, \tag{3.2.6}$$

where the expression on the right-hand side has been obtained by summing a geometric series. In other words the function $T^+(z)$ can be analytically continued into the entire complex plane except for the point p_0, where it has a simple pole. Now, since this function is analytic in C^+, we must have

$$p_0 \in C^- - C. \tag{3.2.7}$$

A similar analysis for the kernel will give all the information required for C, and it is deferred until the next section.

Now, in order to solve (3.2.5), we need to factorize the kernel into a product of the form

$$K(z) = K^+(z)K^-(z), \tag{3.2.8}$$

where $K^+(z)$ and $K^-(z)$ have no zeros in their respective regions of analyticity C^+ and C^-. With this factorisation and in view of (3.2.6), equation (3.2.5) becomes

$$K^+(z)A^+(z) = \frac{ip_0}{(z - p_0)K^-(z)} + \frac{T^-(z)}{K^-(z)}. \tag{3.2.9}$$

The right hand side of this equation is analytic in C^-, except at the point p_0, where it has a simple pole. This pole can be moved to other side with a simple subtraction, that is

$$K^+(z)A^+(z) - \frac{ip_0}{(z-p_0)K^-(p_0)} = \frac{ip_0}{z-p_0}\Big(\frac{1}{K^-(z)} - \frac{1}{K^-(p_0)}\Big) + \frac{T^-(z)}{K^-(z)}. \tag{3.2.10}$$

We have now reached an equation whose left hand side is analytic in C^+ and the right hand side is analytic in C^-. Since the equation holds on C, we can conclude that there exists an entire function $J(z)$ which is the analytic continuation of each side into the entire complex plane. It is clear that this function vanishes in the limit $z \to \infty$ (see (2.3.8) and note that $K^-(z)$ is analytic at infinity), and therefore from Liouville's theorem we have $J(z) = 0$. Thus,

$$A^+(z) = \frac{ip_0}{K^-(p_0)(z-p_0)K^+(z)}, \tag{3.2.11}$$

and

$$T^-(z) = \frac{-ip_0}{z-p_0}\Big(1 - \frac{K^-(z)}{K^-(p_0)}\Big). \tag{3.2.12}$$

3.3 The kernel and its approximate factorisation

In this section we examine the physical and mathematical nature of the kernel with the aim to obtain an approximate factorisation. First we need to specify the form of the kernel in the $\mathcal{Z}$-transformed domain. This can be accomplished through the process of analytic continuation if we separate negative and positive powers of z, i.e. we write

$$K(z) = -if_0^{-1} + i\mathcal{S}_0 + i\sum_{n=1}^{\infty}\mathcal{S}_n z^n + i\sum_{n=1}^{\infty}\mathcal{S}_{-n}z^{-n}, \tag{3.3.1}$$

which in view of (3.1.22), and (3.1.23) becomes

$$K(z) = -if_0^{-1} + i\mathcal{S}_0 + \frac{2i}{ka_1}\sum_{n=1}^{\infty}\sum_{j=-\infty}^{\infty}\frac{(p_j^{-1}z)^n}{\sin\psi_j} + \frac{2i}{ka_1}\sum_{n=1}^{\infty}\sum_{j=-\infty}^{\infty}\frac{(\tau_j z^{-1})^n}{\sin\psi_j}. \tag{3.3.2}$$

Now, we sum the two infinite series in (3.3.2) in their respective region of convergence and obtain

$$K(z) = -if_0^{-1} + i\mathcal{S}_0 - \frac{2i}{ka_1}\sum_{j=-\infty}^{\infty}\frac{1}{\sin\psi_j}\Big(\frac{z}{z-p_j} - \frac{1}{\tau_j z - 1}\Big). \tag{3.3.3}$$

It is clear from the last formula that the kernel has infinitely many poles located at the points at p_j and τ_j^{-1}, and two nonisolated essential singularities at zero and infinity.

The representation (3.3.3) can also help us to specify the position of the singularities of the kernel relative to C. Note that in order to formulate the problem in the $\mathcal{Z}$–transformed domain we assumed that $K_n \in \mathscr{Z}(C)$, i.e.

$$K_n = \frac{1}{2\pi i} \oint_C K(z) z^{-n-1} dz, \qquad n \in \mathbb{Z}. \tag{3.3.4}$$

and in view of (3.2.4), (3.1.22), and (3.1.23) this is a valid representation if and only if

$$p_j \in C^- - C, \quad \text{and} \quad \tau_j^{-1} \in C^+ - C, \quad \forall j \in \mathbb{Z}, \tag{3.3.5}$$

which is in agreement with the condition (3.2.7).

3.3.1 Symmetry

The kernel has important symmetry properties that are not immediately apparent. In the case of a rectangular lattice, where $\eta_1 = 0$, we have $\tau_j = p_j$, meaning that $K(1/z) = K(z)$. More generally, if we write f_0 and $\mathcal{S}_0$ explicitly using (1.2.21) and (B.2.5), then, after some algebra, we find that

$$K(z) = \frac{2}{\pi} \ln\left(\frac{a_1}{2\pi\ell}\right) + \sum_{\substack{j=-\infty \\ j\neq 0}}^{\infty} \left(\frac{2i}{ka_1 \sin\psi_j} - \frac{1}{|j|\pi}\right) - \frac{(2i/ka_1)(\tau_0 p_0 - 1)z}{\sin\psi_0 (z - p_0)(\tau_0 z - 1)} - \sum_{\substack{j=-\infty \\ j\neq 0}}^{\infty} \frac{2i}{ka_1 \sin\psi_j} \left(\frac{z}{z - p_j} - \frac{1}{\tau_j z - 1}\right). \tag{3.3.6}$$

From this expression and the conditions (3.1.25), and (3.1.26) we can conclude that

$$K^*(1/z^*) = K(z). \tag{3.3.7}$$

3.3.2 Approximate factorisation

We now introduce an approximate kernel by truncating the second sum over j in (3.3.6). The physical meaning of this approximation is important, and can be understood as follows. We begin by noting that if we define

$$\boldsymbol{\beta}(z) = (k\cos\psi_0, \lambda(z)) \quad \text{with} \quad \lambda(z) = \frac{i\log z - \eta_1 k\cos\psi_0}{\eta_2}. \tag{3.3.8}$$

then

$$e^{i\mathbf{R}_{jn}\cdot\boldsymbol{\beta}(z)} = e^{ijka_1\cos\psi_0}\, z^{-n}. \tag{3.3.9}$$

Hence, using the definition of $\mathcal{S}_n$ (3.1.17) and (3.1.18) in (3.3.1), we obtain

$$K(z) = -if_0^{-1} + i\sum_{n=-\infty}^{\infty}{\sum_{j=-\infty}^{\infty}}' e^{i\mathbf{R}_{jn}\cdot\boldsymbol{\beta}(z)} H_0(kR_{jn}), \tag{3.3.10}$$

i.e. the kernel can be expressed in the form of a two-dimensional lattice sum, representing the effect at the origin of sources at all other lattice points, the complex amplitude of the source located at $\mathbf{r} = \mathbf{R}_{jn}$ being $e^{i\mathbf{R}_{jn}\cdot\boldsymbol{\beta}(z)}$. Using the alternative representation (B.2.11) in (3.3.10) we can retrieve (3.3.3) and subsequently (3.3.6). Note that (B.2.11) originates from the the spectral representations of the quasi-periodic functions G_0^+ and G_0^- (see appendix B.1.3) and this observation can clarify the physical meaning of the infinite sum in (3.3.3). It describes the interactions between distinct rows of scatterers, and the representations (B.1.32) and (B.1.33) show that these interactions are caused by an infinite sum of modes (exponential solutions to the Helmholtz equation) propagating between the rows. However, all but one of these modes is evanescent, and the rate of decay increases rapidly with the modulus of the summation index j. Thus, in truncating this sum, we are discarding interaction effects due to strongly damped modes, and in fact this amounts to a standard method for treating scattering by multiple linear arrays [4, 42]. On the other hand, the first sum over j in (3.3.6) originates from the one-dimensional lattice sum $\sigma_0^{(1)}$, and describes the interactions between the scatterers within each row. Now the

approximate kernel

$$K_\nu(z) = \frac{2}{\pi}\ln\left(\frac{a_1}{2\pi\ell}\right) + \sum_{\substack{j=-\infty \\ j\neq 0}}^{\infty}\left(\frac{2i}{ka_1\sin\psi_j} - \frac{1}{|j|\pi}\right) - \frac{(2i/ka_1)(\tau_0 p_0 - 1)z}{\sin\psi_0(z-p_0)(\tau_0 z - 1)} - \sum_{\substack{j=-\nu \\ j\neq 0}}^{\nu}\frac{2i}{ka_1\sin\psi_j}\left(\frac{z}{z-p_j} - \frac{1}{\tau_j z - 1}\right), \quad (3.3.11)$$

is a rational function with simple poles at the points $z = p_0$, $z = 1/\tau_0$, $z = p_j$ and $z = 1/\tau_j$, $j = \pm 1, \pm 2, \ldots, \pm\nu$, which also satisfies the symmetry relation (3.3.7). Taking the limit $z \to \infty$, we find that

$$K_\nu(z) \to C_\nu, \quad (3.3.12)$$

where

$$C_\nu = \frac{2}{\pi}\left(\ln\left(\frac{a_1}{2\pi\ell}\right) - \sum_{j=1}^{\nu}\frac{1}{j}\right) + \sum_{|j|>\nu}\left(\frac{2i}{ka_1\sin\psi_j} - \frac{1}{|j|\pi}\right). \quad (3.3.13)$$

Note that C_ν is real, and by choosing ν to be sufficiently large, we can always ensure that it is nonzero. This being the case, if we write

$$K_\nu(z) = P_\nu(z)\prod_{j=-\nu}^{\nu}\frac{1}{(z-p_j)(z-1/\tau_j)}, \quad (3.3.14)$$

where $P_\nu(z)$ is a polynomial, then C_ν represents its leading coefficient. Hence we can conclude that $K_\nu(z)$ has exactly $4\nu + 2$ zeros. Initially, we will assume that there are no zeros that lie on the unit circle; later we will show how the theory can be adjusted to account for this case.

Now the symmetry relation (3.3.7) shows that there are $2\nu + 1$ zeros outside the unit circle located at the points $z = z_j$, $j = -\nu, \ldots, \nu$, say, and an equal number of zeros inside the unit circle, located at the points $z = 1/z_j^*$. The actual values of z_j must be determined numerically from (3.3.11). However, we can determine the locations of the zeros of $K_\nu(z)$ relative to the inversion contour C by considering their implications for the behaviour of A_{0n} as $n \to \infty$. Equation (3.2.11) shows that a zero of $K_\nu^+(z)$ corresponds to a pole of $A^+(z)$. Moreover, all of the poles of $A^+(z)$ must lie in the region where $|z| \geq 1$, or else the coefficients A_{0n}

grow exponentially as $n \to \infty$, which is unphysical. Hence, the points $z = 1/z_j^*$, $j = -\nu, \ldots, \nu$ must be zeros of $K_\nu^-(z)$. Now, the condition (3.3.5) implies that $K_\nu^-(z)$ has $2\nu + 1$ poles at the points τ_j^{-1}, and since this function must also be analytic and zero free at infinity, we can conclude that it can not possess any other zeros besides $z = 1/z_j^*$. Therefore, the remaining points $z = z_j$ must be zeros of $K_\nu^+(z)$. To summarise we have the following condition

$$z_j \in C^- - C, \quad \text{and} \quad 1/z_j^* \in C^+ - C, \quad \text{for} \quad j = -\nu, \ldots, \nu \tag{3.3.15}$$

and the factorisation of the approximate kernel may now be expressed as

$$K_\nu^+(z) = C_\nu \prod_{j=-\nu}^{\nu} \frac{z - z_j}{z - p_j}, \tag{3.3.16}$$

and

$$K_\nu^-(z) = \prod_{j=-\nu}^{\nu} \frac{z - 1/z_j^*}{z - 1/\tau_j}. \tag{3.3.17}$$

Note that the factors are related via

$$\left[\frac{K_\nu^+(1/z^*)}{K_\nu^+(0)}\right]^* = \frac{z - 1/\tau_0}{z - p_0} K_\nu^-(z), \tag{3.3.18}$$

which means that

$$(z - p_0)(z - 1/\tau_0) K_\nu(z) = \frac{(z - p_0)^2}{[K_\nu^+(0)]^*} \left|K_\nu^+(z)\right|^2, \quad |z| = 1, \tag{3.3.19}$$

because in this case $1/z^* = z$.

Next consider the case in which the approximate kernel $K_\nu(z)$ has N zeros on the unit circle. The symmetry relation dictates that N is an even number. Thus, suppose that $N = 2$, for example

$$K_\nu(z_0) = K_\nu(z_0') = 0, \quad \text{with} \quad |z_0| = |z_0'| = 1. \tag{3.3.20}$$

As before, the zeros $1/z_j^*$, $j = -\nu, \ldots, -1, 1, \ldots, \nu$ located inside the unit circle are zeros of $K_\nu^-(z)$, and since this function must be analytic and zero free at infinity, it should posses only one additional zero. For rectangular or hexagonal ($a_1 = 2\eta_1$) lattices we can prove that this zero should be located on the unit circle. If we suppose on the contrary that it lies outside the unit circle, then $K^+(z)$ must have

two zeros on the unit circle, which in turn implies that $A^+(z)$ must have two poles on the unit circle. These points are z_0 and $z_0' = 1/z_0$, and we will see in §3.5.2 that they correspond to the existence of two Bloch waves propagating through the lattice. It is not difficult to see that the y-component of the group velocity [18, eq. 23] of these two waves differs only by sign, meaning that one of them is incoming and the other is outgoing. Clearly the first one violates the radiation condition at infinity and therefore we can conclude that the function $A^+(z)$ should have only one pole on the unit circle. In other words, the zeros of the kernel that are on the unit circle should be shared between the approximate factors. The last statement is assumed to be valid for skewed lattices as well, since we have not encountered situations in which the numerical calculations have suggested otherwise. Now, we may assume without loss of generality that

$$K_\nu^+(z_0) = 0, \quad K_\nu^-(z_0') = 0, \quad \text{and} \quad K_\nu^+(z_0')K_\nu^-(z_0) \neq 0. \tag{3.3.21}$$

Given a pair of zeros on the unit circle, determining which to treat as z_0 and which to treat as z_0' is not straight forward; we will return to this matter in §3.5.2 and §3.6. Note that the locations of z_0 and z_0' are not necessarily related to each other, but (3.3.7) still holds because on the unit circle we have $z = 1/z^*$. Therefore the form of $K_\nu^-(z)$ must be changed slightly; in fact

$$K_\nu^-(z) = \frac{z - z_0'}{z - 1/\tau_0} \prod_{\substack{j=-\nu \\ j\neq 0}}^{\nu} \frac{z - 1/z_j^*}{z - 1/\tau_j}, \tag{3.3.22}$$

whereas K_ν^+ is still given by (3.3.16). The relationship between the two factors (3.3.18) must be also be adjusted (a multiplicative factor $(z - z_0)/(z - z_0')$ must be introduced to the right-hand side), and so in place of (3.3.19), we now have

$$(z - p_0)(z - 1/\tau_0)K_\nu(z) = \frac{(z - p_0)^2(z - z_0')}{[K_\nu^+(0)]^*(z - z_0)} \left|K_\nu^+(z)\right|^2, \quad |z| = 1. \tag{3.3.23}$$

Finally, note that z_0 and z_0' may actually coincide with each other, in which case K_ν^+ and K_ν^- share a common zero. However, this situation is not problematic, because the expressions obtained for $A^+(z)$ (3.2.11) and $T^-(z)$ (3.2.12) remain valid. In particular, such a point is a pole of $A^+(z)$, but is neither a pole nor a zero of $T^-(z)$, and must therefore lie outside the contour C.

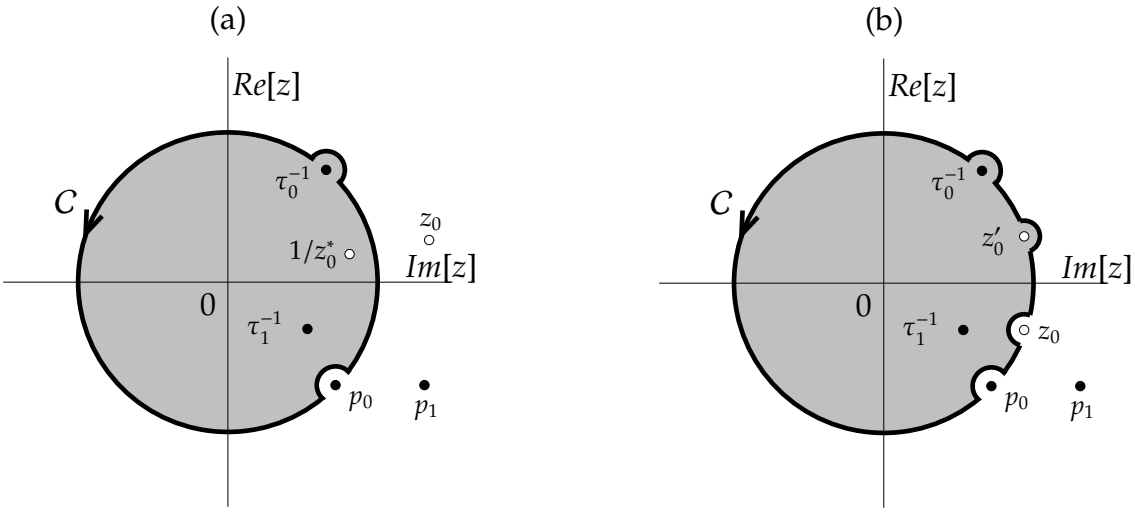

Figure 3.2: *Schematic diagram illustrating the possible situations in the z plane. The black disks are poles of K(z), and the white disks represent zeros; (a) shows the case where there K(z) has no zeros on the unit circle, whereas there is one pair of these in (b). Functions with a superscript '+' ('−') are analytic in the (un)shaded region.*

3.4 Explicit solution

Having determined the factorization of the kernel, we can substitute (3.3.16) in (3.2.11) and obtain

$$A^+(z) = \frac{ip_0}{C_\nu K_\nu^-(p_0)(z-z_0)} \prod_{\substack{j=-\nu \\ j\neq 0}}^{\nu} \frac{z-p_j}{z-z_j}, \tag{3.4.1}$$

and the amplitudes can now be calculated from the integral

$$A_{0n} = \frac{1}{2\pi i} \oint_C A^+(z)\, z^{-n-1}\, dz. \tag{3.4.2}$$

The contour of integration may be chosen to be the unit circle indented so as to include the pole at $z = 1/\tau_0$ and exclude the pole at $z = p_0$ (see figure 3.2(a)), and further indentations are required in the case where the kernel has zeros on the unit circle (see figure 3.2(b)). Clearly (3.4.2) evaluates to zero for $n < 0$; otherwise A_{0n} can be calculated by collecting the residues from the poles[2] outside C (see

[2]for simplicity we assume that z_m are distinct, so that the poles are simple.

[64, p. 380]), that is

$$A_{0n} = -\sum_{m=-\nu}^{\nu} z_m^{-n-1}\rho_m, \quad n = 0, 1, \ldots. \tag{3.4.3}$$

with

$$\rho_m = \operatorname*{Res}_{z=z_m} A^+(z) = \frac{ip_0}{C_\nu K_\nu^-(p_0)} \prod_{j=-\nu}^{\nu} \frac{(z_m - p_j)^{(1-\delta_{j0})}}{(z_m - z_j) + \delta_{jm}}. \tag{3.4.4}$$

3.4.1 Remarks

An important question regarding our method of solution is what value should be assigned to the approximation parameter ν in order to obtain results of high accuracy. From (3.4.3) it is evident that the amplitudes depend on the zeros of the approximate kernel that lie outside the closed curve C, and the leading order behaviour comes from the zero that is either on, or closest to the unit circle. Let w_ν be that zero for a given parameter ν. If

$$w_\nu \to w \quad \text{as} \quad \nu \to \infty, \tag{3.4.5}$$

for some point w, then $K(w) = 0$. In table 3.1, we give results that confirm (3.4.5), and it appears that a small value of ν is sufficient to provide a good approximation of w by w_ν.

The rate of convergence of the infinite sum in (3.3.6) depends on the exponential growth rate of the poles p_j and τ_j which in turn depends on the parameters ka_1 and $k\eta_2$ (see (B.1.16) and (B.1.12)). In particular, the rate of convergence of the kernel is increased in cases where either ka_1 is fixed and $k\eta_2$ is increased, or $k\eta_2$ is fixed and ka_1 is decreased. In physical terms, as we pointed out in the beginning of §3.3.2, the effect of approximating the kernel is to take into account some (2ν) evanescent modes who play significant role in the interaction effects between distinct rows, and discard the rest as strongly damped modes. A large value of $k\eta_2$ in effect means that the distance (in wavelengths) the evanescent modes have to travel before they interact with the next row is large and consequently when they do reach the next row they are considerably weakened. The

Table 3.1: *The value of the zero of the approximate kernel w_ν, which is either on, or closest to the unit circle, for different values of ν, ka_1 and $k\eta_2$. The parameters in use are $\psi_0 = \pi/6$, $\ell = 0.05$, and $\eta_1 = 0$.*

a_1	k	η_2	w_1	w_2	w_3
0.5	1	1	27.1117	27.1117	27.1117
1	1	1	6.53812	6.53805	6.53805
1	2	0.5	2.99878	2.99470	2.99459
1.5	2	0.5	1.33153	1.32897	1.32880
3	1	1	1.27714	1.27445	1.27427
3	1	2	$0.975676 - 0.219216i$	$0.975573 - 0.219677i$	$0.975572 - 0.219680i$
3	1	3	$0.686014 + 0.727588i$	$0.686009 + 0.727593i$	$0.686009 + 0.727593i$
1	3	3	-1.87542	-1.87542	-1.87542

second block of table 3.1 presents data for the case where ka_1 is fixed and $k\eta_2$ is increased. The last two rows indicate that for large values of $k\eta_2$ the interaction effect of two evanescent modes ($\nu = 1$) is sufficient to obtain accurate results. On the other hand, keeping $k\eta_2$ fixed and increasing ka_1 has the opposite effect and this is shown on the first block of table 3.1. In this case, as ka_1 increases the decay rate of the evanescent modes slows down, and consequently more than two of these modes ($\nu > 1$) are required in order to capture the significant interaction effects. To summarise, in view of the data of table 3.1 we can estimate that for $a_1 \leq \eta_2$, the choice $\nu = 1$ is adequate for our method to produce accurate results, whereas for $a_1 > \eta_2$, we need to increase ν in order to achieve high accuracy.

The last statement can be also confirmed alternatively as follows. From equation (3.4.3), it is clear that $A_{0n} \to 0$ as $n \to \infty$, if and only if the kernel has no zeros on the unit circle. In this case there is an alternative way to calculate the amplitudes which is to truncate the system (3.1.16) and then invert it numerically. Results that have been obtained using the two methods for different sets of parameters, are consistent with each other. In table 3.2 and 3.3, we display the first ten amplitudes obtained by each method for the case $a_1 = \eta_2$ ($\nu = 1$) and $a_1 > \eta_2$ ($\nu = 2$), respectively. Note that if the kernel possesses a

Table 3.2: *The first ten amplitudes calculated by numerical truncation and via the Wiener-Hopf technique. The parameters in use are* $k\ell = 0.01$, $\psi_0 = \pi/4$, $a_1 = \eta_2 = 1$, *and* $\eta_1 = 0$. *For the numerical method the order of truncation in the system* (3.1.16) *is* 200, *and the Wiener–Hopf technique has been carried out with* $\nu = 1$.

Amplitudes	Numerical truncation	Wiener–Hopf technique
A_{00}	$-271593\times10^{-1}-701286\times10^{-2}i$	$-271593\times10^{-1}-701286\times10^{-2}i$
A_{01}	$-827986\times10^{-2}-213795\times10^{-2}i$	$-827987\times10^{-2}-213795\times10^{-2}i$
A_{02}	$-253255\times10^{-2}-653934\times10^{-3}i$	$-253254\times10^{-2}-653932\times10^{-3}i$
A_{03}	$-774649\times10^{-3}-200023\times10^{-3}i$	$-774646\times10^{-3}-200022\times10^{-3}i$
A_{04}	$-236947\times10^{-3}-611826\times10^{-4}i$	$-236946\times10^{-3}-611822\times10^{-4}i$
A_{05}	$-724769\times10^{-4}-187143\times10^{-4}i$	$-724763\times10^{-4}-187142\times10^{-4}i$
A_{06}	$-221690\times10^{-4}-572430\times10^{-5}i$	$-221688\times10^{-4}-572424\times10^{-5}i$
A_{07}	$-678101\times10^{-5}-175093\times10^{-5}i$	$-678092\times10^{-5}-175091\times10^{-5}i$
A_{08}	$-207415\times10^{-5}-535571\times10^{-6}i$	$-207412\times10^{-5}-535563\times10^{-6}i$
A_{09}	$-634437\times10^{-6}-163819\times10^{-6}i$	$-634427\times10^{-6}-163816\times10^{-6}i$

Table 3.3: *The first ten amplitudes calculated by numerical truncation and via the Wiener-Hopf technique. The parameters in use are* $k\ell = 0.1$, $\psi_0 = \pi/6$, $a_1 = 1$, $\eta_2 = 0.8$, *and* $\eta_1 = 0$. *For the numerical method the order of truncation in the system* (3.1.16) *is* 200, *and the Wiener–Hopf technique has been carried out with* $\nu = 2$.

Amplitudes	Numerical truncation	Wiener–Hopf technique
A_{00}	$-230216\times10^{-1}-854630\times10^{-3}i$	$-230216\times10^{-1}-854630\times10^{-3}i$
A_{01}	$-194845\times10^{-2}-723323\times10^{-4}i$	$-194845\times10^{-2}-723323\times10^{-4}i$
A_{02}	$-203636\times10^{-3}-755958\times10^{-5}i$	$-203636\times10^{-3}-755957\times10^{-5}i$
A_{03}	$-209931\times10^{-4}-779327\times10^{-6}i$	$-209930\times10^{-4}-779325\times10^{-6}i$
A_{04}	$-216656\times10^{-5}-804292\times10^{-7}i$	$-216655\times10^{-5}-804288\times10^{-7}i$
A_{05}	$-223581\times10^{-6}-830000\times10^{-8}i$	$-223580\times10^{-6}-829995\times10^{-8}i$
A_{06}	$-230729\times10^{-7}-856535\times10^{-9}i$	$-230727\times10^{-7}-856528\times10^{-9}i$
A_{07}	$-238105\times10^{-8}-883917\times10^{-10}i$	$-238103\times10^{-8}-883910\times10^{-10}i$
A_{08}	$-245717\times10^{-9}-912175\times10^{-11}i$	$-245715\times10^{-9}-912166\times10^{-11}i$
A_{09}	$-253573\times10^{-10}-941335\times10^{-12}i$	$-253570\times10^{-10}-941326\times10^{-12}i$

zero on the unit circle, then A_{0n} does not tend to zero as $n \to \infty$, and therefore a comparison between the two methods is not possible.

It is important to underline that the parameter $k\ell$ has not been considered in the data of table 3.1 because it doesn't play any role in the approximation of the kernel. In fact, we consider cases where $k\ell > 1$ and the results we obtained from the Wiener-Hopf technique and the numerical truncation are consistent with each other. However, the parameter $k\ell$ plays crucial role in the small scatterer approximation and it must be kept low in order to have a good accuracy on the boundary condition (see for example figure 5.1 (a)).

3.5 The far field pattern

The far field pattern depends on whether or not the kernel has zeros on the unit circle, or in other words, whether or not one of the poles of $A^+(z)$ located at the points $z = z_j$ lies on the unit circle. We shall examine these two cases separately.

3.5.1 $A^+(z)$ is analytic on the unit circle

In the case where the kernel has no zeros on the unit circle, the function $A^+(z)$ is analytic inside and on the unit circle, which means that it has the following Taylor expansion

$$A^+(z) = \sum_{n=0}^{\infty} A_{0n} z^n, \quad \text{for} \quad |z| \leqslant 1. \tag{3.5.1}$$

Recall that the scattered field is given by

$$u_{sc}(\mathbf{r}) = \sum_{n=0}^{\infty} \sum_{j=-\infty}^{\infty} A_{0n} e^{ijka_1 \cos\psi_0} H_0(k|\mathbf{r} - \mathbf{R}_{jn}|), \tag{3.5.2}$$

which alternatively, can be expressed in the form

$$u_{sc}(\mathbf{r}) = \sum_{n=0}^{\infty} A_{0n} G_0^{(1)}(\mathbf{r} - n\mathbf{a}_2, k\cos\psi_0), \tag{3.5.3}$$

where G_0^1 is the 1D quasi-periodic function defined in (B.1.19). Using the spectral representation (B.1.23), yields

$$u_{sc}(\mathbf{r}) = \frac{2}{ka_1} \sum_{n=0}^{\infty} \sum_{j=-\infty}^{\infty} \frac{A_{0n}}{\sin\psi_j} e^{ik\left((x-n\eta_1)\cos\psi_j + |y-n\eta_2|\sin\psi_j\right)}. \tag{3.5.4}$$

From the last expression and the Taylor expansion (3.5.1) we can determine the behaviour of u_{sc} in the limit $y \to \pm\infty$.

In the upper half plane, and in particular for $N\eta_2 < y < (N+1)\eta_2$, from (3.5.4) we have that

$$u_{sc}(\mathbf{r}) = \frac{2}{ka_1} \sum_{j=-\infty}^{\infty} \frac{e^{ikx\cos\psi_j}}{\sin\psi_j} \left(e^{iky\sin\psi_j} \sum_{n=0}^{N} \left(A_{0n} p_j^n\right) + e^{-iky\sin\psi_j} \sum_{n=N+1}^{\infty} \left(A_{0n}\, \tau_j^{-n}\right) \right). \tag{3.5.5}$$

Taking the limit $N \to \infty$, which in turn implies that $y \to \infty$, causes the second sum over n to disappear, and since $\sin\psi_j$ is positive imaginary for $j \neq 0$, only the term with $j = 0$ contributes to the final result. That is,

$$u_{sc}(\mathbf{r}) \sim c_0^+ e^{ik(x\cos\psi_0 + y\sin\psi_0)} \quad \text{as} \quad y \to \infty, \tag{3.5.6}$$

with

$$c_0^+ = \frac{2A^+(p_0)}{ka_1 \sin\psi_0}. \tag{3.5.7}$$

Moreover, from (3.4.1) we have that

$$A^+(p_0) = \frac{ip_0}{K_\nu^-(p_0)\,\mathrm{Res}_{z=p_0} K_\nu^+(z)}, \tag{3.5.8}$$

or equivalently

$$A^+(p_0) = \frac{ip_0}{\mathrm{Res}_{z=p_0} K_\nu(z)} = -\frac{ka_1}{2}\sin\psi_0, \tag{3.5.9}$$

and therefore

$$c_0^+ = -1. \tag{3.5.10}$$

Thus, in the far field limit $y \to \infty$, the scattered field exactly cancels the incident wave, regardless of the value chosen for ν in performing the approximate kernel factorisation.

The field in the lower half plane is easier to determine, because in this case there is no need to split the sum over n in (3.5.4). For $y < 0$, we have that

$$u_{sc}(\mathbf{r}) = \sum_{j=-\infty}^{\infty} c_j^- e^{ik(x\cos\psi_j - y\sin\psi_j)}, \tag{3.5.11}$$

with

$$c_j^- = \frac{2A^+(\tau_j^{-1})}{ka_1 \sin\psi_j}, \tag{3.5.12}$$

and since ψ_j is positive imaginary for $j \neq 0$, the far field form of u_{sc} consists of a single term, corresponding to a reflected plane wave, that is

$$u_{sc}(\mathbf{r}) \sim c_0^- e^{ik(x\cos\psi_0 - y\sin\psi_0)} \quad \text{as} \quad y \to -\infty. \tag{3.5.13}$$

In this case, the exact value of the coefficient c_0^- depends on the choice of parameters, nevertheless, we can prove that

$$|c_0^-| = 1, \tag{3.5.14}$$

which is a necessary condition for energy to be conserved (see §3.6). For the proof, note that

$$A^+(\tau_0^{-1}) = \frac{ip_0}{K_\nu^-(p_0)(\tau_0^{-1} - p_0)K_\nu^+(\tau_0^{-1})}. \tag{3.5.15}$$

Evaluating the left-hand side of (3.3.19) at $z = p_0$ and $z = \tau_0^{-1}$ shows that

$$\left|(\tau_0^{-1} - p_0)K_\nu^+(\tau_0^{-1})\right| = \left|\mathrm{Res}_{z=p_0} K_\nu^+(z)\right|, \tag{3.5.16}$$

which in view of (3.5.8), yields

$$\left|A^+(\tau_0^{-1})\right| = \left|A^+(p_0)\right| = \frac{ka_1}{2}\sin\psi_0, \tag{3.5.17}$$

and the condition (3.5.14) follows immediately; again this is independent of the value taken for ν.

Figure 3.3 shows how $\arg[c_0^-]$ (the only far field parameter for which we do not have a simple expression) varies with ψ_0, for three different wavenumbers and two different lattices. Data for these plots and also for subsequent figures were computed with $\nu = 1$, which means that the interactions between each pair of consecutive rows are modelled using two plane waves (one propagating upwards and one propagating downwards) and four evanescent modes. Increasing the value of ν was found to lead to negligible changes in the results. The behaviour exhibited in figure 3.3 is typical of the cases in which there is no propagation through the lattice. When $\arg[c_0^-] = \pi$, the far field behaviour

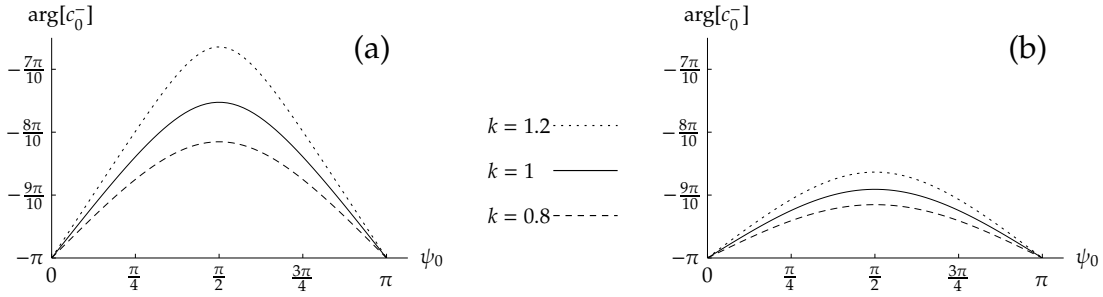

Figure 3.3: *Plots showing how the argument of the reflection coefficient c_0^- varies with the angle of incidence ψ_0. No Bloch waves are present, and so $|c_0^-| = 1$ in all cases shown. The parameters in use are $a_1 = 1$, $\eta_1 = 0$, $\eta_2 = 1$ and (a) $\ell = 0.01$, (b) $\ell = 0.05$.*

is identical to that which would occur if the lattice were to be replaced with a continuous sound-soft barrier on the line $y = 0$. Here, this occurs in the grazing limits $\psi_0 \to 0$ and $\psi_0 \to \pi$, which is to be expected, because $\tau_0^{-1} \to p_0$ as $\sin\psi_0 \to 0$, and (3.5.10) holds in all cases. The greatest deviation from this occurs at head-on incidence (i.e. $\psi_0 = \pi/2$), and the height of the peak increases with frequency.

3.5.2 $A^+(z)$ has a pole on the unit circle

We now consider the case where the function $A^+(z)$ has a simple pole on the unit circle, at $z = z_0$, say. To account for this, we use (3.4.4) to split the amplitudes into two terms

$$A_{0n} = \hat{A}_{0n} - \rho_0 z_0^{-n-1}, \tag{3.5.18}$$

where

$$\hat{A}_{0n} = -\sum_{\substack{m=-\nu \\ m\neq 0}}^{\nu} \rho_m z_m^{-n-1}. \tag{3.5.19}$$

Accordingly, we split the scattered field into two parts

$$u_{sc}(\mathbf{r}) = u_a(\mathbf{r}) + u_b(\mathbf{r}) \tag{3.5.20}$$

where

$$u_a(\mathbf{r}) = \sum_{n=0}^{\infty}\sum_{j=-\infty}^{\infty} \hat{A}_{0n} e^{ijka_1\cos\psi_0} H_0(k|\mathbf{r}-\mathbf{R}_{jn}|), \tag{3.5.21}$$

and

$$u_b(\mathbf{r}) = -\frac{\rho_0}{z_0}\sum_{n=0}^{\infty}\sum_{j=-\infty}^{\infty} e^{i\mathbf{R}_{jn}\cdot\boldsymbol{\beta}(z_0)} H_0(k|\mathbf{r}-\mathbf{R}_{jn}|), \tag{3.5.22}$$

with $\boldsymbol{\beta}(z)$ defined in (3.3.8) (we also used (3.3.9)). Since $\sum_{n=0}^{\infty}\left|\hat{A}_{0n}\right| < \infty$, the far field analysis for u_a can be carried out in the same manner as in §3.5.1. We first set

$$\hat{A}(z) = \sum_{n=0}^{\infty} \hat{A}_{0n} z^n, \quad \text{for} \quad |z| \leqslant 1, \tag{3.5.23}$$

and then substitute $\hat{A}_{0n} = A_{0n} + \rho_0 z_0^{-n-1}$ and use analytical continuation arguments to obtain

$$\hat{A}(z) = A^+(z) - \frac{\rho_0}{z - z_0}. \tag{3.5.24}$$

From the last two equations and the representation (see (3.5.2)-(3.5.4))

$$u_a(\mathbf{r}) = \frac{2}{ka_1}\sum_{n=0}^{\infty}\sum_{j=-\infty}^{\infty} \frac{\hat{A}_{0n}}{\sin\psi_j}\, e^{ik\left((x-n\eta_1)\cos\psi_j + |y-n\eta_2|\sin\psi_j\right)}, \tag{3.5.25}$$

we find that

$$u_a(\mathbf{r}) \sim \hat{c}_0^{\pm} e^{ik(x\cos\psi_0 \pm y\sin\psi_0)}, \quad \text{as} \quad y \to \pm\infty, \tag{3.5.26}$$

where

$$\hat{c}_0^{+} = \frac{2}{ka_1\sin\psi_0}\left(A^+(p_0) - \frac{\rho_0}{p_0 - z_0}\right), \tag{3.5.27}$$

and

$$\hat{c}_0^{-} = \frac{2}{ka_1\sin\psi_0}\left(A^+(\tau_0^{-1}) - \frac{\rho_0}{\tau_0^{-1} - z_0}\right). \tag{3.5.28}$$

The far field pattern of u_b can be determined by expressing it in terms of the function $G^{\pm}$ defined in (B.1.24), and then make use the spectral form (B.1.32) and (B.1.33). Note that these representations are valid in the upper and lower half plane respectively. With this in mind, for $y > 0$, we write

$$u_b(\mathbf{r}) = -\frac{\rho_0}{z_0}\left(G_0^{(2)}(\mathbf{r}, \boldsymbol{\beta}(z_0)) - G_0^{+}(\mathbf{r}, \boldsymbol{\beta}(z_0))\right), \tag{3.5.29}$$

where $G_0^{(2)}$ represents the two dimensional quasi-periodic Green's function defined in (B.1.5). We can now use (B.1.32) and obtain

$$u_b(\mathbf{r}) \sim -\frac{\rho_0}{z_0} G_0^{(2)}(\mathbf{r}, \boldsymbol{\beta}(z_0)) \\ - \frac{2\rho_0}{ka_1 \sin\psi_0 (z_0 - p_0)} e^{ik(x\cos\psi_0 + y\sin\psi_0)} \quad \text{as} \quad y \to \infty. \tag{3.5.30}$$

On the other hand, for $y < 0$, we write

$$u_b(\mathbf{r}) = -\frac{\rho_0}{z_0}\Big(G_0^{(1)}(\mathbf{r}, k\cos\psi_0) + G_0^{-}(\mathbf{r}, \boldsymbol{\beta}(z_0))\Big), \tag{3.5.31}$$

where $G_0^{(1)}$ is the one dimensional quasi-periodic Green's function, defined in (B.1.3). Substituting the spectral representations (B.1.23) and (B.1.33) in (3.5.31), yields

$$u_b(\mathbf{r}) \sim \frac{2\rho_0}{ka_1 \sin\psi_0 (\tau_0^{-1} - z_0)} e^{ik(x\cos\psi_0 - y\sin\psi_0)} \quad \text{as} \quad y \to -\infty. \tag{3.5.32}$$

To summarise, in the upper half plane in view of (3.5.9), (3.5.26), (3.5.27) and (3.5.30) we have that

$$u_{sc}(\mathbf{r}) \sim -\frac{\rho_0}{z_0} G_0^{(2)}(\mathbf{r}, \boldsymbol{\beta}(z_0)) - e^{ik(x\cos\psi_0 + y\sin\psi_0)} \quad \text{as} \quad y \to \infty, \tag{3.5.33}$$

and so the far field pattern takes the form of a Bloch wave, with complex amplitude $-\rho_0 z_0^{-1}$, plus a plane wave which cancels the incident wave. In the lower half plane (3.5.26), (3.5.28) and (3.5.32) reveal that the scattered field is again given by (3.5.13), only this time the reflected coefficient c_0^- does not satisfy the condition (3.5.14). To determine $|c_0^-|$, evaluate the left-hand side of (3.3.23) at the points $z = p_0$ and $z = \tau_0^{-1}$, which yields

$$\left|(\tau_0^{-1} - p_0) K_\nu^+(\tau_0^{-1})\right| = f(z_0, z_0')\left|\operatorname{Res}_{z=p_0} K_\nu^+(z)\right|, \tag{3.5.34}$$

where

$$f(z_0, z_0') = \sqrt{\left|\frac{(\tau_0^{-1} - z_0)(p_0 - z_0')}{(\tau_0^{-1} - z_0')(p_0 - z_0)}\right|}. \tag{3.5.35}$$

Hence, from (3.5.8) and (3.5.15),

$$\left|A^+(\tau_0^{-1})\right| = \frac{\left|A^+(p_0)\right|}{f(z_0, z_0')} = \frac{ka_1 \sin\psi_0}{2 f(z_0, z_0')}, \tag{3.5.36}$$

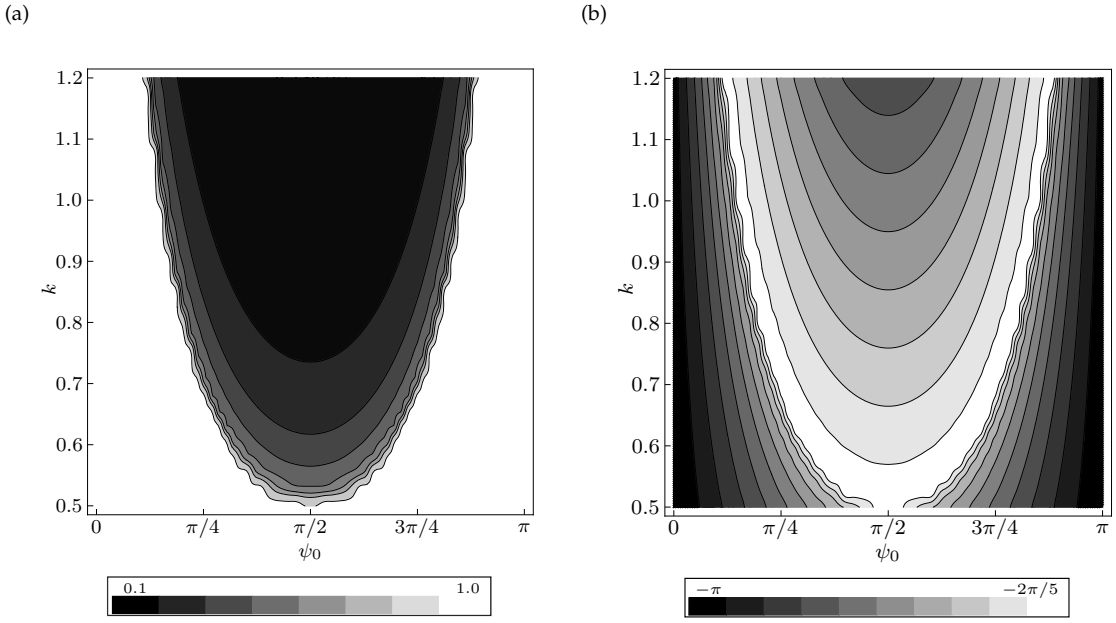

Figure 3.4: *Contour plots showing the (a) modulus and (b) phase of the reflection coefficient c_0^- for the case where $l = 0.001$, $a_1 = 2$, $\eta_1 = 0$ and $\eta_2 = 2$.*

and therefore the modulus of the reflection coefficient is given by

$$|c_0^-| = \frac{1}{f(z_0, z_0')}. \tag{3.5.37}$$

We now return to the matter of classifying zeros of $K_\nu(z)$ that occur on the unit circle as zeros of K_ν^+ or of K_ν^-. Clearly, any Bloch wave that is excited must be outgoing as $y \to \infty$, but there is no meaningful way to define the phase velocity of such phenomena; for example we can add $2q\pi/\eta_2$, $q \in \mathbb{Z}$ to $\lambda(z_0)$ without affecting the value of $\mathbf{R}_{jp} \cdot \boldsymbol{\beta}(z_0)$ (see [18, pp. 40–43] for full details). One possibility is to calculate the direction of energy propagation (group velocity) of the Bloch waves; another is to consider the rate of energy flux parallel to the y-axis (see §3.6, below). Provided that $K_\nu(z)$ has a single pair of zeros on the unit circle, so that only one Bloch wave is excited, a simple alternative is to use the value $f(z_0, z_0')$ given in (3.5.35). Since $f(z_0', z_0) = 1/f(z_0, z_0')$, this provides a simple means of distinguishing z_0 from z_0' —the wrong choice leads to a reflected wave whose amplitude is greater than one, which is clearly unphysical. Also, note that $|c_0^-| = 1$ can only occur when $z_0 = z_0'$.

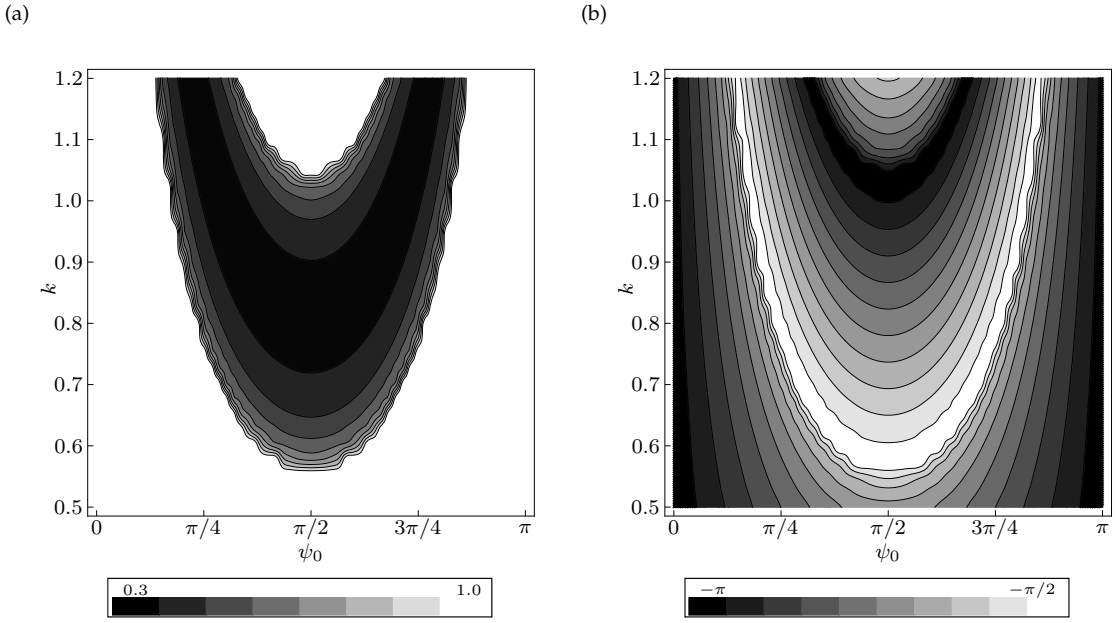

Figure 3.5: *Contour plots showing the (a) modulus and (b) phase of the reflection coefficient* c_0^- *for the case where* $l = 0.001$, $a_1 = 1$, $\eta_1 = 0$, *and* $\eta_2 = 3$.

Figures 3.4 and 3.5 show contour plots of the modulus and phase of the reflection coefficient, for all possible values of ψ_0, and $k \in [0.5, 1.2]$, with the lattice parameters fixed. Since the scattered field includes only two terms that propagate energy into the far field (the reflected field and the Bloch wave), these figures give a fairly comprehensive picture of the behaviour of the solution for the lattices in question. In particular, the proportion of incident field energy reflected back into the region $y < 0$ is $|c_0^-|^2$ (see §3.6, below). At grazing incidence (i.e. when $\sin\psi_0 \approx 0$), and also for very small k, we have $|c_0^-| = 1$, meaning that the parameters are in a band gap, and there is no propagation through the lattice. In the former case, we also have $\arg[c_0^-] \approx \pi$ (see §3.5.1, above). On the other hand, when $\pi/4 \lesssim \psi_0 \lesssim \pi/2$, there are values of k in both cases for which $|c_0^-| < 1$, meaning that a Bloch wave has been excited. In figure 3.4, the range of angles for which this wave exists widens as k is increased, and it persists up to the maximum value of k shown. In figure 3.5, a second band gap appears at $k \gtrsim 1.05$ and $\psi_0 \approx \pi/2$, and widens as k is increased. The modulus of the reflection coefficient decreases significantly as the parameters are moved away

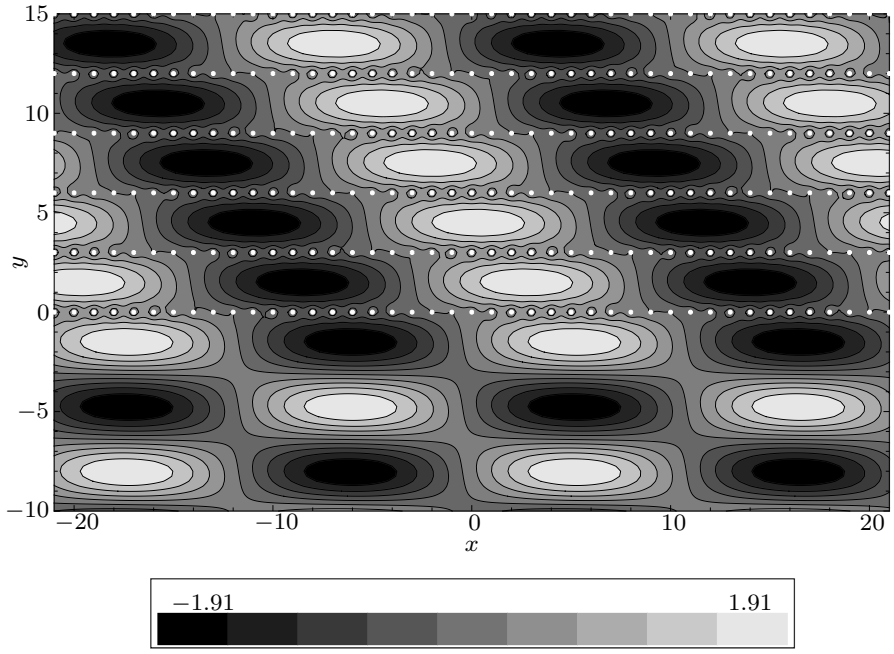

Figure 3.6: *Contour plot showing* $Re[u^t(\mathbf{r})]$, *for* $k = 1$, $l = 0.1$, $a_1 = 1$, $\eta_1 = 0$, $\eta_2 = 3$ *and* $\psi_0 = 0.41\pi$.

from the band edges and into the interior; in figure 3.4(a), the minimum value of $|c_0^-|$ is approximately 0.1, meaning that around 99% of the incident field energy is transmitted into the lattice. There is also significant variation in the argument of the reflection coefficient in these regimes; interestingly the largest deviation from the grazing incidence behaviour ($\arg[c_0^-] = -\pi$) occurs at the lower edge of the pass-band in both cases.

Figure 3.6 shows the value of $Re[u(\mathbf{r})]$ in the region $-20 \leq x \leq 20, -10 \leq y \leq 15$ for the case where $a_1 = 1$, $\eta_1 = 0$, $\eta_2 = 3$, $l = 0.1$, $k = 1$ and $\psi_0 = 0.41\pi$. These parameters were chosen because the value of $\boldsymbol{\beta}(z_0)$ (3.3.8) is significantly different from that of $\mathbf{k}$ (3.1.4); in fact we have that the y-component of $\mathbf{k}$ is $k \sin \psi_0 \approx 0.225$, whereas of $\boldsymbol{\beta}(z_0)$ is $\lambda(z_0) \approx 0.960$ (the x-components are of course equal). The different nature of the field in the regions $y < 0$ and $y > 0$ is clearly evident. Note that the transition from plane waves in the lower half plane to a Bloch wave in the upper half plane is extremely rapid. It is also interesting to note that $|c_0^-| \approx 0.912$ in this case, which means that approximately 83% of the incident field energy is reflected back into the region $y < 0$. Nevertheless, the amplitude

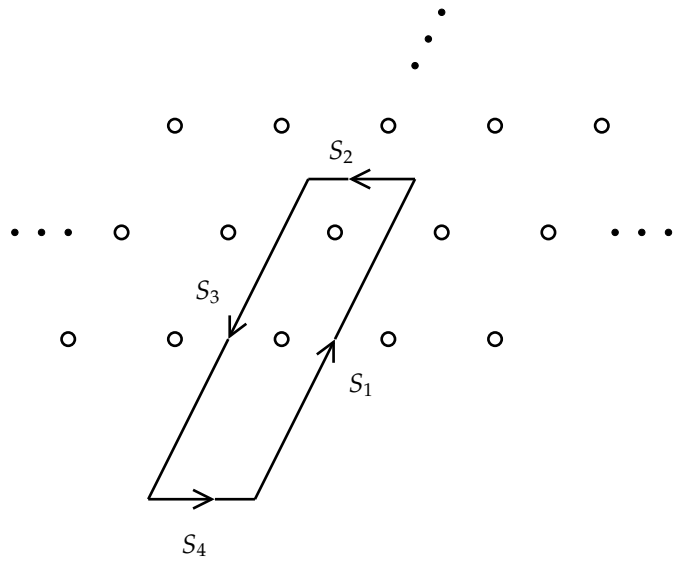

Figure 3.7: *The contour S, consisting of the four elements $S_1, \ldots, S_4$.*

range inside the lattice is very similar to that outside.

3.6 Conservation of energy

To establish that the energy is conserved, we begin by noting that the acoustic intensity $\mathbf{I}$, that is the rate of working of the pressure fluctuation, is given by [5, pp. 40–44]

$$\mathbf{I} = -P_0 \frac{\partial U}{\partial t} \nabla U, \tag{3.6.1}$$

where P_0 is the quiescent pressure, and $U(\mathbf{r}, t) = Re[u(\mathbf{r})e^{-i\omega t}]$ is the total acoustic potential (with ω representing the angular frequency see §1.1). The problem that we are considering is uniform in the z-direction, and so we can calculate the flux across a contour S in the (x, y) plane, by which we strictly mean the flux across S per unit length in z. Following the procedure in [34, pp. 19–20], it is not difficult to show that the average energy flux over one time period is given by the line integral

$$\langle E_S \rangle = -\frac{P_0 \omega}{2} Im \int_S u(\mathbf{r}) \left(\frac{\partial u(\mathbf{r})}{\partial n} \right)^* ds, \tag{3.6.2}$$

where the derivative is taken in the direction of the outgoing normal to S. Clearly, conservation of energy requires that this integral must vanish for any closed

contour, a result that can be obtained directly by applying Green's theorem [34, p. 85] to u and its complex conjugate. We take S to be the parallelogram with vertices at the points

$$\mathbf{r} = \pm\tfrac{1}{2}\mathbf{a}_1 \pm \left(N + \tfrac{1}{2}\right)\mathbf{a}_2, \tag{3.6.3}$$

so that we have

$$I_1 + I_2 + I_3 + I_4 = 0, \tag{3.6.4}$$

where

$$I_j = -\frac{P_0\omega}{2} Im \int_{S_j} u(\mathbf{r}) \left(\frac{\partial u(\mathbf{r})}{\partial n}\right)^* ds, \tag{3.6.5}$$

and $S_1, \ldots, S_4$ represent the four sides of S; see figure 3.7. In view of the quasi-periodicity relation (3.1.13), it is clear that the only difference between the integrals along S_1 and S_3 is caused by the fact that the derivatives are taken in opposite directions; hence

$$I_1 + I_3 = 0, \tag{3.6.6}$$

for all N. For the horizontal portions of S, we take the limit $N \to \infty$ so that we can discard contributions that decay as $y \to \pm\infty$. Thus, on S_4, we have

$$u \sim e^{ikx\cos\psi_0}\left(e^{iky\sin\psi_0} + c_0^- e^{-iky\sin\psi_0}\right), \tag{3.6.7}$$

and so the integral trivially evaluates to yield

$$I_4 = -\frac{P_0\omega^2}{2c}\, a_1 \sin\psi_0 \left(1 - |c_0^-|^2\right), \tag{3.6.8}$$

where c represents the speed of sound. If there are no Bloch waves, the total field decays exponentially as $y \to \infty$ (see §3.5.1), and so the integral along S_2 evaluates to zero. We also have $|c_0^-| = 1$ in this case, and so $I_4 = 0$ as well. On the other hand, if a Bloch wave is present, then $|c_0^-| < 1$ (see §3.5.2, above) and so I_4 is negative, corresponding to the fact that energy is propagating across S_4 in the direction opposite to the outgoing normal, i.e. from the exterior of S to the interior. Also, from (3.5.33), we have

$$I_2 = -\frac{P_0\omega|\rho|^2}{2} Im \int_{S_2} G_0^{(2)}(\mathbf{r}, \boldsymbol{\beta}(z_0)) \frac{\partial}{\partial y}\left[G_0^{(2)}(\mathbf{r}, \boldsymbol{\beta}(z_0))\right]^* ds, \tag{3.6.9}$$

where the path of integration has the following parametrisation

$$S_2 \,:\, \mathbf{r}(t) = (t + N\eta_1/2,\ N\eta_2/2), \quad -a_1/2 \le t \le a_1/2. \tag{3.6.10}$$

From (B.1.6), it is clear that the integrand is independent of N, and so we choose the value $N = 1$ so as to enable the use of (B.1.36). Hence, on this particular path we have that

$$G_0^{(2)}(\mathbf{r}(t), \boldsymbol{\beta}(z_0)) = -\frac{2}{ka_1} \sum_{j=-\infty}^{\infty} \frac{e^{ikt\cos\psi_j}}{\sin\psi_j} \left(\frac{p_j^{1/2}}{z_0 - p_j} - \frac{\tau_j^{1/2}}{\tau_j z_0 - 1} \right), \tag{3.6.11}$$

$$\frac{\partial}{\partial y} \left[G_0^{(2)}(\mathbf{r}(t), \boldsymbol{\beta}(z_0)) \right]^* = \frac{2i}{a_1} \sum_{j=-\infty}^{\infty} e^{-ikt\cos\psi_j} \left(\frac{p_j^{1/2}}{z_0 - p_j} + \frac{\tau_j^{1/2}}{\tau_j z_0 - 1} \right)^*, \tag{3.6.12}$$

and

$$\begin{aligned} G_0^{(2)}(\mathbf{r}(t), \boldsymbol{\beta}(z_0)) \frac{\partial}{\partial y} \left[G_0^{(2)}(\mathbf{r}(t), \boldsymbol{\beta}(z_0)) \right]^* = &- \frac{4i}{ka_1^2} \sum_{j=-\infty}^{\infty} \sum_{n=-\infty}^{\infty} \frac{e^{2it(j-n)\pi/a_1}}{\sin\psi_j} \\ &\times \left(\frac{p_j^{1/2}}{z_0 - p_j} - \frac{\tau_j^{1/2}}{\tau_j z_0 - 1} \right) \left(\frac{p_n^{1/2}}{z_0 - p_n} + \frac{\tau_n^{1/2}}{\tau_n z_0 - 1} \right)^*. \end{aligned} \tag{3.6.13}$$

Now, if we substitute the last equation in (3.6.9) and perform the integration over t, then only the terms in which $j = n$ are non zero. In fact

$$\begin{aligned} I_2 = Re \sum_{j=-\infty}^{\infty} &\frac{2P_0 c|\rho_0|^2}{a_1 \sin\psi_j} \left(\frac{|p_j|}{|z_0 - p_j|^2} - \frac{|\tau_j|}{|\tau_j z_0 - 1|^2} \right) \\ &+ \frac{4iP_0 c|\rho_0|^2}{a_1 \sin\psi_j} Im \left[\frac{\left(p_j \tau_j^*\right)^{1/2}}{(z_0 - p_j)(\tau_j z_0 - 1)^*} \right]. \end{aligned} \tag{3.6.14}$$

Finally, we take into account the fact that $\tau_j^* = p_j$ for $j \neq 0$, and that $\sin\psi_j$ is real when $j = 0$ and positive imaginary otherwise, to obtain

$$I_2 = \frac{2P_0 c|\rho_0|^2}{a_1 \sin\psi_0} \left(\frac{1}{|z_0 - p_0|^2} - \frac{1}{|\tau_j z_0 - 1|^2} \right) - \sum_{\substack{j=-\infty \\ j\neq 0}}^{\infty} \frac{4P_0 c|\rho_0|^2}{a_1 |\sin\psi_j|} Im \left[\frac{p_j z_0}{(p_j - z_0)^2} \right]. \tag{3.6.15}$$

Since $I_4 \le 0$, we must have $I_2 \ge 0$, with equality holding in both cases if and only if $|c_0^-| = 1$, i.e. $z_0 = z_0'$. In this case, the y-component of the Bloch wave group velocity is zero, and so no energy is transported into the lattice. Otherwise, we

must have $I_2 > 0$, which corresponds to the fact that any Bloch wave excited in the far field can only transport energy across S_2 in the direction of the outgoing normal (i.e. increasing y). The fact that $I_2 + I_4 = 0$ serves as a useful check on our numerical results; in fact our calculations indicate that this is always satisfied to a high degree of accuracy, regardless of the value chosen for the parameter ν in approximating the kernel.

Equation (3.6.15) can also be used to distinguish between zeros of K_ν^+ and those of K_ν^- when these occur on the unit circle. Thus, zeros of $K_\nu^-(z)$ on the unit circle correspond to Bloch waves that can propagate through an infinite lattice, but that cannot be excited here, because they are incoming from infinity, that is the y component of their group velocity is oriented in the direction of decreasing y. Therefore replacing z_0 with a zero of $K_\nu^-(z)$ in (3.6.15) leads to a negative result, in contrast to zeros of K_ν^+, which yield positive results. This method is more general than using (3.5.35), in that it applies regardless of the number of zeros that occur on the unit circle.

Chapter 4

The general case

The method used in the previous chapter needs to be generalised to account for cases where Neumann boundary conditions are imposed on the cylinders surfaces, or where the assumption (3.1.5) is dropped, so that the cylinders are no longer treated as point scatterers. In the first case, in order to correctly capture the behaviour of the field, both monopole and dipole terms are required in the expansion of the field radiating from each scatterer (see §1.2). Consequently, there are three amplitude coefficients associated with each scatterer, and this leads to a system of three coupled Wiener–Hopf equations, or equivalently a matrix Wiener–Hopf equation of order three. For the general case, more terms are required in the expansion of the field, and the dimension of the matrix grows larger.

In the first two sections we present the details regarding the formulation which leads to the matrix Wiener–Hopf equation, and in §4.3 we prove an important symmetry property of the matrix kernel. Each one of the elements of the kernel is expressed as an infinite sum of partial fractions, and it has an infinite number of poles, plus two nonisolated essential singularities at the origin and at infinity. As in the previous chapter, these sums are truncated and thereby a rational matrix kernel is obtained. In contrast to the scalar case a factorisation of a rational matrix is not trivial. However, a new method which essentially

solves a rational matrix Wiener–Hopf problem without the need of a product factorisation is presented in §4.4.

In the same fashion seen in chapter 3, we present the far field analysis in §4.5, and useful identities provided by the principle of the conservation of energy are given in §4.6. Finally, in the last section we examine the band structure of the lattice by presenting some numerical results.

4.1 Formulation

In general, the field radiating from each cylinder of the semi-infinite lattice can be expressed in terms of a multipole expansion series (1.2.10). Therefore, using the same notation as in §3.1, the total field is represented by the expansion

$$u(\mathbf{r}) = u_{inc}(\mathbf{r}) + \sum_{q=-Q}^{Q} \sum_{p=0}^{\infty} \sum_{j=-\infty}^{\infty} A_{jp}^{q} \mathcal{H}_q(\mathbf{r}_{jp}). \tag{4.1.1}$$

Here we have introduced the parameter Q which denotes the order of truncation of the multipole expansion. Recall that for 'small-sized' sound-soft cylinders we can take $Q = 0$, whereas, for sound-hard cylinders we can take $Q = 1$ (see 1.2.4). However, as the size of the cylinder or the frequency increases, the value of Q needs to be significantly higher (some representative values are given in [35]).

In order to find the amplitudes A_{jp}^{q} we will apply the boundary condition on the surface of an arbitrary chosen cylinder, at $\mathbf{r} = \mathbf{R}_{mn}$, say. To do this, we need to express the total field in terms of the polar coordinates $\mathbf{r}_{mn} = (r_{mn}, \theta_{mn})$. For the incident wave, we note that $u_{inc}(\mathbf{r}) = e^{i\mathbf{k}\cdot(\mathbf{R}_{mn}+\mathbf{r}_{mn})}$, and use Jacobi's formula (1.2.12), to obtain

$$u_{inc}(\mathbf{r}_{mn}) = e^{i\mathbf{k}\cdot\mathbf{R}_{mn}} \sum_{\mu=-\infty}^{\infty} e^{i\mu(\pi/2-\psi_0)} \mathcal{J}_{\mu}(\mathbf{r}_{mn}). \tag{4.1.2}$$

For the wavefunctions $\mathcal{H}_q(\mathbf{r}_{jp})$ in (4.1.1), we can use Graf's addition theorem. Thus, assuming that $r_{mn} < R_{m-j,n-p}$, for every j and p with $(j,p) \neq (m,n)$, Graf's

formula (1.3.1) yields

$$\mathcal{H}_q(\mathbf{r}_{jp}) = \sum_{\mu=-\infty}^{\infty} \mathcal{H}_{q-\mu}(\mathbf{R}_{m-j,n-p})\mathcal{J}_\mu(\mathbf{r}_{mn}). \tag{4.1.3}$$

Hence, in the vicinity of the chosen cylinder, and with the aid of (4.1.2) and (4.1.3), the total field can be written solely in terms of the coordinates $\mathbf{r}_{mn}$; that is

$$u(\mathbf{r}_{mn}) = e^{i\mathbf{k}\cdot\mathbf{R}_{mn}} \sum_{\mu=-\infty}^{\infty} e^{i\mu(\pi/2-\psi_0)}\mathcal{J}_\mu(\mathbf{r}_{mn}) + \sum_{q=-Q}^{Q} A_{mn}^q \mathcal{H}_q(\mathbf{r}_{mn}) + \sum_{q=-Q}^{Q}\sum_{p=0}^{\infty}{\sum_{j=-\infty}^{\infty}}' A_{jp}^q \sum_{\mu=-\infty}^{\infty} \mathcal{H}_{q-\mu}(\mathbf{R}_{m-j,n-p})\mathcal{J}_\mu(\mathbf{r}_{mn}). \tag{4.1.4}$$

Recall that the prime on the summation symbol is used to indicate that the term in which the argument of the Hankel function vanishes (in this case $(j,p) = (m,n)$) is to be omitted from the series. We can now apply the boundary condition on the surface of the cylinder, and use the orthogonality of the functions $e^{iq\theta_{mn}}$, to obtain the system of algebraic equations

$$A_{mn}^\mu + Z_\mu \sum_{q=-Q}^{Q}\sum_{p=0}^{\infty}{\sum_{j=-\infty}^{\infty}}' A_{jp}^q \mathcal{H}_{q-\mu}(\mathbf{R}_{m-j,n-p}) = -Z_\mu e^{i\mathbf{k}\cdot\mathbf{R}_{mn}} e^{i\mu(\pi/2-\psi_0)}, \qquad \mu = -Q,\dots Q, \quad n = 0,1,\dots, \quad m \in \mathbb{Z}, \tag{4.1.5}$$

where Z_μ is defined in (1.2.15). Note that the periodicity condition (3.1.13) still holds, and so we seek a solution with the property

$$A_{jp}^q = A_{0p}^q e^{ij\mathbf{k}\cdot\mathbf{a}_1}. \tag{4.1.6}$$

Now, multiply the system (4.1.5) by $iZ_\mu^{-1}e^{-im\mathbf{k}\cdot\mathbf{a}_1}$, and use (4.1.6) to obtain the reduced system

$$iZ_\mu^{-1}A_{0n}^\mu + i\sum_{q=-Q}^{Q}\sum_{p=0}^{\infty} A_{0p}^q \mathcal{S}_{n-p}^{q-\mu} = -ie^{in\mathbf{k}\cdot\mathbf{a}_2}e^{i\mu(\pi/2-\psi_0)}, \qquad \mu = -Q,\dots Q, \quad n = 0,1,\dots, \tag{4.1.7}$$

where

$$\mathcal{S}_0^q = \sum_{\substack{j=-\infty \\ j\neq 0}}^{\infty} e^{ij\mathbf{k}\cdot\mathbf{a}_1}\mathcal{H}_q(-j\mathbf{a}_1), \tag{4.1.8}$$

and

$$\mathcal{S}_n^q = \sum_{j=-\infty}^{\infty} e^{ij\mathbf{k}\cdot\mathbf{a}_1}\mathcal{H}_q(n\mathbf{a}_2 - j\mathbf{a}_1), \quad n \in \mathbb{Z} - \{0\}. \tag{4.1.9}$$

Note that

$$\mathcal{S}_n^q = \begin{cases} (-1)^q \sigma_q^{(1)}(k\cos\psi_0), & n = 0, \\ G_q^{(1)}(n\mathbf{a}_2, k\cos\psi_0), & n \neq 0, \end{cases} \tag{4.1.10}$$

where $\sigma_q^{(1)}$ is the 1D lattice sum of order q, and $G_q^{(1)}$ is the 1D quasi-periodic array of singularities of order q, the definition of which can be found in the appendix B. In particular, for $n \neq 0$, we can use the scattering angles (B.1.12), the points p_j, τ_j defined in (B.1.16), and the representation (B.1.23) to obtain

$$\mathcal{S}_n^q = \frac{2(-i)^q}{ka_1} \sum_{j=-\infty}^{\infty} \frac{e^{iq\psi_j} p_j^{-n}}{\sin\psi_j}, \quad \text{for} \quad n > 0, \tag{4.1.11}$$

and

$$\mathcal{S}_n^q = \frac{2(-i)^q}{ka_1} \sum_{j=-\infty}^{\infty} \frac{e^{-iq\psi_j} \tau_j^{n}}{\sin\psi_j}, \quad \text{for} \quad n < 0. \tag{4.1.12}$$

4.2 The matrix Wiener–Hopf equation

So far we have dealt with the $\mathcal{Z}$-transformation of a single infinite system of algebraic equations into a scalar Wiener–Hopf equation. Now, since (4.1.7) defines $2Q + 1$ coupled infinite systems of equations we expect that a similar transformation will yield a system of $2Q + 1$ coupled Wiener–Hopf equations, which essentially defines a matrix Wiener–Hopf equation. The transformation process remains the same (see §2.3); first we extend the validity of (4.1.7) by setting

$$A_{0n}^m = 0, \quad \text{for} \quad n < 0, \tag{4.2.1}$$

and write it in the equivalent form

$$\sum_{q=-Q}^{Q} \sum_{p=-\infty}^{\infty} K_{n-p}^{\mu q} A_{0p}^q = T_n^{\mu^+} + T_n^{\mu^-}, \quad \mu = -Q, \ldots Q, \quad n \in \mathbb{Z}, \tag{4.2.2}$$

where

$$T_n^{\mu^+} = \begin{cases} -ip_0^{-n} e^{i\mu(\pi/2-\psi_0)}, & n \geqslant 0, \\ 0, & n < 0, \end{cases} \qquad T_n^{\mu^-} = \begin{cases} 0, & n \geqslant 0, \\ \sum_{q=-Q}^{Q} \sum_{p=0}^{\infty} K_{n-p}^{\mu q} A_{0p}^{q}, & n < 0, \end{cases} \tag{4.2.3}$$

and

$$K_n^{\mu q} = \begin{cases} iZ_q^{-1}\delta_{\mu q} + i\mathcal{S}_0^{q-\mu}, & n = 0, \\ i\mathcal{S}_n^{q-\mu}, & n \neq 0. \end{cases} \tag{4.2.4}$$

Next, we assume that all the terms in the system (4.2.2) are members of the class $\mathscr{Z}(C)$ for all $\mu,\ q = -Q, \ldots Q$, so as to transform it into the system of functional equations

$$\sum_{q=-Q}^{Q} K_{\mu q}(z) A_q^+(z) = T_\mu^+(z) + T_\mu^-(z), \quad \mu = -Q \ldots Q, \quad z \in C. \tag{4.2.5}$$

The known functions in this system are $K_{\mu q}(z)$ and $T_\mu^+(z)$, and these are given by $\mathcal{Z}(K_n^{\mu q})$ and $\mathcal{Z}(T_n^{\mu^+})$, respectively. We seek to determine $A_q^+(z)$ and $T_\mu^-(z)$. Note that the following condition must hold (see (2.3.8))

$$T_\mu^-(z) \to 0 \qquad \text{as} \qquad z \to \infty. \tag{4.2.6}$$

The '+' and '−' signs indicate analyticity in the sets C^+ and C^-, where C^+ consists of all the points that lie inside and on C, and C^- consists of all the points that lie outside and on C. We also know that C is a closed curve that encircles the origin, and its exact form will be determined once we specify the singularity structure of the functions $K_{\mu q}(z)$ and $T_\mu^+(z)$. Finally, we write the system (4.2.5) in the form of a matrix Wiener–Hopf equation; that is

$$\mathbf{K}(z)\mathbf{A}^+(z) = \mathbf{T}^+(z) + \mathbf{T}^-(z), \tag{4.2.7}$$

where the kernel is the $(2Q+1) \times (2Q+1)$ matrix

$$\mathbf{K}(z) = \left[K_{\mu q}(z)\right]_{\mu=-Q,\ldots Q; q=-Q\ldots Q}, \tag{4.2.8}$$

and the other terms are the column vectors

$$\mathbf{A}^+(z) = \left[A_q^+(z)\right]_{q=-Q,\ldots,Q}, \tag{4.2.9}$$

$$\mathbf{T}^+(z) = \left[T_q^+(z)\right]_{q=-Q,\ldots,Q}, \tag{4.2.10}$$

$$\text{and} \quad \mathbf{T}^-(z) = \left[T_q^-(z)\right]_{q=-Q,\ldots,Q}. \tag{4.2.11}$$

We now examine the form of the functions $T_q^+(z)$ and $K_{\mu q}(z)$ in the $\mathcal{Z}$-transformed domain, with the aim of revealing their singularities, and also to determine which of these lies inside and which outside the contour C. For the first set of functions, we simply sum a geometric series to obtain

$$T_\mu^+(z) = e^{i\mu(\pi/2-\psi_0)}\frac{ip_0}{z-p_0}, \quad \mu = -Q,\dots,Q, \tag{4.2.12}$$

and since these functions are analytic in C^+ we must have

$$p_0 \in C^- - C. \tag{4.2.13}$$

For the elements of the kernel, we have that

$$K_{\mu q}(z) = iZ_q^{-1}\delta_{\mu q} + i\sum_{j=-\infty}^{\infty} \mathcal{S}_j^{q-\mu} z^j, \quad \mu, q = -Q,\dots,Q, \tag{4.2.14}$$

and with the aid of (4.1.11) and (4.1.12), the last equation becomes

$$K_{\mu q}(z) = iZ_q^{-1}\delta_{\mu q} + i\mathcal{S}_0^{q-\mu} + \frac{2i^{\mu-q+1}}{ka_1}\sum_{n=1}^{\infty}\sum_{j=-\infty}^{\infty}\frac{e^{i(q-\mu)\psi_j}}{\sin\psi_j}\left(p_j^{-1}z\right)^n + \frac{2i^{\mu-q+1}}{ka_1}\sum_{n=1}^{\infty}\sum_{j=-\infty}^{\infty}\frac{e^{i(\mu-q)\psi_j}}{\sin\psi_j}\left(\tau_j^{-1}z^{-1}\right)^n. \tag{4.2.15}$$

We can now evaluate the two sums over n in their respective region of convergence to obtain

$$K_{\mu q}(z) = i\left(Z_q^{-1}\delta_{\mu q} + \mathcal{S}_0^{q-\mu}\right) - \frac{2i^{\mu-q+1}}{ka_1}\sum_{j=-\infty}^{\infty}\frac{1}{\sin\psi_j}\left(\frac{e^{i(q-\mu)\psi_j}z}{z-p_j} - \frac{e^{i(\mu-q)\psi_j}}{z\tau_j-1}\right). \tag{4.2.16}$$

Note that we assumed that $K_n \in \mathscr{Z}(C)$ (see definition 1 in §2.2.1), i.e.

$$K_n^{\mu q} = \frac{1}{2\pi i}\oint_C K_{\mu q}(z)z^{-n-1}dz, \qquad n \in \mathbb{Z}. \tag{4.2.17}$$

and in view of (4.2.16), (4.1.11), (4.1.12) and (4.2.4) this is a valid representation if and only if

$$p_j \in C^- - C, \quad \text{and} \quad \tau_j^{-1} \in C^+ - C, \quad \forall j \in \mathbb{Z}, \tag{4.2.18}$$

which is in agreement with the condition (4.2.13).

4.3 Symmetry

In this section we will prove an important symmetry property of the matrix kernel. In order to achieve this we will do some calculations similar to those given in §3.3.1. We begin by splitting each element of the kernel $K_{\mu q}(z)$ into three parts as follows:

$$K_{\mu q}(z) = c_{\mu q} + K^1_{\mu q}(z) + K^2_{\mu q}(z), \tag{4.3.1}$$

where

$$c_{\mu q} = i(Z_q^{-1}\delta_{\mu q} + \mathcal{S}_0^{q-\mu}) - \frac{2i^{\mu-q+1}}{ka_1}\sum_{j\in\mathcal{M}}\frac{e^{-i|\mu-q|\operatorname{sgn}(j)\psi_j}}{\sin\psi_j}, \tag{4.3.2}$$

is a constant

$$K^1_{\mu q}(z) = \frac{2i^{\mu-q+1}}{ka_1}\sum_{j\in\mathcal{M}}\frac{e^{-i|\mu-q|\operatorname{sgn}(j)\psi_j}}{\sin\psi_j} - \frac{2i^{\mu-q+1}}{ka_1}\sum_{j\in\mathcal{M}}\frac{1}{\sin\psi_j}\left(\frac{e^{i(q-\mu)\psi_j}z}{z-p_j} - \frac{e^{i(\mu-q)\psi_j}}{z\tau_j-1}\right), \tag{4.3.3}$$

is a function, which has singularities only on the unit circle, and finally

$$K^2_{\mu q}(z) = -\frac{2i^{\mu-q+1}}{ka_1}\sum_{j\in\mathcal{N}}\frac{1}{\sin\psi_j}\left(\frac{e^{i(q-\mu)\psi_j}z}{z-p_j} - \frac{e^{i(\mu-q)\psi_j}}{z\tau_j-1}\right). \tag{4.3.4}$$

is a function that is analytic on the unit circle. The sets $\mathcal{M}$ and $\mathcal{N}$ are defined in (B.1.13) and (B.1.14), respectively, and

$$\operatorname{sgn}(j) = \begin{cases} +1, & j \geqslant 0, \\ -1, & j < 0. \end{cases} \tag{4.3.5}$$

We first examine the diagonal elements of the matrix, each one of which may be written as a sum of the constant

$$c_{qq} = iZ_q^{-1} + i\mathcal{S}_0^0 - \frac{2i}{ka_1}\sum_{j\in\mathcal{M}}\frac{1}{\sin\psi_j}, \tag{4.3.6}$$

and the term

$$K^1_{qq}(z) + K^2_{qq}(z) = -\frac{2i}{ka_1}\sum_{j\in\mathcal{M}}\frac{(\tau_j p_j - 1)z}{\sin\psi_j(z-p_j)(\tau_j z-1)} - \frac{2i}{ka_1}\sum_{j\in\mathcal{N}}\frac{1}{\sin\psi_j}\left(\frac{z}{z-p_j} - \frac{1}{z\tau_j-1}\right). \tag{4.3.7}$$

In the last equation, if we replace z with $1/z^*$ and take the complex conjugate of the whole expression, then with the aid of (B.1.17), and (B.1.18), we find that

$$\Big(K^1_{qq}(1/z^*) + K^2_{qq}(1/z^*)\Big)^* = K^1_{qq}(z) + K^2_{qq}(z), \quad q = -Q \dots Q. \tag{4.3.8}$$

Returning to (4.3.6), if we write $\mathcal{S}^0_0$ explicitly using (B.2.5), we obtain

$$c_{qq} = i(Z_q^{-1} - 1) + \frac{2}{\pi}\Big(\mathfrak{c} + \ln\frac{ka_1}{4\pi}\Big) - \frac{1}{\pi}\sum_{\substack{j\in\mathcal{M}\\ j\neq 0}}\frac{1}{|j|} + \sum_{j\in\mathcal{N}}\Big(\frac{2i}{ka_1\sin\psi_j} - \frac{1}{\pi|j|}\Big). \tag{4.3.9}$$

Observe that $i(Z_q^{-1} - 1)$ is real for all $q \in \mathbb{Z}$, and also that $\sin\psi_j$ is positive imaginary for all $j \in \mathcal{N}$. Thus, c_{qq} is real for all $q \in \mathbb{Z}$, which in view of (4.3.8), reveals the symmetry property

$$\Big(K_{qq}(1/z^*)\Big)^* = K_{qq}(z), \quad q = -Q \dots Q. \tag{4.3.10}$$

We now turn our attention to the non-diagonal elements with the aim to generalise (4.3.10). In what follows, we may assume without loss that

$$\mu < q. \tag{4.3.11}$$

We begin by proving that

$$\Big(K^i_{\mu q}(1/z^*)\Big)^* = K^i_{q\mu}(z) \quad \text{for} \quad i = 1, 2. \tag{4.3.12}$$

For $i = 2$, this can be verified easily from (4.3.4) by taking into acount (B.1.18) and the fact that $i/\sin\psi_j$ and $e^{i\psi_j}$ are both real for all $j \in \mathcal{N}$. On the other hand, for $i = 1$ we have that

$$K^1_{\mu q}(z) = \frac{2i^{\mu-q+1}}{ka_1}\Bigg(\sum_{\substack{j\in\mathcal{M}\\ j\geqslant 0}}\frac{e^{i(\mu-q)\psi_j}z\tau_j(z-p_j) - e^{i(q-\mu)\psi_j}z(z\tau_j-1)}{\sin\psi_j(z-p_j)(z\tau_j-1)} + \sum_{\substack{j\in\mathcal{M}\\ j<0}}\frac{e^{i(\mu-q)\psi_j}(z-p_j) - e^{i(q-\mu)\psi_j}p_j(z\tau_j-1)}{\sin\psi_j(z-p_j)(z\tau_j-1)}\Bigg), \tag{4.3.13}$$

and

$$K^1_{q\mu}(z) = \frac{2i^{q-\mu+1}}{ka_1}\left(\sum_{\substack{j\in\mathcal{M}\\ j\geqslant 0}} \frac{e^{i(q-\mu)\psi_j}(z-p_j) - e^{i(\mu-q)\psi_j}p_j(z\tau_j-1)}{\sin\psi_j(z-p_j)(z\tau_j-1)}\right.$$
$$\left. + \sum_{\substack{j\in\mathcal{M}\\ j<0}} \frac{e^{i(q-\mu)\psi_j}z\tau_j(z-p_j) - e^{i(\mu-q)\psi_j}z(z\tau_j-1)}{\sin\psi_j(z-p_j)(z\tau_j-1)}\right). \quad (4.3.14)$$

Using (B.1.17), and the fact that ψ_j is real for $j \in \mathcal{M}$, we can substitute $1/z^*$ in (4.3.13) and then take the conjugate of the whole expression to arrive at (4.3.14). We now move on to examine how the constant parts of the non-diagonal elements are related. In view of (4.1.10) and (B.2.6) , we have that

$$c_{\mu q} = (-1)^{q-\mu} i^{q-\mu+1}\left(\frac{2}{ka_1}\sum_{j=-\infty}^{\infty}\frac{e^{i(q-\mu)\operatorname{sgn}(j)\psi_j}}{\sin\psi_j} + i\mathcal{B}_{q-\mu}\right)$$
$$- \frac{2i^{\mu-q+1}}{ka_1}\sum_{j\in\mathcal{M}}\frac{e^{i(\mu-q)\operatorname{sgn}(j)\psi_j}}{\sin\psi_j}, \quad (4.3.15)$$

whereas (see also (B.2.8)),

$$c_{q\mu} = i^{q-\mu+1}\left(\frac{2}{ka_1}\sum_{j=-\infty}^{\infty}\frac{e^{i(q-\mu)\operatorname{sgn}(j)\psi_j}}{\sin\psi_j} + i\mathcal{B}_{q-\mu}\right) - \frac{2i^{q-\mu+1}}{ka_1}\sum_{j\in\mathcal{M}}\frac{e^{i(\mu-q)\operatorname{sgn}(j)\psi_j}}{\sin\psi_j}. \quad (4.3.16)$$

where $\mathcal{B}_q$, is real for $q = 1, 2, \ldots$, and its definition is given in (B.2.7). From the last two equations we can derive some useful conclusions. If $q - \mu$ is an odd number, then observe that $c_{\mu q} = -c_{q\mu}$, and also after some algebra we can show that $c_{\mu q}$ is pure imaginary. On the other hand, if $q - \mu$ is an even number then $c_{\mu q} = c_{q\mu}$, and $c_{\mu q} \in \mathbb{R}$. Thus, in any case we have that

$$c^*_{\mu q} = c_{q\mu}. \quad (4.3.17)$$

To sumarise, in view of (4.3.10), (4.3.12), and (4.3.17), we can conclude that the elements of the kernel are related via

$$\left(K_{\mu q}(1/z^*)\right)^* = K_{q\mu}(z), \quad q = -Q, \ldots, Q, \;\; \mu = -Q, \ldots, Q, \quad (4.3.18)$$

or equivalently, the kernel has the symmetry property

$$\left(\mathbf{K}(1/z^*)\right)^* = \mathbf{K}(z). \tag{4.3.19}$$

Note that the asterisk is used to denote the conjugate of a function, whereas when it is applied to a matrix it denotes the conjugate transpose.

4.4 The method of solution

The standard method to solve the matrix Wiener–Hopf equation (4.2.7), is to decompose the matrix kernel into the product

$$\mathbf{K}(z) = \mathbf{K}^-(z)\mathbf{K}^+(z), \tag{4.4.1}$$

where $\mathbf{K}^\pm(z)$ denotes a matrix whose elements are functions analytic in $C^\pm$ and also that its determinant is zero free in $C^\pm$. Substituting this factorisation in (4.2.7) we have that

$$\mathbf{K}^+(z)\mathbf{A}^+(z) = \left(\mathbf{K}^-(z)\right)^{-1}\mathbf{T}^+(z) + \left(\mathbf{K}^-(z)\right)^{-1}\mathbf{T}^-(z). \tag{4.4.2}$$

We now move the pole that the elements of $\mathbf{T}^+(z)$ have at the point $z = p_0$ to the left hand side by subtracting from both sides the column vector $\left(\mathbf{K}^-(p_0)\right)^{-1}\mathbf{T}^+(z)$, that is

$$\begin{aligned}\mathbf{K}^+(z)\mathbf{A}^+(z) - \left(\mathbf{K}^-(p_0)\right)^{-1}\mathbf{T}^+(z)& \\ = \left(\left(\mathbf{K}^-(z)\right)^{-1} - \left(\mathbf{K}^-(p_0)\right)^{-1}\right)\mathbf{T}^+(z) + \left(\mathbf{K}^-(z)\right)^{-1}\mathbf{T}^-(z).&\end{aligned} \tag{4.4.3}$$

The left-hand side of the last equation is a column vector whose elements are analytic in C^+, whereas the elements of the vector in right-hand side are analytic in C^-. Therefore, there exists a column vector $\mathbf{V}(z)$ whose elements are entire functions and which represents the analytic continuation of both sides of (4.4.3). Note that from the condition (4.2.6) we must have $\mathbf{V}(z) \to \mathbf{0}$ as $z \to \infty$. Thus, Liouville's theorem dictates that $\mathbf{V}(z) = \mathbf{0}$, and consequently

$$\mathbf{A}^+(z) = \left(\mathbf{K}^+(z)\right)^{-1}\left(\mathbf{K}^-(p_0)\right)^{-1}\mathbf{T}^+(z). \tag{4.4.4}$$

As we pointed out in §2.5.1 the factorisation (4.4.1) always exists, but in practice it is extremely difficult to find it. However, in this particular problem, an alternative approach to solve (4.2.7) is possible. To proceed we first approximate the functions $K_{\mu q}(z)$ given in (4.2.16) by truncating the sum over j. We introduce the parameter ν which denotes the order of truncation and write

$$\mathcal{K}_{\mu q}(z) = i\Big(Z_q^{-1}\delta_{\mu q} + \mathcal{S}_0^{q-\mu}\Big) - \frac{2i^{\mu-q+1}}{ka_1}\sum_{j=-\nu}^{\nu}\frac{1}{\sin\psi_j}\left(\frac{e^{i(q-\mu)\psi_j}z}{z-p_j} - \frac{e^{i(\mu-q)\psi_j}}{z\tau_j - 1}\right). \tag{4.4.5}$$

The physical meaning of this approximation is explained in §3.3.2.

4.4.1 The form of the unknown functions

The method that will be used to solve (4.2.7) is quite similar to the Wiener–Hopf procedure. The major difference is that we will sum-split the kernel instead of decomposing it into a product. The idea is to determine the column vector $\mathbf{T}^-(z)$, and then use this result to obtain $\mathbf{A}^+(z)$. We begin with the sum decomposition

$$\mathbf{K}(z) = \mathbf{K}^+(z) + \mathbf{K}^-(z), \tag{4.4.6}$$

where

$$\mathbf{K}^\pm(z) = \left[\mathcal{K}^\pm_{\mu q}(z)\right]_{\mu=-Q,\ldots,Q;\ q=-Q,\ldots,Q}, \tag{4.4.7}$$

with

$$\mathcal{K}^+_{\mu q}(z) = i\Big(Z_q\delta_{\mu q} + \mathcal{S}_0^{q-\mu}\Big) - \frac{2i^{\mu-q+1}}{ka_1}\sum_{j=-\nu}^{\nu}\frac{e^{i(q-\mu)\psi_j}z}{\sin\psi_j(z-p_j)}, \tag{4.4.8}$$

and

$$\mathcal{K}^-_{\mu q}(z) = \frac{2i^{\mu-q+1}}{ka_1}\sum_{j=-\nu}^{\nu}\frac{e^{i(\mu-q)\psi_j}}{\sin\psi_j(z\tau_j - 1)}. \tag{4.4.9}$$

Substituting (4.4.6) into (4.2.7), yields

$$\mathbf{K}^+(z)\mathbf{A}^+(z) + \mathbf{K}^-(z)\mathbf{A}^+(z) - \mathbf{T}^+(z) = \mathbf{T}^-(z). \tag{4.4.10}$$

The right-hand side of this equation is analytic in C^-, whereas the left-hand side is analytic in C^+ except at the points $z = \tau_j^{-1}$, where the matrix $\mathbf{K}^-(z)$ has simple

poles. To move these poles to the right-hand side we introduce the column vector

$$\mathbf{M}^-(z) = \left[\frac{2i}{ka_1}\sum_{j=-\nu}^{\nu}\frac{e^{i\mu(\psi_j+\pi/2)}}{\sin\psi_j(z\tau_j-1)}\sum_{q=-Q}^{Q}e^{-iq(\psi_j+\pi/2)}A_q^+(\tau_j^{-1})\right]_{\mu=-Q,\ldots,Q} \tag{4.4.11}$$

which we subtract from both sides to obtain

$$\mathbf{K}^+(z)\mathbf{A}^+(z) + \mathbf{K}^-(z)\mathbf{A}^+(z) - \mathbf{M}^-(z) - \mathbf{T}^+(z) = \mathbf{T}^-(z) - \mathbf{M}^-(z). \tag{4.4.12}$$

In this way we have reached an equation in which the left-hand side is analytic in C^+ and the right-hand side is analytic C^-. Hence, we can conclude that the two sides represent the analytic continuation of each other, and moreover that both actually represent the same entire function. Since the right-hand side tends to zero as $z \to \infty$ (see (4.2.6)), Liouville's theorem dictates that the entire function must be zero, and therefore

$$\mathbf{T}^-(z) = \mathbf{M}^-(z). \tag{4.4.13}$$

From the last equation, and (4.4.11) we can conclude that the entries of the column vector $\mathbf{T}^-(z)$, are meromorphic functions with simple poles at the points $z = 1/\tau_j$, for $j = -\nu, \ldots, \nu$. Moreover, the exact form of these functions depends on the $(2Q+1)(2\nu+1)$ unknowns $A_q^+(1/\tau_j)$. The crucial observation here is that in order to determine $T_\mu^-(z)$, we do not need to explicitly specify all the unknowns. Instead, since they appear in combinations, we can write

$$T_\mu^-(z) = \frac{2i}{ka_1}\sum_{j=-\nu}^{\nu}\frac{e^{i\mu(\psi_j+\pi/2)}}{\sin\psi_j(z\tau_j-1)}X_j, \quad \mu = -Q, \ldots, Q, \tag{4.4.14}$$

where

$$X_j = \sum_{q=-Q}^{Q}e^{-iq(\psi_j+\pi/2)}A_q^+(\tau_j^{-1}), \quad j = -\nu, \ldots \nu, \tag{4.4.15}$$

and then determine the $2\nu + 1$ unknown parameters X_j. This will be addressed in §4.4.3, where we will construct a system of $2\nu+1$ system of algebraic equation for X_j.

So far, we have relied on an implicit description of the closed curve C, which was given by the condition (4.2.18), and as it turns out the fact that

$$\tau_j^{-1} \in C^+ - C, \quad \text{for} \quad j = -\nu, \ldots, \nu, \tag{4.4.16}$$

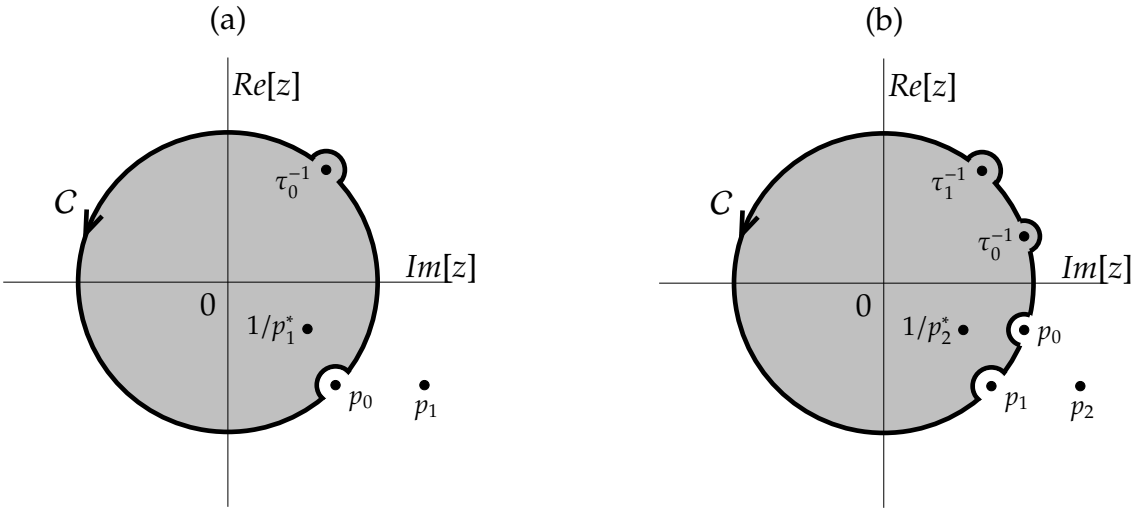

Figure 4.1: *The closed curve C where the Wiener–Hopf equation holds in the case where $A_q^+(z)$ is free of singularities on the unit circle, and also in the case of (a) $\mathcal{M} = \{0\}$ and (b) $\mathcal{M} = \{0, 1\}$. Functions with a superscript '+' ('−') are analytic in the (un)shaded region.*

is a necessary and sufficient condition to establish the analyticity of the functions $T_\mu^-(z)$ in C^-. The shape of C can become more specific, if we examine the form of the functions $A_q^+(z)$. It is clear these functions must be meromorphic, and in addition, all of their poles must lie in the region where $|z| \geqslant 1$, or else the coefficients A_{0n}^q grow exponentially as $n \to \infty$, which is unphysical. Using this information we can conclude that in the case where all of these poles lie in the region $|z| > 1$, the closed curve C may chosen to be the unit circle indented so as to include the points τ_j^{-1} and to exclude the points p_j, for all $j \in \mathcal{M}$; see figure 4.1. On the other hand, if it turns out that $A_q^+(z)$ has a pole on the unit circle then an extra indentation will be required in order for C to exclude this pole.

4.4.2 The kernel in terms of a polynomial matrix

The zeros of the determinant of the kernel play crucial role in the solution of the problem, and to simplify the linear algebra required for our method, we will write the matrix kernel in polynomial form by pulling out its poles. To begin,

we introduce the polynomials

$$\mathcal{P}(z) = \prod_{n=-\nu}^{\nu}(z - p_n), \qquad \mathcal{T}(z) = \prod_{n=-\nu}^{\nu}(z - \tau_n^{-1}), \tag{4.4.17}$$

$$\mathcal{P}_j(z) = \prod_{\substack{n=-\nu \\ n\neq j}}^{\nu}(z - p_n), \qquad \mathcal{T}_j(z) = \prod_{\substack{n=-\nu \\ n\neq j}}^{\nu}(z - \tau_n^{-1}), \quad j = -\nu, \ldots \nu, \tag{4.4.18}$$

and

$$\begin{aligned} P_{\mu q}(z) = {} & i\Big(Z_q^{-1}\delta_{\mu q} + \mathcal{S}_0^{q-\mu}\Big)\mathcal{P}(z)\mathcal{T}(z) \\ & - \frac{2i^{\mu-q+1}}{ka_1}\sum_{j=-\nu}^{\nu}\frac{1}{\sin\psi_j}\Big(ze^{i(q-\mu)\psi_j}\mathcal{P}_j(z)\mathcal{T}(z) - \tau_j^{-1}e^{i(\mu-q)\psi_j}\mathcal{P}(z)\mathcal{T}_j(z)\Big). \end{aligned} \tag{4.4.19}$$

With this notation, the matrix kernel can be written

$$\mathbf{K}(z) = \frac{1}{\mathcal{P}(z)\mathcal{T}(z)}\mathbf{P}(z), \tag{4.4.20}$$

where

$$\mathbf{P}(z) = \Big[P_{\mu q}(z)\Big]_{\mu=-Q,\ldots,Q;\ q=-Q,\ldots,Q}. \tag{4.4.21}$$

Suppose that $D(z)$ denotes the determinant of $\mathbf{P}(z)$, then the symmetry property (4.3.19) dictates that

$$D(z) = 0 \Leftrightarrow D(1/z^*) = 0. \tag{4.4.22}$$

It is evident that the degree of $D(z)$ is at most d, where $d = 2(2Q+1)(2\nu+1)$, and therefore we can write

$$D(z) = \sum_{j=0}^{d} a_j z^j. \tag{4.4.23}$$

In fact, it turns out that that there are only two possibilities: either the degree is precisely d, or $D(z)$ is the zero function. To see this, we begin by noting that (4.4.22) yields

$$\det\Big(\mathbf{K}(0)\Big) = \frac{a_0}{\mathcal{P}^{2Q+1}(0)\mathcal{T}^{2Q+1}(0)}. \tag{4.4.24}$$

Since $\mathcal{P}(z)$ and $\mathcal{T}(z)$ are monic polynomials of degree $2\nu+1$, we also have

$$\lim_{z\to\infty}\det\Big(\mathbf{K}(z)\Big) = a_d. \tag{4.4.25}$$

In view of the symmetry relation (4.3.19), we may conclude that

$$a_d^* = \frac{a_0}{\mathcal{P}^{2Q+1}(0)\mathcal{T}^{2Q+1}(0)}. \tag{4.4.26}$$

Thus, if $a_d = 0$, then $a_0 = D(0) = 0$. However, equation (4.4.24) now shows that $D(z) \to 0$ as $z \to \infty$, meaning that $D(z)$ is the zero function. We have not encountered any parameters for which this pathological case actually occurs, and in any case we are free to increase ν, thereby altering the approximate kernel matrix. Consequently, in what follows, we will assume that $D(z)$ is not the zero function, and therefore that its degree is precisely d. Clearly, this means that no two rows of $\mathbf{P}(z)$ are linearly dependent for arbitrary z. That is, no linear combination of rows yields the zero function, and so the rank of the polynomial matrix $\mathbf{P}(z)$ is $2Q+1$. However, if we fix a particular value of z, we may find that the resulting constant matrix has a lower rank. Such values are called *latent roots* of $\mathbf{P}(z)$. Crucially, these latent roots are precisely the zeros of the determinant $D(z)$ (see appendix A.4 for details).

Now $\mathcal{P}(p_j) = 0$ and $\mathcal{P}_n(p_j) = 0$ if $n \neq j$, so (4.4.19) yields

$$P_{\mu q}(p_j) = -\frac{2ip_j}{ka_1 \sin\psi_j}\mathcal{P}_j(p_j)\mathcal{T}(p_j)i^{\mu-q}e^{i(q-\mu)\psi_j}, \tag{4.4.27}$$

and similarly

$$P_{\mu q}(\tau_j^{-1}) = \frac{2i\tau_j^{-1}}{ka_1 \sin\psi_j}\mathcal{P}(\tau_j^{-1})\mathcal{T}_j(\tau_j^{-1})i^{\mu-q}e^{i(\mu-q)\psi_j}. \tag{4.4.28}$$

Thus, each successive row of $\mathcal{P}(p_j)$ is obtained by multiplying the previous row by $ie^{-i\psi_j}$, meaning no two are linearly independent, and so p_j is a latent root of rank $2Q$. The same reasoning applies to the matrix $\mathbf{P}(\tau_j^{-1})$, and so property (i) in appendix A.4 now shows that

$$D(z) = \mathcal{P}^{2Q}(z)\mathcal{T}^{2Q}(z)D_1(z), \tag{4.4.29}$$

where $D_1(z)$ is a polynomial of degree $4\nu + 2$. Furthermore, it now follows from property (ii) in appendix A.4 that

$$\operatorname{adj}\Big(\mathbf{P}(z)\Big) = \mathcal{P}^{2Q-1}(z)\mathcal{T}^{2Q-1}(z)\mathbf{F}(z), \tag{4.4.30}$$

for some polynomial matrix $\mathbf{F}(z)$.

4.4.3 The solution

We are now in the position to determine the elements of the column vector $\mathbf{T}^-(z)$ by forming a system of $2\nu+1$ equations for the unknown parameters X_j, $j=-\nu,\dots\nu$. We begin by substituting (4.4.20) into the Wiener–Hopf equation (4.2.7), to obtain

$$\frac{1}{\mathcal{P}(z)\mathcal{T}(z)}\mathbf{P}(z)\mathbf{A}^+(z)=\mathbf{T}^+(z)+\mathbf{T}^-(z). \tag{4.4.31}$$

Next, we multiply (4.4.31) by the adjugate of $\mathbf{P}(z)$, which in view of (4.4.30), and (4.4.29), yields

$$D_1(z)\mathbf{A}^+(z)=\mathbf{F}(z)\Big(\mathbf{T}^+(z)+\mathbf{T}^-(z)\Big). \tag{4.4.32}$$

Initially, we assume that none of the zeros of $D_1(z)$ lies on the unit circle. From the symmetry relation (4.4.22) we can conclude that there are $2\nu+1$ zeros outside the unit circle at the points $z=z_j$, $j=-\nu,\dots,\nu$, say and an equal number of zeros inside the unit circle, located at the points $z=1/z_j^*$. Since $\mathbf{A}^+(z)$ is analytic inside the unit circle, equation (4.4.32) yields

$$\mathbf{F}(1/z_j^*)\Big(\mathbf{T}^+(1/z_j^*)+\mathbf{T}^-(1/z_j^*)\Big)=0. \tag{4.4.33}$$

Now consider the case where the points $1/z_j^*$ are distinct. Then property (iii) in appendix A.4 shows that $\mathbf{F}(z_j)$ has rank 1, which means that (4.4.33) yields one linear equation for the $2\nu+1$ unknowns in the vector $\mathbf{T}^-(z)$. Since there are $2\nu+1$ zeros, the required system of equations is formed. The situation that arises if two (or more) zeros coincide is slightly more complicated. Suppose that $1/z_j^*$ is a double zero of $D_1(z)$. Then there are two possibilities. If this is a latent zero of rank two, then properties (ii) and (iii) in appendix A.4 show that the matrix

$$\hat{\mathbf{F}}(z)=\lim_{z\to 1/z_j^*}\frac{\mathbf{F}(z)}{z-1/z_j^*} \tag{4.4.34}$$

exists and has rank two. Therefore we may divide (4.4.32) by $(z-1/z_j^*)$ and set $z=1/z_j^*$ to obtain two equations for the unknowns on the right-hand side. On the other hand, if $1/z_j^*$ is a latent zero of rank one, then not all entries of the matrix $\mathbf{F}(z)$ have $z-1/z_j^*$ as a factor. In this case, setting $z=1/z_j^*$ in (4.4.32) yields one equation, and differentiating before setting $z=1/z_j^*$ yields another, because

$D_1'(1/z_j^*) = 0$. Zeros of multiplicity greater than two can be dealt with in much the same way. It is worth remarking that we have not observed any parameters for which the multiplicity of a zero of $D_1(z)$ is greater than one. Therefore, for simplicity from this point onwards we assume that all the zeros of $D_1(z)$ are distinct.

Once we determine X_j, then $\mathbf{A}^+(z)$ is known and given by

$$\mathbf{A}^+(z) = \frac{1}{D_1(z)}\mathbf{F}(z)\Big(\mathbf{T}^+(z) + \mathbf{T}^-(z)\Big). \tag{4.4.35}$$

and the amplitudes can be calculated from the integral

$$A_{0n}^{\mu} = \frac{1}{2\pi i}\oint_C A_{\mu}^+(z)\, z^{-n-1}\, dz, \quad \mu = -Q, \ldots, Q, \quad n = 0, 1, \ldots. \tag{4.4.36}$$

where the contour of integration is shown in figure 4.1. Equivalently, we can collect the residues from the poles outside the unit circle, that is

$$A_{0n}^{\mu} = -\sum_{m=-\nu}^{\nu} z_m^{-n-1}\rho_m^{\mu}, \quad \mu = -Q, \ldots, Q, \quad n = 0, 1, \ldots, \tag{4.4.37}$$

with

$$\rho_m^{\mu} = \operatorname*{Res}_{z=z_m} A_{\mu}^+(z), \quad \mu = -Q, \ldots, Q. \tag{4.4.38}$$

In case where the determinant of the kernel has N zeros on the unit circle we can use the symmetry property (4.3.19) to deduce that N is an even number. First we consider the case $N = 2$. The question arises as to how many of these zeros correspond to a pole of the function $A_{\mu}^+(z)$. To answer this question we need to look at the form of the solution that we would have obtained if had we followed the standard Wiener–Hopf procedure (see the beginning of §4.4). Although we do not know the exact form of the factors $\mathbf{K}^{\pm}(z)$ in (4.4.1), we do know (from (4.2.18)) that the points p_j should be poles of $\det\Big(\mathbf{K}^+(z)\Big)$ and the points τ_j^{-1} should be poles of $\det\Big(\mathbf{K}^-(z)\Big)$. Moreover, from (4.4.20) and (4.4.29), we have that

$$\det\Big(\mathbf{K}(z)\Big) = \frac{D_1(z)}{\mathcal{P}(z)\mathcal{T}(z)}. \tag{4.4.39}$$

Hence, we can write

$$\det\Big(\mathbf{K}^+(z)\Big) = \frac{D_1^+(z)}{\mathcal{P}(z)}, \quad \text{and} \quad \det\Big(\mathbf{K}^-(z)\Big) = \frac{D_1^-(z)}{\mathcal{T}(z)}, \tag{4.4.40}$$

where $D_1^{\pm}(z)$ is a polynomial that is zero free in $C^{\pm}$, such that

$$D_1(z) = D_1^{+}(z)D_1^{-}(z). \tag{4.4.41}$$

Now, since

$$\Big(\mathbf{K}^{+}(z)\Big)^{-1} = \frac{\mathcal{P}(z)}{D_1^{+}(z)}\,\mathrm{adj}\Big(\mathbf{K}^{+}(z)\Big), \tag{4.4.42}$$

a zero of $D_1^{+}(z)$ corresponds to a pole for the column vector $\mathbf{A}^{+}(z)$ (see (4.4.4)), and this means that all the zeros of $D_1(z)$ which lie inside the unit circle (in total 2ν) should be zeros of $D_1^{-}(z)$. Also, since the matrix

$$\Big(\mathbf{K}^{-}(z)\Big)^{-1} = \frac{\mathcal{T}(z)}{D_1^{-}(z)}\,\mathrm{adj}\Big(\mathbf{K}^{-}(z)\Big), \tag{4.4.43}$$

must be analytic at infinity, $D_1^{-}(z)$ must possess one additional zero. This zero should be located on the unit circle because otherwise $\mathbf{A}^{+}(z)$ has two poles on the unit circle, and as we will see in the coming sections one of these corresponds to the existence of a Bloch wave propagating energy towards $y = 0$, which is unphysical (see also pp 50–51). To summarise, if z_0 and z_0' are the zeros of $\det\Big(\mathbf{K}(z)\Big)$ that are on the unit circle, then the solution via the standard Wiener–Hopf procedure suggests that precisely one of these is a zero of $\mathbf{K}^{+}(z)$; that is

$$z_0 \in C^{-} - C \quad \text{and} \quad z_0' \in C^{+} - C. \tag{4.4.44}$$

Given a pair of zeros on the unit circle, we will use (4.6.6) and (4.6.12) in order to determine which one to treat as z_0, and which to treat as z_0'. If z_0 is used in this calculation, then the result is positive, corresponding to a pole of $\mathbf{A}^{+}(z)$, and energy propagating into the lattice. On the other hand, if z_0' is used then the result is negative, and cannot correspond to a pole of $\mathbf{A}^{+}(z)$. Situations in which $N > 2$ are much the same; the zeros appear on the unit circle in pairs, and in each pair precisely one corresponds to a pole of $\mathbf{A}^{+}(z)$.

4.5 The far field pattern

The far field analysis is quite similar to the case presented in §3.5, and for this reason we will not elaborate on the details. We shall examine the case where

$\mathbf{A}^+(z)$ is analytic on the unit circle and the case where $\mathbf{A}^+(z)$ has a simple pole on the unit circle.

4.5.1 $\mathbf{A}^+(z)$ is analytic on the unit circle

We first consider the case where the determinant of the kernel is zero free on the unit circle. This means that the functions $A_q^+(z)$ are analytic inside and on the unit circle, and therefore

$$A_q^+(z) = \sum_{n=0}^{\infty} A_{0n}^q z^n, \quad |z| \leqslant 1. \tag{4.5.1}$$

The scattered field can be expressed in the form

$$u_{sc}(\mathbf{r}) = \sum_{q=-Q}^{Q} \sum_{n=0}^{\infty} A_{0n}^q G_q^{(1)}(\mathbf{r} - n\mathbf{a}_2, k\cos\psi_0), \tag{4.5.2}$$

where G_q^1 is the 1D quasi-periodic function defined in (B.1.19). Using the spectral representation (B.1.23), we have that

$$u_{sc}(\mathbf{r}) = \frac{2}{ka_1} \sum_{q=-Q}^{Q} \sum_{n=0}^{\infty} \sum_{j=-\infty}^{\infty} A_{0n}^q \frac{e^{iq\left(\psi_j \operatorname{sgn}(y-n\eta_2)-\pi/2\right)}}{\sin\psi_j} e^{ik\left((x-n\eta_1)\cos\psi_j + |y-n\eta_2|\sin\psi_j\right)}. \tag{4.5.3}$$

From the last expression, the Taylor expansion (4.5.1) and the fact that $\sin\psi_j$ is positive imaginary for $j \in \mathcal{N}$, we can determine the behaviour of the scattered field in the limit $y \to \pm\infty$; thus

$$u_{sc}(\mathbf{r}) \sim \sum_{j\in\mathcal{M}} c_j^{\pm} e^{ik(x\cos\psi_j \pm y\sin\psi_j)} \quad \text{as} \quad y \to \pm\infty, \tag{4.5.4}$$

where

$$c_j^- = \frac{2}{ka_1\sin\psi_j} \sum_{q=-Q}^{Q} A_q^+(\tau_j^{-1}) e^{-iq(\psi_j+\pi/2)}, \tag{4.5.5}$$

and

$$c_j^+ = \frac{2}{ka_1\sin\psi_j} \sum_{q=-Q}^{Q} A_q^+(p_j) e^{iq(\psi_j-\pi/2)}. \tag{4.5.6}$$

Note that from (4.4.15)

$$c_j^- = \frac{2X_j}{ka_1\sin\psi_j}. \tag{4.5.7}$$

A further simplification of (4.5.6) occurs if we multiply both sides of (4.4.31) by $(z - p_j)$, take the limit $z \to p_j$, and use (4.4.27). In this way we find that

$$c_j^+ = \begin{cases} -1, & j = 0, \\ 0, & j \neq 0, \end{cases} \tag{4.5.8}$$

and hence,

$$u_{sc}(\mathbf{r}) \sim -e^{ik(x\cos\psi_0 + y\sin\psi_0)} \quad \text{as} \quad y \to +\infty, \tag{4.5.9}$$

which means that the scattered field cancels out the incident wave in this limit.

4.5.2 $\mathbf{A}^+(z)$ has a pole on the unit circle

We now consider the case where $\mathbf{A}^+(z)$ is analytic inside and on the unit circle except at the point $z = z_0$, where it has a simple pole. We first use (4.4.37) to split the amplitudes into two terms

$$A_{0n}^q = \hat{A}_{0n}^q - \rho_0^q z_0^{-n-1}, \tag{4.5.10}$$

where

$$\hat{A}_{0n}^q = -\sum_{\substack{m=-\nu \\ m\neq 0}}^{\nu} \rho_m^q z_m^{-n-1}, \tag{4.5.11}$$

and ρ_m^q is given by (4.4.38). Accordingly, we split the scattered field into two parts

$$u_{sc}(\mathbf{r}) = u_a(\mathbf{r}) + u_b(\mathbf{r}), \tag{4.5.12}$$

where

$$u_a(\mathbf{r}) = \sum_{q=-Q}^{Q} \sum_{n=0}^{\infty} \sum_{j=-\infty}^{\infty} \hat{A}_{0n}^q e^{ijka_1\cos\psi_0} \mathcal{H}_q(\mathbf{r} - \mathbf{R}_{jn}), \tag{4.5.13}$$

and

$$u_b(\mathbf{r}) = -\frac{1}{z_0} \sum_{q=-Q}^{Q} \rho_0^q \sum_{n=0}^{\infty} \sum_{j=-\infty}^{\infty} e^{i\mathbf{R}_{jn}\cdot\boldsymbol{\beta}(z_0)} \mathcal{H}_q(\mathbf{r} - \mathbf{R}_{jn}), \tag{4.5.14}$$

with $\boldsymbol{\beta}(z)$ defined in (3.3.8) (we also used (3.3.9)). For the first field, since $\sum_{n=0}^{\infty} |\hat{A}_{0n}^q| < \infty$, we can use the method of §3.5.2 to obtain

$$u_a(\mathbf{r}) \sim \sum_{j\in\mathcal{M}} \hat{c}_j^{\pm} e^{ik(x\cos\psi_j \pm y\sin\psi_j)} \quad \text{as} \quad y \to \pm\infty, \tag{4.5.15}$$

where now

$$\hat{c}_j^- = \frac{2}{ka_1 \sin\psi_j} \sum_{q=-Q}^{Q} \left(A_q^+(\tau_j^{-1}) - \frac{\rho_0^q}{\tau_j^{-1} - z_0} \right) e^{-iq(\psi_j + \pi/2)}, \tag{4.5.16}$$

and

$$\hat{c}_j^+ = \frac{2}{ka_1 \sin\psi_j} \sum_{q=-Q}^{Q} \left(A_q^+(p_j) - \frac{\rho_0^q}{p_j - z_0} \right) e^{iq(\psi_j - \pi/2)}. \tag{4.5.17}$$

The last coefficient can be simplified (see previous section) to

$$\hat{c}_j^+ = -\delta_{j0} - \frac{2}{ka_1 \sin\psi_j} \sum_{q=-Q}^{Q} \rho_0^q \frac{e^{iq(\psi_j - \pi/2)}}{p_j - z_0}. \tag{4.5.18}$$

The behaviour of the field u_b in the limit $y \to \pm\infty$ can be determined by first expressing it in terms of quasi-periodic arrays of singularities defined in appendix B. For $y > 0$, we have

$$u_b(\mathbf{r}) = -\frac{1}{z_0} \sum_{q=-Q}^{Q} \rho_0^q \Big(G_q^{(2)}(\mathbf{r}, \boldsymbol{\beta}(z_0)) - G_q^+(\mathbf{r}, \boldsymbol{\beta}(z_0)) \Big), \tag{4.5.19}$$

where $G_q^{(2)}$ is defined in (B.1.5) and G_q^+ is given by (B.1.24). Using (B.1.32) and the fact that $i \sin\psi_j < 0$ for $j \in \mathcal{N}$ yields

$$\begin{aligned} u_b(\mathbf{r}) \sim & -\frac{1}{z_0} \sum_{q=-Q}^{Q} \rho_0^q G_q^{(2)}(\mathbf{r}, \boldsymbol{\beta}(z_0)) \\ & + \frac{2}{ka_1} \sum_{q=-Q}^{Q} \rho_0^q \sum_{j \in \mathcal{M}} \frac{e^{iq(\psi_j - \pi/2)}}{\sin\psi_j (p_j - z_0)} e^{ik(x\cos\psi_j + y\sin\psi_j)} \quad \text{as} \quad y \to +\infty. \end{aligned} \tag{4.5.20}$$

On the other hand, for $y < 0$, we write

$$u_b(\mathbf{r}) = -\frac{1}{z_0} \sum_{q=-Q}^{Q} \rho_0^q \Big(G_q^{(1)}(\mathbf{r}, k\cos\psi_0) + G_q^-(\mathbf{r}, \boldsymbol{\beta}(z_0)) \Big), \tag{4.5.21}$$

where $G_q^{(1)}$ is given in (B.1.3). Substituting the spectral representations (B.1.23) and (B.1.33) in (4.5.21), yields

$$u_b(\mathbf{r}) \sim \frac{2}{ka_1} \sum_{q=-Q}^{Q} \rho_0^q \sum_{j \in \mathcal{M}} \frac{e^{-iq(\psi_j + \pi/2)}}{\sin\psi_j (\tau_j^{-1} - z_0)} e^{ik(x\cos\psi_j - y\sin\psi_j)} \quad \text{as} \quad y \to -\infty. \tag{4.5.22}$$

To summarise, in the upper half plane in view of (4.5.15), (4.5.18), and (4.5.20), we have that

$$u_{sc}(\mathbf{r}) \sim -\frac{1}{z_0}\sum_{q=-Q}^{Q}\rho_0^q G_q^{(2)}(\mathbf{r},\boldsymbol{\beta}(z_0)) - e^{ik(x\cos\psi_0+y\sin\psi_0)} \quad \text{as} \quad y\to+\infty, \tag{4.5.23}$$

and so the far field pattern of takes the form of a Bloch waves with a Bloch wave vector $\boldsymbol{\beta}(z_0)$, plus a plane wave which cancels the incident wave. In the lower half plane (4.5.15), (4.5.16) and (4.5.22) reveal that the behaviour of the scattered field in the limit $y\to-\infty$ is again given by (4.5.4) and (4.5.7).

4.6 Conservation of energy

As we have seen in §3.6, the principle of conversation of energy dictates that

$$-\frac{P_0\omega}{2}Im\int_S u(\mathbf{r})\left(\frac{\partial u(\mathbf{r})}{\partial n}\right)^* ds = 0, \tag{4.6.1}$$

where S is chosen to be the parallelogram whose vertices are given in (3.6.3) (see figure 3.7). Using the same notation we denote the integrals along the side of this parallelogram by $I_1,\dots,I_4$, and equation (3.1.13) shows that

$$I_1 + I_3 = 0. \tag{4.6.2}$$

Therefore, in order to show that energy is conserved we need only to evaluate the integrals I_2 and I_4. Following the same procedure as in §3.6, we take the limit $N\to\infty$ (where N is associated with the vertices of S; see (3.6.3)), in order to discard contributions that decay as $y\to\pm\infty$. In the lower half plane we use the asymptotic formula

$$u(\mathbf{r}) \sim e^{ik(x\cos\psi_0+y\sin\psi_0)} + \sum_{j\in\mathcal{M}} c_j^- e^{ik(x\cos\psi_j-y\sin\psi_j)} \quad \text{as} \quad y\to-\infty, \tag{4.6.3}$$

to obtain

$$I_4 = -\frac{P_0\omega^2}{2c}a_1\left(\sin\psi_0 - \sum_{j\in\mathcal{M}}|c_j^-|^2\sin\psi_j\right). \tag{4.6.4}$$

In the upper half plane the integral I_2 depends on whether or not $\mathbf{A}^+(z)$ has a pole on the unit circle. If $\mathbf{A}^+(z)$ is analytic on the unit circle then we have

that $u(\mathbf{r}) \to 0$, as $y \to \infty$, which means that $I_2 = 0$. On the other hand, if $\mathbf{A}^+(z)$ possesses a pole that lies on the unit circle, then a Bloch wave is presented in the far field, and from (4.5.23) we have

$$u(\mathbf{r}) \sim -\frac{1}{z_0} \sum_{q=-Q}^{Q} \rho_0^q G_q^{(2)}(\mathbf{r}, \boldsymbol{\beta}(z_0)), \quad \text{as} \quad y \to +\infty. \tag{4.6.5}$$

In this situation the integral I_2 can be decomposed as follows

$$I_2 = -\frac{P_0 \omega}{2} \sum_{q=-Q}^{Q} \sum_{m=-Q}^{Q} Im\left[\rho_0^q (\rho_0^m)^* \mathcal{I}_{qm}\right], \tag{4.6.6}$$

where

$$\mathcal{I}_{qm} = \int_{S_2} G_q^{(2)}(\mathbf{r}, \boldsymbol{\beta}(z_0)) \frac{\partial}{\partial y}\left[G_m^{(2)}(\mathbf{r}, \boldsymbol{\beta}(z_0))\right]^* ds. \tag{4.6.7}$$

To evaluate the integrals $\mathcal{I}_{qm}$ we introduce the parametrisation

$$S_2 \,:\, \mathbf{r}(t) = (t + N\eta_1/2,\ N\eta_2/2), \quad -a_1/2 \le t \le a_1/2. \tag{4.6.8}$$

From (B.1.6), it is evident that the integrand in (4.6.7) is independent of N, and so we choose the value $N = 1$ so as to enable the use of (B.1.36). Hence, on this particular path we have

$$G_q^{(2)}(\mathbf{r}(t), \boldsymbol{\beta}(z_0)) = -\frac{2(-i)^q}{ka_1} \sum_{j=-\infty}^{\infty} \frac{e^{ikt\cos\psi_j}}{\sin\psi_j}\left(\frac{p_j^{1/2} e^{iq\psi_j}}{z_0 - p_j} - \frac{\tau_j^{1/2} e^{-iq\psi_j}}{\tau_j z_0 - 1}\right), \tag{4.6.9}$$

$$\frac{\partial}{\partial y}\left[G_m^{(2)}(\mathbf{r}(t), \boldsymbol{\beta}(z_0))\right]^* = \frac{2i^{m+1}}{a_1} \sum_{j=-\infty}^{\infty} e^{-ikt\cos\psi_j}\left(\frac{p_j^{1/2} e^{im\psi_j}}{z_0 - p_j} + \frac{\tau_j^{1/2} e^{-im\psi_j}}{\tau_j z_0 - 1}\right)^*, \tag{4.6.10}$$

and

$$G_q^{(2)}(\mathbf{r}(t), \boldsymbol{\beta}(z_0)) \frac{\partial}{\partial y}\left[G_m^{(2)}(\mathbf{r}(t), \boldsymbol{\beta}(z_0))\right]^* = -\frac{4i^{m-q+1}}{ka_1^2} \sum_{j=-\infty}^{\infty} \sum_{n=-\infty}^{\infty} \frac{e^{2it(j-n)\pi/a_1}}{\sin\psi_j} \times \left(\frac{p_j^{1/2} e^{iq\psi_j}}{z_0 - p_j} - \frac{\tau_j^{1/2} e^{-iq\psi_j}}{\tau_j z_0 - 1}\right)\left(\frac{p_n^{1/2} e^{im\psi_n}}{z_0 - p_n} + \frac{\tau_n^{1/2} e^{-im\psi_n}}{\tau_n z_0 - 1}\right)^*. \tag{4.6.11}$$

Now, if we substitute the last equation in (4.6.7), and perform the integration over t, then only the terms in which $j = n$ are non zero, and therefore

$$\mathcal{I}_{qm} = -\frac{4i^{m-q+1}}{ka_1} \sum_{j=-\infty}^{\infty} \frac{1}{\sin\psi_j}\left(\frac{p_j^{1/2} e^{iq\psi_j}}{z_0 - p_j} - \frac{\tau_j^{1/2} e^{-iq\psi_j}}{\tau_j z_0 - 1}\right)\left(\frac{p_j^{1/2} e^{im\psi_j}}{z_0 - p_j} + \frac{\tau_j^{1/2} e^{-im\psi_j}}{\tau_j z_0 - 1}\right)^*, \tag{4.6.12}$$

where in the numerator of the fractions inside the sum, the exponent of the poles is divided by two (see (B.1.16)). In the last series, since the points p_j and τ_j grow exponentially (see (B.1.16)), only a few terms are required for numerical calculations. In fact taking the truncation point to be ν is sufficient to verify that the equation $I_2 + I_4 = 0$ is satisfied to a high degree of accuracy.

4.7 Numerical Results

In this section we present numerical results that illustrate the band structure of the semi-infinite lattice. Most of the selected parameters for our calculations have been chosen so that an easy comparison can be made with the results given by Nicorovici et al. [43]. In particular, we aim to show that the band gaps predicted by our method are consistent with those appearing in [43, fig. 5, 6, and 7] and in addition, to reproduce the plot seen in [43, fig. 9] for Dirichlet boundary conditions, which illustrates the effect the radius of the cylinders has on the size of the first band gap. These issues are addressed in the plots seen in figure 4.2 and 4.3, and a satisfying agreement is evident in all cases.

First, we consider sound-hard cylinders, and we will restrict ourselves to cases where

$$ka_1 < \pi. \tag{4.7.1}$$

The purpose of this restriction is to ensure that $\mathcal{M} = \{0\}$ (see (B.1.13)), which in turn implies that the scattered field in the limit $y \to -\infty$ takes the form of a single plane wave of amplitude c_0^- (see (4.5.4)). Furthermore, the formula (4.6.4), which measures the difference of the energy reflected from the lattice and the energy of the incident field, reduces to

$$I_4 = -\frac{P_0\omega^2}{2c} a_1 \sin\psi_0 \Big(1 - |c_0^-|^2\Big). \tag{4.7.2}$$

From the last formula we can identify that $100 \times \left(1 - |c_0^-|^2\right)$ is the percentage of the energy transmitted into lattice and $100 \times |c_0^-|^2$ is the percentage of the energy reflected from the lattice. Hence, contour plots of the reflection coefficient $|c_0^-|$

Table 4.1: *The zero of the approximate kernel which is either on, or closest to the unit circle, for different set of parameters, with $\psi_0 = \pi/6$ and $\eta_1 = 0$ fixed, and Neumann boundary conditions are imposed on the cylinders' surface.*

Q	a_1	η_2	ℓ	k	$\nu = 1$	$\nu = 2$	$\nu = 3$
1	1	1	0.02	3	$0.066906 - 0.997759i$	$0.066906 - 0.997759i$	$0.066906 - 0.997759i$
2	1	1	0.02	3	$0.066902 - 0.997760i$	$0.066902 - 0.997760i$	$0.066902 - 0.997760i$
1	0.1	1	0.03	2	$0.498740 - 0.866752i$	$0.498740 - 0.866752i$	$0.498740 - 0.866752i$
2	0.1	1	0.03	2	$0.498635 - 0.866812i$	$0.498635 - 0.866812i$	$0.498635 - 0.866812i$
1	1	1	0.25	1	$0.786230 - 0.617933i$	$0.786232 - 0.617931i$	$0.786232 - 0.617931i$
2	1	1	0.25	1	$0.782988 - 0.622037i$	$0.782986 - 0.622039i$	$0.782986 - 0.622039i$
3	1	1	0.25	1	$0.782938 - 0.622100i$	$0.782936 - 0.622103i$	$0.782936 - 0.622103i$
1	1	3	0.25	1	$-0.098504 - 0.995137i$	$-0.098504 - 0.995137i$	$-0.098504 - 0.995137i$
2	1	3	0.25	1	$-0.103428 - 0.994637i$	$-0.103428 - 0.994637i$	$-0.103428 - 0.994637i$
3	1	3	0.25	1	$-0.103456 - 0.994634i$	$-0.103456 - 0.994634i$	$-0.103456 - 0.994634i$
1	0.6	1	0.25	1	$0.731016 - 0.682360i$	$0.731016 - 0.682360i$	$0.731016 - 0.682360i$
2	0.6	1	0.25	1	$0.713723 - 0.700428i$	$0.713723 - 0.700428i$	$0.713723 - 0.700428i$
3	0.6	1	0.25	1	$0.706679 - 0.707535i$	$0.706679 - 0.707535i$	$0.706679 - 0.707535i$
2	1	1	0.472	2	-1.18553	-1.24711	-1.24756
3	1	1	0.472	2	-1.60763	-1.68123	-1.68205
4	1	1	0.472	2	-1.61840	-1.68335	-1.68406

will give a comprehensive picture of the scattering effect. We stress that (4.7.1) is simply a convenient regime in which to display results, and that the methods we have presented are not limited to this case.

From (4.4.37) we can see that the leading order behaviour of the amplitudes A_{0n}^q comes from the zero of the determinant of the kernel that is located outside C and which is either on, or closest to the unit circle. In table 4.1, we investigate how fast this zero converges to a specific value as the approximation parameters Q and ν increase. It appears that the convergence rate with respect to Q is fast for small cylinders, and it slows down when either the nondimensional size $k\ell$ of the cylinders increases, or the nondimensional distance ka_1 between them in each row decreases. On the other hand for fixed Q, the convergence rate with respect to ν accelerates when either ka_1 is decreased or $k\eta_2$ is increased. For a normalised square lattice ($\eta_1 = 0$ and $a_1 = \eta_2 = 1$) and $k < \pi$, the data in table 4.1 suggest that our method of solution can be carried out effectively with

$Q = \nu = 1$ for the case of small cylinders, and $Q = \nu = 3$ for large cylinders close to touching.

A table of plots is given in figure 4.2, which illustrate how the energy is distributed between transmitted and reflected waves. The case under consideration is a square lattice for three different sizes of cylinders. The value of $|c_0^-|$ as ψ_0 varies, for all the other parameters fixed, follows a general pattern. At grazing incidence ($\sin\psi_0 = 0$), we have $|c_0^-| = 1$, and as the angle of incidence increases the value $|c_0^-|$ decreases rapidly. There is a critical angle in the interval $(0, \pi/2)$, at $\psi_0 = \widetilde{\psi}_0$ say, where $|c_0^-|$ takes its minimum value. Note that all the plots are symmetric with respect to $\psi_0 = \pi/2$, and therefore $\pi - \widetilde{\psi}_0$ is also a critical angle. More specificly, for $\ell = 0.25$, the argument of the reflected coefficient at the critical angle $\widetilde{\psi}_0$, appears to have a discontinuity. This means that in the complex plane the point c_0^- passes through (or very close to) the origin as ψ_0 varies in the vicinity of $\widetilde{\psi}_0$, and therefore, we can conclude that (almost) full transmission occurs for $\psi_0 = \widetilde{\psi}_0$. In this respect, the contour plot of $|c_0^-|$ displays information of full transmission in black, total reflection in white, and partial transmission and reflection in shades of gray.

As the size of the cylinders increases, the amount of the energy reflected from the lattice increases as well. This is illustrated in the contour plots generated for $\ell = 0.42$ and $\ell = 0.472$. For the first case, we see that a local band gap is opening up at $k \approx 1.8$ and $\psi_0 = \pi/2$, and widens as k increases to take the form of a full band gap for $k \gtrsim 2.95$. Note that the plot of the phase of the reflected coefficient is continuous for $k = 3$, which is expected for the parameters being in a total band gap.

For cylinders of radius $\ell = 0.472$, we can see a total band gap extending from $k \approx 2.05$ up to $k = 3.1$. Interestingly, the argument of c_0^- is continuous even for parameters in a pass band, which means that in this case c_0^- does not pass through (or very close to) the origin as ψ_0 varies in the vicinity of $\widetilde{\psi}_0$. In fact, the minimum value of $|c_0|$ is approximately 0.1, meaning that around 99% of the incident field energy is transmitted into the lattice. This suggests that cases

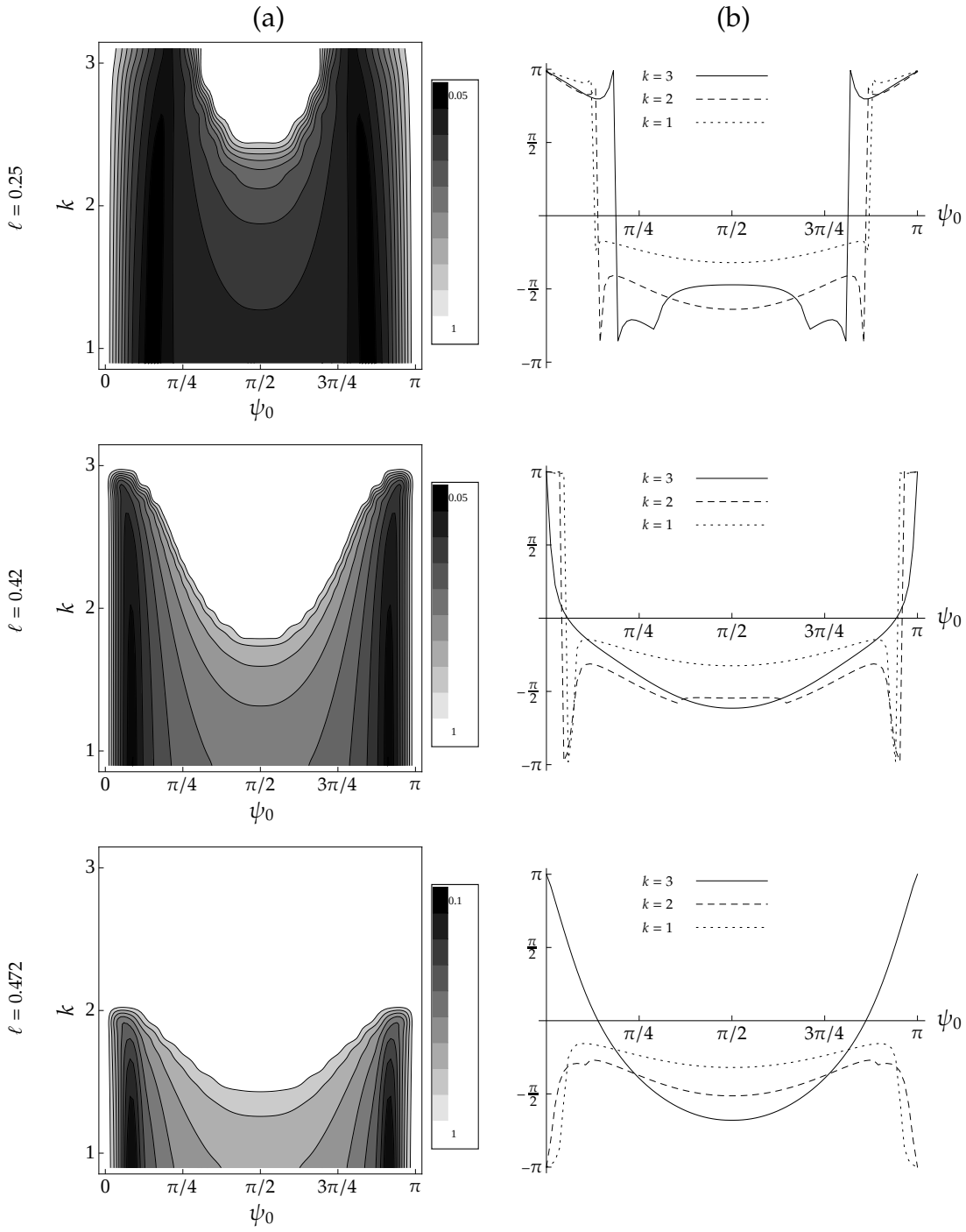

Figure 4.2: *Plots of the reflected coefficient for three different sizes ($\ell = 0.25, 0.42$ and 0.472) of cylinders. Column (a) consists of contour plots of the modulus of the reflected coefficient, and plots of its argument are shown in column (b) for three different wavenumbers ($k = 1, 2$ and 3). The parameter of the lattice are $a_1 = 1$, $\eta_1 = 0$, and $\eta_2 = 1$.*

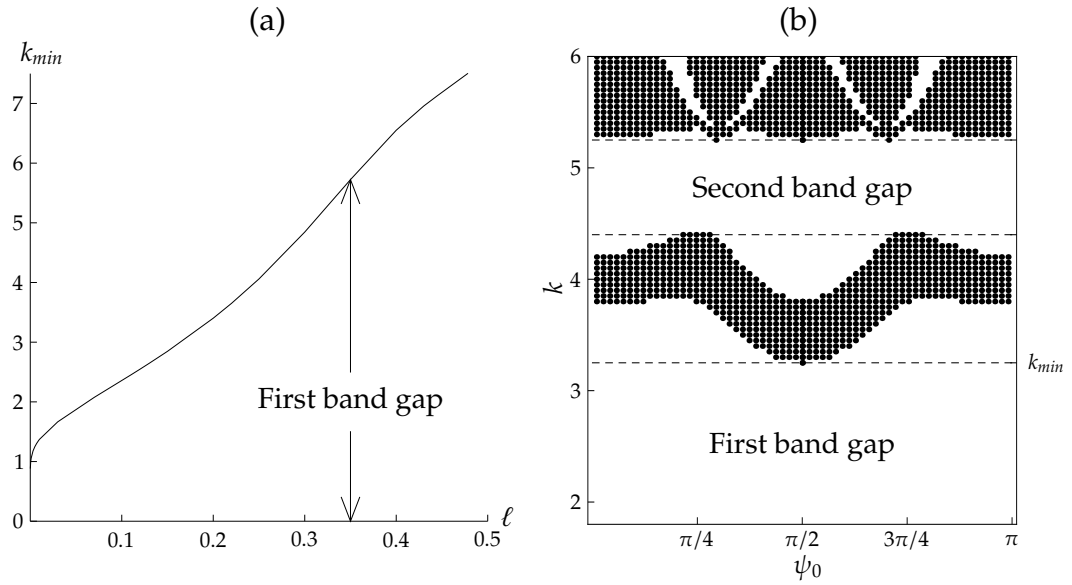

Figure 4.3: *The plot of k_{min} against the radius of the cylinders for a square lattice ($a_1 = \eta_2 = 1$ and $\eta_1 = 0$) of sound-soft cylinders is given in (a). For the same lattice of cylinders with specific radius $\ell = 0.187$ we plotted the points (k, ψ_0) which indicate pass bands in (b).*

where cylinders are close to touching prohibit full transmission phenomena to occur. In contrast, dilute lattices allow almost full transmission even between the critical angles $\widetilde{\psi}_0$ and $\pi - \widetilde{\psi}_0$. For example, we found that for cylinders of radius $\ell = 0.02$, the maximum value of $|c_0^-|$ in the region $k \in [1, 3]$ and $\psi_0 \in [\widetilde{\psi}_0, \pi - \widetilde{\psi}_0]$ is 0.018. Hence, for any parameters in this region it is guaranteed that at least 99.97% of the incident field energy would be transmitted into the lattice.

We now turn our attention to the case where Dirichlet boundary condition is imposed on the cylinders' surface. For the figures we will use a simple method to extract information about the band structure of a lattice, which does not require the restriction (4.7.1). A total band gap appears whenever the determinant of the kernel is zero free on the unit circle for all $\psi_0 \in [0, \pi]$. On the contrary, if for a given set of parameters the determinant has a zero on the unit circle, then this leads to an excitation of a Bloch wave propagating through the lattice. Therefore, we can easily identify band gaps and pass bands by plotting the points (k, ψ_0) which correspond to the presence of zeros on the unit circle. This approach is illustrated in figure 4.3 (b) where we examine the band structure of

a square lattice of sound-soft cylinders with radius $\ell = 0.187$. Two band gaps appear in this case, with the upper bound of the first one being $k = 3.25$, whereas the second one extends from $k = 4.4$ to $k = 5.25$. Note that band diagrams for a lattice with the same parameters have been previously calculated and displayed in figure 1.9 (a). The two figures are in agreement with respect to the region of the two band gaps.

In figure 4.3 (b) it is evident that there exists a minimum value of k and in particular $k_{min} = 3.25$, for which a Bloch wave can be excited. This has been observed also in figure 3.4 (a) and 3.5 (a). It appears also that this minimum occurs at head-on incidence, in which case the Bloch vector (see (3.3.8)) takes the form

$$\boldsymbol{\beta}(z_0) = \left(0, i \log z_0/\eta_2\right), \tag{4.7.3}$$

where z_0 is a zero of the determinant of the kernel which is on the unit circle. Note that the case where $z_0 = 1$ indicates the threshold between band gaps and pass bands, and also the presence of a Bloch wave with $\boldsymbol{\beta}(z_0) = \mathbf{0}$. Also as we have seen in figure 1.9 (a) (see also the relative figures in [43] and [46]), k_{min} is obtained when the Bloch wave vector passes from the centre of the Brillouin zone (i.e. when it is the zero vector). Therefore, in order to determine k_{min} for a given lattice we do not need to consider all the possible values of ψ_0. Instead we can set the angle of incidence at $\psi_0 = \pi/2$ and then a simple bisection and iteration is sufficient for our task. This approach has been used to show the dependence of k_{min} (and consequently the size of the first band gap), on the radius ℓ of the cylinders, see figure 4.3 (a). It is worth remarking that k_{min} tends very slowly to zero as $\ell \to 0$.

Chapter 5

Conclusions

The solution of the problem of acoustic wave scattering by a semi-infinite lattice of cylinders has been obtained by means of the Wiener–Hopf technique. In the case where the cylinders are small relative to the wavelength and Dirichlet boundary condition is imposed on their surface, the procedure simply requires a scalar kernel factorisation. On the other hand, the general case presents a much more challenging proposition, since it gives rise to a matrix Wiener–Hopf equation. This has been dealt with a method that does not require the explicit factorisation of the kernel.

The accuracy of the method depends crucially on the approximation parameter Q, since the field radiating from each cylinder can be modelled more accurately by including higher-order multipoles in its expansion. This is evident in figure 5.1 which shows the real part of the total field on the boundary of the cylinder centred at the origin. The plots were produced by first expressing the field radiating from each cylinder solely in monopole terms (plot (a)), and then by including both monopole and dipole terms in its expansion (plot (b)). The scattered field was calculated using its spectral form (3.5.4), and (4.5.3), respectively. Note that these expressions originate from the spectral representation (B.1.22) of the 1D quasi-periodic Green's function $G_q^{(1)}$, and hence (4.5.3) is not valid on the line $y = 0$ (see appendix B.1.2). This explains the high peak at 0 and

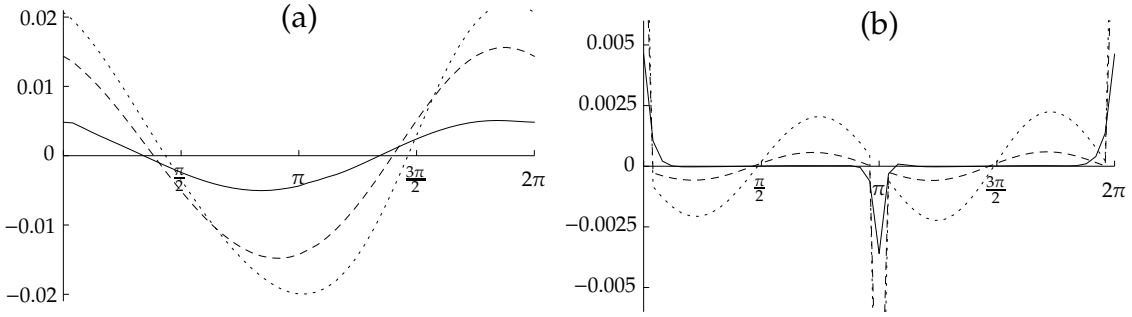

Figure 5.1: *Plots illustrating the accuracy on the boundary of the cylinder centred on the origin for Dirichlet boundary conditions. The function* $Re[u(\ell e^{it})]$ *is plotted against* t *for the approximation parameters (a)* $Q = 0$ *and* $\nu = 1$ *and (b)* $Q = 1$ *and* $\nu = 1$*. The other parameters in use are* $a_1 = 1$, $\eta_1 = 0$, $\eta_2 = 1$, $k = 1$ *and we considered three different values for the radii of the cylinders:* $\ell = 0.01$ *(solid line),* $\ell = 0.05$ *(dashed line) and* $\ell = 0.1$ *(dotted line). The scattered field was calculated form the spectral representation* (3.5.4)*, and* (4.5.3)*, respectively. Note that the latter is not valid on the line* $y = 0$*, hence the anomalies around* 0, π, *and* 2π *in plot (b).*

2π (i.e. the point $(\ell, 0)$ on the (x,y) plane) and the low trough at π (i.e. the point $(-\ell, 0)$), of plot (b). It is clear that by increasing the size of the cylinders had a negative effect on the accuracy. However, the cost in accuracy remains low if we include dipole terms in the expansion of field radiating from each cylinder.

The problem under consideration can be solved regardless of the size of the cylinder and the boundary condition that is imposed on its surface, as long as the approximation parameters Q and ν are sufficiently large. However, there are limitations, since increasing Q causes the dimension of the matrix kernel to increase, and increasing ν makes its elements more complex. Intensive computation are then required in order to calculate the solution. Another issue to be considered is that if we increase the wavenumber or the horizontal distance a_1, then the set of indices $\mathcal{M}$ will grow larger (see (B.1.13)). Recall that this set implicitly defines how many of the poles of the matrix kernel are on the unit circle, (see (B.1.17)). We observed (numerically) that more than one pair of zeros appear on the unit circle in situations where there are more than one pair of poles on the unit circle. Therefore, in such case extra effort is required in order

to determine which of these zeros correspond to a pole of $\mathbf{A}^{+}(z)$. In addition the conservation of energy principle leads to more complicated identities.

To summarise, we were able to devise a method to solve the problem of plane wave scattering by a semi-infinite lattice of cylinders. The objective was to tackle the problem at low frequencies, but this restriction can be relaxed. An analytical approach based on the Wiener–Hopf technique in combination with a valid approximation of the kernel that essentially disregards interaction effects of strongly evanescent modes proved to be sufficient for dealing with a variety of boundary conditions. The far field analysis for the scattered field has been carried out in a straightforward manner, and useful identities that serve as a check on our results have been obtained by applying the principle of conservation of energy.

5.1 Future work

In chapter 4 we have presented a general method of solution which in theory can be applied to any given set of parameters. However, in practice the numerical calculations are effective only at low-frequencies because in this case the approximation parameters Q and ν may be chosen to be sufficiently small. Therefore, the first objective for future work is to write a more powerful numerical code which can handle large values of Q and ν, and subsequently produce results of higher frequencies.

As we pointed out in the introduction, the scattering effect of a large finite array of cylinders can be modelled by its infinite counterpart. In this respect, the study of the semi-infinite lattice provides significant information regarding scattering by a large finite rectangular array. However, this information is valid only in the interior of the finite array, where the edge effects may be considered to be negligible. Thus, in order to correctly capture the behaviour of the scattered field by a large finite array of cylinders we need to take into account the scattering effect of both its edges and corners. This is an interesting

research topic for future work. Another possible research avenue is the study of scattering by defects in the semi-infinite lattice following the work of Thompson & Linton [52].

More generally, since many scattering problems can be reduced to a matrix Wiener–Hopf equation, it would be interesting to investigate whether our method of solution described in §4.4 could be applied in different physical and geometrical settings. Recall that our effort was successful due to an approximation of the kernel by a rational matrix. For arbitrary matrices, such approximations can be achieved by means of Padé approximants. It has been shown that this approach is effective for scalar Wiener–Hopf kernels [1], but the case of matrix kernels requires further investigation.

Appendix A

Miscellaneous functions

A.1 Multiple valued functions

A multiple valued function, as the name suggests, has more than one possible value at a particular point in the complex plane. The square root is a typical example. Roughly speaking, a branch of a multiple valued function is a single valued function, which at every point of its domain assumes exactly one of the various possible values that the multiple valued function can assume. The notion of the branch and the related branch points and branch cuts of multiple valued functions are explained in detail by several complex analysis texts, including Gamelin [13], Sarason [50], and Wunsch [64]. Here, we shall define the branches of two frequently used multiple valued functions.

The first function is

$$\gamma(z) = (z^2 - 1)^{1/2}, \tag{A.1.1}$$

which posses two branch points, located at $z = \pm 1$. The branch cuts are taken along the line sections $(1, 1 + i\infty)$ and $(-1, -1 - i\infty)$ (see fig. A.1), and a branch is chosen so that for real argument we have

$$\gamma(t) = \begin{cases} -i\sqrt{1 - t^2}, & |t| \leqslant 1, \\ \sqrt{t^2 - 1}, & |t| > 1. \end{cases} \tag{A.1.2}$$

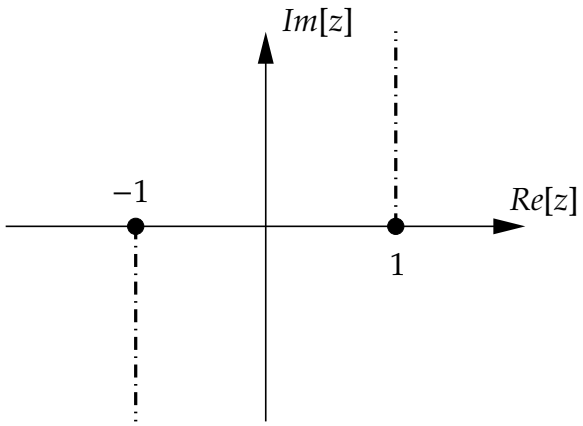

Figure A.1: *Branch cuts for the functions γ and* arccos.

The other function we are interested in is the inverse cosine function, which has three branch points, located at $z = \pm 1$, and the point at infinity. Again, the branch cuts are taken along $(1, 1 + i\infty)$ and $(-1, -1 - i\infty)$ (see fig. A.1) and we can write

$$\arccos(z) = i \log\Big(z + \gamma(z)\Big), \tag{A.1.3}$$

and choose the branch of the logarithm so that $\arccos(z) \in (0, \pi)$ for $z \in (-1, 1)$. It is worth remarking that on the real line outside the interval $(-1, 1)$ the selected branch of the inverse cosine function is given by

$$\arccos t = \begin{cases} i \operatorname{arccosh} t, & t > 1, \\ \pi - i \operatorname{arccosh}(-t), & t < -1, \end{cases} \tag{A.1.4}$$

with $\operatorname{arccosh} t = \ln(t + \sqrt{t^2 - 1})$ for $t > 1$.

A.2 Bessel functions

Bessel's equation is the linear second-order ordinary differential equation

$$z^2 \frac{d^2 f}{dz^2} + z \frac{df}{dz} + (z^2 - q^2) f = 0. \tag{A.2.1}$$

This has two linearly independent solutions $J_q(z)$ and $Y_q(z)$, known as Bessel functions of the first and second kind respectively. For nonnegative integers q,

$J_q(z)$ has the series expansion

$$J_q(z) = \sum_{m=0}^{\infty} \frac{(-1)^m z^{2m+q}}{2^{2m+q} m!(q+m)!}, \tag{A.2.2}$$

and it is not difficult to see that this defines an entire function. For the Bessel function of the second kind we have the expansion

$$\begin{aligned} Y_q(z) = \frac{2}{\pi} J_q(z) \log \frac{z}{2} - \frac{1}{\pi} \sum_{m=0}^{q-1} \frac{(q-m-1)! z^{2m-q}}{2^{2m-q} m!} \\ - \frac{1}{\pi} \sum_{m=0}^{\infty} \frac{(-1)^m z^{2m+q}}{2^{2m+q} m!(q+m)!} [h(m+1) + h(m+q+1)], \end{aligned} \tag{A.2.3}$$

where

$$h(m+1) = -\mathfrak{c} + 1 + \frac{1}{2} + \cdots + \frac{1}{m},$$

and $\mathfrak{c} = 0.57721...$ is Euler's constant. In the case $q = 0$, the first sum in (A.2.3) should be set equal to zero. Clearly the functions $Y_q(z)$ are singular at $z = 0$, since we have

$$Y_0(z) = \frac{2}{\pi} \left(\log \frac{z}{2} + \mathfrak{c} \right) + O(z^2), \quad \text{as} \quad z \to 0, \tag{A.2.4}$$

and for $q \neq 0$,

$$Y_q(z) = O(z^{-q}), \quad \text{as} \quad z \to 0. \tag{A.2.5}$$

Note that for $q = 1, 2, \ldots,$

$$J_{-q}(z) = (-1)^q J_q(z), \tag{A.2.6}$$

and

$$Y_{-q}(z) = (-1)^q Y_q(z). \tag{A.2.7}$$

The Hankel function of the first kind of order q is defined by the linear combination

$$H_q(z) = J_q(z) + i Y_q(z), \tag{A.2.8}$$

and it is regular in the complex plane except at the point $z = 0$. The asymptotic behaviour of the Hankel function for small arguments are

$$H_0(z) = 1 + \frac{2i}{\pi} \left(\log \frac{z}{2} + \mathfrak{c} \right) + O(z^2), \quad \text{as} \quad z \to 0, \tag{A.2.9}$$

and for $q \neq 0$,

$$H_q(z) = O(z^{-q}), \quad \text{as} \quad z \to 0. \tag{A.2.10}$$

On the other hand for large arguments we have (see [2, eq. 9.2.3])

$$H_q(z) \sim \sqrt{\frac{2}{\pi z}} e^{i(z - q\pi/2 - \pi/4)}, \quad \text{as} \quad |z| \to \infty. \tag{A.2.11}$$

Bessel function are amongst the most important special functions, with applications to different branches of mathematics, physics, and engineering. They have been studied in detail and numerous properties, relations and representations can be found in [2, Ch. 9] and [15, Ch. 8–9]. The treatise by Watson [60] is the classic reference on the theory of Bessel functions.

A.3 Integral representations of multipoles

Multipoles can be written in terms of the integral (see [30, B.10])

$$\mathcal{H}_q(\mathbf{r}) = H_q(kr)e^{iq\theta} = \frac{(-i)^{q+1}}{\pi} \int_{-\infty}^{\infty} \frac{e^{-k\gamma(t)|y|}}{\gamma(t)} e^{ikxt} (t - \gamma(t))^{q\,\mathrm{sgn}(y)} dt, \tag{A.3.1}$$

in which $\gamma(t)$ is as defined in (A.1.2) and the path of integration is indented so as to pass above the branch point at $t = -1$ and below that at $t = 1$. For $q \neq 0$ the integral in (A.3.1) converges for all values of y except for $y = 0$, whereas for $q = 0$, we have

$$\mathcal{H}_0(\mathbf{r}) = H_0(kr) = -\frac{i}{\pi} \int_{-\infty}^{\infty} \frac{e^{-k\gamma(t)|y|}}{\gamma(t)} e^{ikxt} dt, \tag{A.3.2}$$

and in this case the integral converges everywhere except the point where $x = y = 0$.

A.4 Polynomial matrices

Here we will prove some crucial results concerning latent roots of polynomial matrices. Further information on this subject is contained in [23, §7].

Let $\mathbf{P}(z)$ be an $n \times n$ polynomial matrix, whose rows are linearly independent, and let $D(z)$ represent the determinant of $\mathbf{P}(z)$. Note that a polynomial matrix with some linearly dependent rows has the zero function as its determinant, and is of no interest here. Suppose that $\mathbf{P}(z)$ has a latent root of rank r at $z = \lambda$, which means that the constant matrix $\mathbf{P}(\lambda)$ has rank $n - r$. Then

(i) $D(z)$ has a root at $z = \lambda$, whose multiplicity is at least r.

(ii) All entries of $\operatorname{adj}\Big(\mathbf{P}(z)\Big)$ are divisible by $(z - \lambda)^{r-1}$.

(iii) The constant matrix

$$\mathbf{F}(\lambda) = \lim_{z \to \lambda} (z - \lambda)^{1-r} \operatorname{adj}\Big(\mathbf{P}(z)\Big) \tag{A.4.1}$$

has rank r.

Proof. By a sequence of elementary row operations, the matrix $\mathbf{P}(\lambda)$ can be reduced to a matrix in which there are r rows whose entries are all zero. Apply this sequence of operations to the polynomial matrix $\mathbf{P}(z)$ to obtain the polynomial matrix $\mathbf{P}'(z)$. Then $\mathbf{P}'(z)$ has r rows in which each entry has a root at $z = \lambda$. Hence, the determinant of $\mathbf{P}'(z)$ has $(z - \lambda)^r$ as a factor. Since determinants are unaffected by row operations, this establishes property (i).

The adjugate of $\mathbf{P}'(z)$ is formed from minors of size $(n-1) \times (n-1)$. In r rows, a factor $(z - \lambda)$ is suppressed, and so all elements in the resulting minors have $(z - \lambda)^{r-1}$ as a factor. In the remaining $n - r$ rows, each element has $(z - \lambda)^r$ as a factor. Moreover, the adjugate of $\mathbf{P}(z)$ can be obtained by applying a sequence of column operations to the adjugate of $\mathbf{P}'(z)$,[1] and so this establishes (ii).

Finally, we observe from equation (A.4.1) that the constant matrix $\mathbf{F}(\lambda)$ has $n - r$ rows in which all entries are zero. The remaining r rows must be linearly

[1] To see this, consider the equation $\mathbf{P}'(z) \operatorname{adj}\Big(\mathbf{P}'(z)\Big) = \det\Big(\mathbf{P}'(z)\Big)\mathbf{I}$, where $\mathbf{I}$ is the identity matrix, and observe that performing a row operation on the matrix $\mathbf{P}'(z)$ creates one additional nonzero entry on the right-hand side. This unwanted entry can be eliminated by performing an appropriate column operation on $\operatorname{adj}\Big(\mathbf{P}'(z)\Big)$.

independent, or else the rank of the latent root at $z = \lambda$ is greater than r. This establishes property (iii). □

Note that the converse of property (i) is not true; for example the determinant of the matrix

$$\mathbf{P}(z) = \begin{bmatrix} z^2 & 0 \\ 0 & 1 \end{bmatrix}$$

has a double root at $z = 0$, but this a latent root of rank one. In general, if $D(z)$ has a root of multiplicity $r > 1$ at $z = \lambda$, then the rank of $\mathbf{P}(z)$ is strictly less than n, but may exceed $n - r$.

Appendix B

Arrays of singularities

Here, we consider some geometrical arrangements of singularities (multipoles) which are of crucial importance in the theory of scattering by periodic structures. For future convenience, we introduce two arrays of points, in the (x, y) plane in terms of the linearly independent vectors

$$\mathbf{a}_1 = (a_1, 0), \quad \text{and} \quad \mathbf{a}_2 = (\eta_1, \eta_2), \tag{B.0.1}$$

with $\eta_1 > 0$ and $\eta_2 \neq 0$. With this notation, we define

$$\mathcal{A}_1 = \{j\mathbf{a}_1,\ j \in \mathbb{Z}\}, \tag{B.0.2}$$

and

$$\mathcal{A}_2 = \{\mathbf{R}_{jm} = j\mathbf{a}_1 + m\mathbf{a}_2,\ j, m \in \mathbb{Z}\}, \tag{B.0.3}$$

representing a grating and a lattice, respectively.

Definition 2. *A function $f : \mathbb{R}^2 \to \mathbb{C}^2$ will be called quasi-periodic if there exist vectors $\boldsymbol{\alpha}$ and $\boldsymbol{\beta}$ such that*

$$f(\mathbf{r} + n\boldsymbol{\alpha}) = e^{in\boldsymbol{\alpha}\cdot\boldsymbol{\beta}} f(\mathbf{r}), \quad \forall n \in \mathbb{Z}. \tag{B.0.4}$$

B.1 Quasi-periodic arrays of singularities

In this section we consider functions of the form

$$G_q^{(d)}(\mathbf{r},\boldsymbol{\beta}) = \sum_{\mathbf{v}\in\mathcal{A}_d} e^{i\mathbf{v}\cdot\boldsymbol{\beta}}\mathcal{H}_q(\mathbf{r}-\mathbf{v}), \quad q\in\mathbb{Z}, \quad d=1,2 \tag{B.1.1}$$

which represent periodic arrays of singularities centred at the points of the array $\mathcal{A}_d$ and modulated by a phase factor governed by the vector

$$\boldsymbol{\beta} = (\beta_x,\beta_y). \tag{B.1.2}$$

For the case in which $d = 1$ we can write

$$G_q^{(1)}(\mathbf{r},\boldsymbol{\beta}) = \sum_{j=-\infty}^{\infty} e^{ij\mathbf{a}_1\cdot\boldsymbol{\beta}}\mathcal{H}_q(\mathbf{r}-j\mathbf{a}_1), \quad q\in\mathbb{Z}, \tag{B.1.3}$$

and we call this the 1D (one-dimensional) quasi-periodic array of singularities, since it is quasi-periodic in one direction (parallel to $\mathbf{a}_1$), i.e.

$$G_q^{(1)}(\mathbf{r}+n\mathbf{a}_1,\boldsymbol{\beta}) = e^{in\mathbf{a}_1\cdot\boldsymbol{\beta}}G_q^{(1)}(\mathbf{r},\boldsymbol{\beta}), \quad \forall n\in\mathbb{Z}. \tag{B.1.4}$$

On the other hand for the case where $d = 2$ we have

$$G_q^{(2)}(\mathbf{r},\boldsymbol{\beta}) = \sum_{m=-\infty}^{\infty}\sum_{j=-\infty}^{\infty} e^{i\mathbf{R}_{jm}\cdot\boldsymbol{\beta}}\mathcal{H}_q(\mathbf{r}-\mathbf{R}_{jm}), \quad q\in\mathbb{Z}, \tag{B.1.5}$$

and it is evident that this function is quasi-periodic in two directions (parallel to $\mathbf{a}_1$ and $\mathbf{a}_2$), since

$$G_q^{(2)}(\mathbf{r}+\mathbf{R}_{np},\boldsymbol{\beta}) = e^{i\mathbf{R}_{np}\cdot\boldsymbol{\beta}}G_q^{(2)}(\mathbf{r},\boldsymbol{\beta}), \quad \forall n\in\mathbb{Z}, \quad \forall p\in\mathbb{Z}. \tag{B.1.6}$$

Accordingly, we call $G_q^{(2)}(\mathbf{r},\boldsymbol{\beta})$ the 2D quasi-periodic array of singularities. Note that for $q = 0$ (B.1.3) and (B.1.5) represent the 1D and 2D quasi-periodic Green's function, respectively (see [29]).

B.1.1 The scattering angles

Quasi-periodic arrays of singularities can be written more conveniently as an infinite sum of modes (exponential solutions to the Helmholtz equation), and

in order to do this we introduce the so-called scattering angles, defined by

$$\psi_j = \arccos \beta_{xj}, \quad j \in \mathbb{Z}, \tag{B.1.7}$$

where

$$\beta_{xj} = \frac{\beta_x}{k} + \frac{2\pi j}{ka_1}. \tag{B.1.8}$$

The branch of arccos is defined in (A.1.3), and for real values we can use (A.1.4). Note that in order to ensure that the scattering angles are well-defined, we must assume that

$$|\beta_{xj}| \neq 1, \quad j \in \mathbb{Z}. \tag{B.1.9}$$

This being the case, it is clear that

$$\cos \psi_j = \beta_{xj}, \qquad \text{and} \qquad \sin \psi_j = i\gamma(\cos \psi_j). \tag{B.1.10}$$

In the main body of the thesis, the x-component of the vector $\boldsymbol{\beta}$ will be given in terms of the wavenumber, and in particular

$$\beta_x = k \cos \psi_0, \quad \text{with} \quad 0 < \psi_0 < \pi, \tag{B.1.11}$$

in which case we have that

$$\cos \psi_j = \cos \psi_0 + \frac{2\pi j}{ka_1}, \qquad \text{and} \qquad \sin \psi_j = i\gamma(\cos \psi_j). \tag{B.1.12}$$

It is evident that $\cos \psi_j$ is real for all $j \in \mathbb{Z}$. On the other hand, if we define the sets

$$\mathcal{M} = \left\{ m \in \mathbb{Z} \ : \ \left| \cos \psi_0 + 2\pi m / ka_1 \right| < 1 \right\}, \tag{B.1.13}$$

and

$$\mathcal{N} = \left\{ n \in \mathbb{Z} \ : \ \left| \cos \psi_0 + 2\pi n / ka_1 \right| > 1 \right\}, \tag{B.1.14}$$

then it follows from (A.1.2), that $\sin \psi_j$ is real for $j \in \mathcal{M}$ and positive imaginary for $j \in \mathcal{N}$. Moreover, in view of (A.1.4) we can conclude that there exists a sequence $\alpha_j : \mathbb{Z} \to \mathbb{R}$, such that

$$\psi_j = \begin{cases} \pi - i\alpha_j, & j \in \mathcal{N} \quad \textit{and} \quad j < 0, \\ \alpha_j, & j \in \mathcal{M}, \\ i\alpha_j, & j \in \mathcal{N} \quad \textit{and} \quad j > 0. \end{cases} \tag{B.1.15}$$

Finally, we introduce the points

$$p_j = e^{-ik(\eta_1 \cos\psi_j + \eta_2 \sin\psi_j)}, \quad \text{and} \quad \tau_j = e^{ik(\eta_1 \cos\psi_j - \eta_2 \sin\psi_j)}, \tag{B.1.16}$$

which will appear throughout the thesis in several formulae. These points have the properties

$$|p_j| = |\tau_j| = 1, \quad \text{for} \quad j \in \mathcal{M}, \tag{B.1.17}$$

$$p_j^* = \tau_j, \quad \text{for} \quad j \in \mathcal{N}, \tag{B.1.18}$$

and note that they grow exponentially as $|j| \to \infty$.

B.1.2 1D Spectral representation

To derive an alternative representations for the 1D quasi periodic array (B.1.3) in cartesian coordinates, we first note that the phase shift $e^{ij\mathbf{a}_1\cdot\boldsymbol{\beta}} = e^{ija_1\beta_x}$ is independent of β_y. Therefore, we can formally write

$$G_q^{(1)}(\mathbf{r}, \beta_x) = \sum_{j=-\infty}^{\infty} e^{ija_1\beta_x} \mathcal{H}_q(\mathbf{r} - j\mathbf{a}_1), \tag{B.1.19}$$

and by inserting the integral representation (A.3.1), this becomes

$$G_q^{(1)}(\mathbf{r}, \beta_x) = \frac{(-i)^{q+1}}{\pi} \sum_{j=-\infty}^{\infty} \int_{-\infty}^{\infty} e^{ij(a_1\beta_x - ka_1 t)} \frac{e^{-k\gamma(t)|y|}}{\gamma(t)} e^{ikxt} (t - \gamma(t))^{q\,\mathrm{sgn}(y)} dt, \tag{B.1.20}$$

where $\gamma(\cdot)$ is defined in (A.1.2). Now, if we change the integration variable to $ka_1 t$, and apply Poisson's summation formula (see [12, eq. 5.8.3])

$$\frac{1}{2\pi} \sum_{j=-\infty}^{\infty} \int_{-\infty}^{\infty} e^{ij(x-t)} f(t)\, dt = \sum_{j=-\infty}^{\infty} f(x + 2\pi j), \tag{B.1.21}$$

then we obtain the spectral representation

$$G_q^{(1)}(\mathbf{r}, \beta_x) = \frac{2(-i)^{q+1}}{ka_1} \sum_{j=-\infty}^{\infty} \frac{e^{-k\gamma(\beta_{xj})|y|}}{\gamma(\beta_{xj})} e^{ikx\beta_{xj}} \Big(\beta_{xj} - \gamma(\beta_{xj})\Big)^{q\,\mathrm{sgn}(y)}, \tag{B.1.22}$$

where β_{xj} is defined in (B.1.8). For $q \neq 0$ the representation (B.1.22) is valid for all values of y except $y = 0$, whereas for $q = 0$, it is valid everywhere except the

point where $x = y = 0$. Using (B.1.10), we can rewrite (B.1.22) in terms of the scattering angles

$$G_q^{(1)}(\mathbf{r}, \beta_x) = \frac{2(-i)^q}{ka_1} \sum_{j=-\infty}^{\infty} \frac{e^{iq\,\mathrm{sgn}(y)\psi_j}}{\sin\psi_j} e^{ik(x\cos\psi_j + |y|\sin\psi_j)}. \tag{B.1.23}$$

B.1.3 Spectral representation for a semi-infinite lattice

Now we turn our attentions to the functions

$$G_q^{\pm}(\mathbf{r}, \boldsymbol{\beta}) = \sum_{m=1}^{\infty} \sum_{j=-\infty}^{\infty} e^{i\mathbf{R}_{j,\mp m}\cdot\boldsymbol{\beta}} \mathcal{H}_q(\mathbf{r} - \mathbf{R}_{j,\mp m}), \quad q \in \mathbb{Z}, \tag{B.1.24}$$

representing a semi-infinite lattice of singularities modulated by a phase factor, and located either in the upper or the lower half plane. Note that the functions $G_q^+(\mathbf{r}, \boldsymbol{\beta})$ and $G_q^-(\mathbf{r}, \boldsymbol{\beta})$ are free from singularities in the regions

$$D^+ = \{(x, y)/\ y > -\eta_2\}, \quad \text{and} \quad D^- = \{(x, y)/\ y < \eta_2\}, \tag{B.1.25}$$

respectively. For fixed $\boldsymbol{\beta} = (\beta_x, \beta_y)$, with $\beta_x,\ \beta_y \in \mathbb{R}$ the double sum in (B.1.24) does not converge absolutely (see (A.2.11)) and therefore considerable care is needed regarding the order of summation. Our aim is to transform (B.1.24) into a form more suitable for calculations. To do this we will assume that the wavenumber k has a positive imaginary part, i.e. $k = Re[k] + i\epsilon$, which ensures the absolute convergence of the sum. Therefore, with this assumption we are at liberty to manipulate the series without the need to specify the order of summation. Once we have obtained an alternative representation, we can take the limit $\epsilon \to 0$. This is a standard mechanism to treat multi-dimensional conditional convergent series in scattering problems. Further discussion on this subject can be found in [30, §1.5]. Thus provided that $\boldsymbol{\beta}$ is independent of k, we can write

$$G_q^{\pm}(\mathbf{r}, \boldsymbol{\beta}) = \sum_{m=1}^{\infty} e^{\mp im\mathbf{a}_2\cdot\boldsymbol{\beta}} G_q^{(1)}(\mathbf{r} \pm m\mathbf{a}_2, \beta_x), \tag{B.1.26}$$

and inserting the spectral form (B.1.22), we obtain

$$G_q^{\pm}(\mathbf{r}, \boldsymbol{\beta}) = \frac{2(-i)^{q+1}}{ka_1} \sum_{m=1}^{\infty} \sum_{j=-\infty}^{\infty} \frac{e^{\mp k\gamma(\beta_{xj})y + ikx\beta_{xj}}}{\gamma(\beta_{xj})} e^{m\overline{w}_j^{\pm}\left(\beta_{xj} - \gamma(\beta_{xj})\right)^{q\,\mathrm{sgn}(y)}}, \tag{B.1.27}$$

$$\text{for} \quad \mathbf{r} \in D^{\pm},$$

where

$$w_j^{\pm} = -k\gamma(\beta_{xj})\eta_2 \pm i(2\pi j\eta_1/a_1 - \eta_2\beta_y), \tag{B.1.28}$$

and β_{xj} is given by (B.1.8). Assuming that $\beta_x,\ \beta_y \in \mathbb{R}$, it is not difficult to prove that the real part of $w_j^{\pm}$ is negative for all $j \in \mathbb{Z}$. This means that we can sum with respect to m in (B.1.27) and obtain

$$G_q^{\pm}(\mathbf{r},\boldsymbol{\beta}) = \frac{2(-i)^{q+1}}{ka_1}\sum_{j=-\infty}^{\infty}\frac{e^{\mp k\gamma(\beta_{xj})y+ikx\beta_{xj}}}{\gamma(\beta_{xj})}\frac{e^{w_j^{\pm}}}{1-e^{w_j^{\pm}}}\Big(\beta_{xj}-\gamma(\beta_{xj})\Big)^{q\,\mathrm{sgn}(y)}, \quad \text{for} \quad \mathbf{r}\in D^{\pm}. \tag{B.1.29}$$

We can now take the limit $\epsilon \to 0$, and write (B.1.29) in terms of the scattering angles (B.1.10), i.e.

$$G_q^{\pm}(\mathbf{r},\boldsymbol{\beta}) = \frac{2(-i)^{q}}{ka_1}\sum_{j=-\infty}^{\infty}\frac{e^{\pm iq\psi_j}}{\sin\psi_j}e^{ik(x\cos\psi_j\pm y\sin\psi_j)}\frac{e^{w_j^{\pm}}}{1-e^{w_j^{\pm}}}, \quad \text{for} \quad \mathbf{r}\in D^{\pm}. \tag{B.1.30}$$

Having obtained the alternative representation (B.1.30) we can consider situations in which $\boldsymbol{\beta}$ depends on k and (or) $\beta_x,\ \beta_y \in \mathbb{C}$. For example, we will need to use the spectral representation of $G_q^{\pm}(\mathbf{r},\boldsymbol{\beta}(z))$ for

$$\boldsymbol{\beta}(z) = (k\cos\psi_0, \lambda(z)) \quad \text{with} \quad \lambda(z) = \frac{i\log z - \eta_1 k\cos\psi_0}{\eta_2}, \tag{B.1.31}$$

in which case we have that

$$G_q^{+}(\mathbf{r},\boldsymbol{\beta}(z)) = -\frac{2(-i)^{q}}{ka_1}\sum_{j=-\infty}^{\infty}\frac{e^{iq\psi_j}}{\sin\psi_j}e^{ik(x\cos\psi_j+y\sin\psi_j)}\frac{z}{z-p_j}, \quad \text{for} \quad \mathbf{r}\in D^{+}, \tag{B.1.32}$$

and

$$G_q^{-}(\mathbf{r},\boldsymbol{\beta}(z)) = \frac{2(-i)^{q}}{ka_1}\sum_{j=-\infty}^{\infty}\frac{e^{-iq\psi_j}}{\sin\psi_j}e^{ik(x\cos\psi_j-y\sin\psi_j)}\frac{1}{\tau_j z-1}, \quad \text{for} \quad \mathbf{r}\in D^{-}. \tag{B.1.33}$$

where the points p_j and τ_j are given by (B.1.16).

B.1.4 2D Spectral representation

To derive a spectral representation for the 2D quasi-periodic array of singularities (B.1.5) we note first that

$$G_q^{(2)}(\mathbf{r},\boldsymbol{\beta}) = G_q^{+}(\mathbf{r},\boldsymbol{\beta}) + G_q^{(1)}(\mathbf{r},\beta_x) + G_q^{-}(\mathbf{r},\boldsymbol{\beta}). \tag{B.1.34}$$

Now if we restrict ourselves to the strip $0 < y < \eta_2$, then we can use (B.1.30) and (B.1.23) to obtain

$$G_q^{(2)}(\mathbf{r},\boldsymbol{\beta}) = \frac{2(-i)^q}{ka_1}\sum_{j=-\infty}^{\infty}\frac{e^{ikx\cos\psi_j}}{\sin\psi_j}\left(\frac{e^{i(ky\sin\psi_j+q\psi_j)}}{1-e^{w_j^+}}+\frac{e^{-i(ky\sin\psi_j+q\psi_j+iw_j^-)}}{1-e^{w_j^-}}\right), \tag{B.1.35}$$

where $w_j^{\pm}$ is defined in (B.1.28). From the quasi-periodicity relation (B.1.6) we can conclude that $G_q^{(2)}(\mathbf{r},\boldsymbol{\beta})$ can be evaluated using (B.1.35) even at points outside the strip $0 < y < \eta_2$. Note that $G_0^{(2)}(\mathbf{r},\boldsymbol{\beta})$ can be calculated at all regular points. However, for $q \neq 0$ we cannot calculate $G_q^{(2)}(\mathbf{r},\boldsymbol{\beta})$ in this way on the lines $y = n\eta_2$, where $n \in \mathbb{Z}$.

For the particular case where $\boldsymbol{\beta}(z)$ is given by (B.1.31) we have that

$$G_q^{(2)}(\mathbf{r},\boldsymbol{\beta}(z)) = -\frac{2(-i)^q}{ka_1}\sum_{j=-\infty}^{\infty}\frac{e^{ikx\cos\psi_j}}{\sin\psi_j}\left(\frac{p_j e^{i(ky\sin\psi_j+q\psi_j)}}{z-p_j}-\frac{e^{-i(ky\sin\psi_j+q\psi_j)}}{\tau_j z-1}\right), \tag{B.1.36}$$

where p_j and τ_j are defined in (B.1.16).

B.2 Lattice sums

The lattice sums are defined by

$$\sigma_q^{(d)}(\boldsymbol{\beta}) = \sum_{\mathbf{R}_j\in\mathcal{A}_d^\star} e^{i\mathbf{R}_j\cdot\boldsymbol{\beta}}\mathcal{H}_q(\mathbf{R}_j), \quad q\in\mathbb{Z}, \quad d = 1,2, \tag{B.2.1}$$

and they describe the effect at the origin of multipoles located at the points of the array $\mathcal{A}_d^\star = \mathcal{A}_d - \{\mathbf{0}\}$, $d = 1,2$, and modulated by a phase factor governed by the vector $\boldsymbol{\beta}$. The sum in (B.2.1) converges slowly and in this section we will present alternative formulae suitable for calculations. A comprehensive review on lattice sums is given by Linton [30].

B.2.1 1D spectral representation

The phase shift in the 1D lattice sum is dependent only on β_x, thus we can formally write

$$\sigma_q^{(1)}(\beta_x) = \sum_{\substack{j=-\infty\\ j\neq 0}}^{\infty} e^{ija_1\beta_x}\mathcal{H}_q(j\mathbf{a}_1). \tag{B.2.2}$$

It is worth remarking that the sum in the right hand side of (B.2.2) is also referred in the literature as Schlömilch series; see [60, Ch. 19]. Note that

$$\sigma_q^{(1)}(\beta_x) = \lim_{\mathbf{r}\to 0}\Big(G_q^{(1)}(\mathbf{r}, -\beta_x) - \mathcal{H}_q(\mathbf{r})\Big), \tag{B.2.3}$$

and from this limit spectral representations can be derived. For $q = 0$, we can use (B.1.22) to obtain (see details in [30, §3.3]),

$$\sigma_0^{(1)}(\beta_x) = -1 - \frac{2i}{\pi}\Big(\mathfrak{c} + \ln\frac{ka_1}{4\pi}\Big) - \frac{2i}{ka_1\gamma(\beta_x/k)} - \sum_{\substack{j=-\infty\\ j\neq 0}}^{\infty}\Big(\frac{2i}{ka_1\gamma(\beta_x/k + 2\pi j/ka_1)} - \frac{i}{\pi|j|}\Big), \tag{B.2.4}$$

where $\mathfrak{c}$ is Euler's constant and γ is defined in (A.1.2). More conveniently, we can write (B.2.4) in terms of the scattering angles defined in (B.1.10), that is

$$\sigma_0^{(1)}(\beta_x) = -1 - \frac{2i}{\pi}\Big(\mathfrak{c} + \ln\frac{ka_1}{4\pi}\Big) + \frac{2}{ka_1\sin\psi_0} + \sum_{\substack{j=-\infty\\ j\neq 0}}^{\infty}\Big(\frac{2}{ka_1\sin\psi_j} + \frac{i}{\pi|j|}\Big). \tag{B.2.5}$$

The spectral representations for the lattice sums for $q > 0$, are much harder to obtain. An outline of the method is given in [30, §3.3] and a more detailed description can be found in [56]. Here, we will use the formula [30, eq. 3.38] expressed as follows

$$\sigma_q^{(1)}(\beta_x) = i^q\left(\frac{2}{ka_1}\sum_{j=-\infty}^{\infty}\frac{e^{iq\,\mathrm{sgn}(j)\psi_j}}{\sin\psi_j} + i\mathcal{B}_q\right), \quad q > 0, \tag{B.2.6}$$

where

$$\mathcal{B}_q = \frac{2}{q\pi}\cos\frac{q\pi}{2} + \frac{1}{\pi}\sum_{m=0}^{[(q-1)/2]}(-1)^m\frac{(q-m-1)!}{m!(q-2m)!}\Big(\frac{4\pi}{ka_1}\Big)^{q-2m}B_{q-2m}\Big(\frac{ka_1\cos\psi_0}{2\pi}\Big). \tag{B.2.7}$$

In the last expression $B_m(\cdot)$ represents a Bernoulli polynomial, and $[x]$ denotes the largest integer not greater than x. Note that $\sigma_q^{(1)}(\beta_x)$ can be calculated for negative values of q from the relation

$$\sigma_{-q}^{(1)}(\beta_x) = (-1)^q\sigma_q^{(1)}(\beta_x). \tag{B.2.8}$$

B.2.2 2D spectral representation

The 2D lattice sum is given by

$$\sigma_q^{(2)}(\boldsymbol{\beta}) = \sum_{m=-\infty}^{\infty} {\sum_{j=-\infty}^{\infty}}' e^{i\mathbf{R}_{jm}\cdot\boldsymbol{\beta}} \mathcal{H}_q(\mathbf{R}_{jm}), \tag{B.2.9}$$

where the prime on the summation symbol indicates that the term $(j, m) = (0, 0)$ is to be omitted. An alternative representation can be obtained by first noting that

$$\sigma_q^{(2)}(\boldsymbol{\beta}) = G_q^+(\mathbf{0}, \boldsymbol{\beta}) + \sigma_q^{(1)}(\beta_x) + G_q^-(\mathbf{0}, \boldsymbol{\beta}), \tag{B.2.10}$$

and then use the spectral form of the terms in the right hand side. For example, in the case where $\boldsymbol{\beta}(z)$ is given by (B.1.31), we can use (B.1.32) and (B.1.33) to obtain

$$\sigma_q^{(2)}\Big(\boldsymbol{\beta}(z)\Big) = \sigma_q^{(1)}(k\cos\psi_0) - \frac{2(-i)^q}{ka_1} \sum_{j=-\infty}^{\infty} \frac{1}{\sin\psi_j}\Big(\frac{ze^{iq\psi_j}}{z-p_j} - \frac{e^{-iq\psi_j}}{\tau_j z - 1}\Big), \tag{B.2.11}$$

where the points p_j and τ_j are given in (B.1.16).

Bibliography

[1] I. D. Abrahams. *The application of Pàde approximants to Wiener-Hopf factorization*. IMA Journal of Applied Mathematics, vol. 65: pp. 257–281, 2000.

[2] M. Abramowitz and I. A. Stegun. *Handbook of Mathematical Functions*. Dover Publications, New York, 1965.

[3] H. Bart, I. Gohberg, M. A. Kaashoek, and A. C. M. Ran. *Factorization of Matrix and Operator Functions: The State Space Method*. Birkhäuser Verlag, 2008.

[4] L. G. Bennetts and V. A. Squire. *Wave scattering by multiple rows of circular ice floes*. Journal of Fluid Mechanics, vol. 639: pp. 213–238, 2009.

[5] J. Billingham and A. C. King. *Wave Motion*. Cambridge Texts In Applied Mathematics. Cambridge University Press, 2000.

[6] F. Bloch. *Über die Quantenmechanik der Elektronen in Kristallgittern*. Zeitschrift für Physik, vol. 52(7–8): pp. 555–600, 1929.

[7] N. G. D. Bruijn. *Asymplotic Methods in Analysis*. Dover Publications, 1981.

[8] A. Calderón, F. Spitzer, and H. Widom. *Inversion of Toeplitz matrices*. Illinois Journal of Mathematics, vol. 3(4): pp. 490–498, 1959.

[9] F. Capolino and M. Albani. *Truncation effects in a semi-infinite periodic array of thin strips: A discrete Wiener–Hopf formulation*. Radio Science, vol. 44: pp. RS2S91 (1–14), 2009.

[10] D. Colton and R. Kress. *Integral Equation Methods in Scattering Theory*. John Wiley & Sons, New York, 1983.

[11] J. W. Dettman. *Mathematical Methods in Physics and Engineering*. Dover Publications, 1988.

[12] D. G. Duffy. *Green's Functions with Applications*. Chapman Hall/CRC, 2001.

[13] T. W. Gamelin. *Complex Analysis*. Springer-Verlag New York, 2001.

[14] I. C. Gohberg and M. G. Krein. *Systems of integral equations on a half-line with kernels depending on the difference of arguments*. American Mathematical Society translations. Series 2, pp. 217–287, 1960.

[15] I. S. Gradshteyn and I. M. Ryzhik. *Table of Integrals, Series and Products*. Academic Press, New York, 4th ed., 1980.

[16] N. L. Hills and S. N. Karp. *Semi-infinite diffraction gratings–I*. Communication on Pure and Applied Mathematics, vol. 18: pp. 203–233, 1965.

[17] N. L. Hills and S. N. Karp. *Semi-infinite diffraction gratings. II. Inward resonance*. Communication on Pure and Applied Mathematics, vol. 18: pp. 389–395, 1965.

[18] J. D. Joannopoulos, S. G. Johnson, J. N. Winn, and R. D. Meade. *Photonic Crystals. Molding the Flow of Light*. Princeton University Press, 2nd ed., 2008.

[19] D. S. Jones. *A simplifying technique in the solution of a class of diffraction problems*. The Quarterly Journal of Mathematics, vol. 3: pp. 189–196, 1952.

[20] D. S. Jones. *Commutative Wiener–Hopf factorization of a matrix*. Proceedings of the Royal Society of London, Series A, vol. 393: pp. 185–192, 1984.

[21] R. Kleinman and B. Vainberg. *Full low-frequency asymptotic expansion for second-order elliptic equations in two dimensions*. Mathematical Methods in the Applied Sciences, vol. 17(4): pp. 989–1004, 1994.

[22] A. Krynkin and P. McIver. *Approximations to wave propagation through a lattice of Dirchlet scatterers*. Waves in Random and Complex Media, vol. 19(2): pp. 347–365, 2009.

[23] P. Lancaster and M. Timenetsky. *The Theory of Matrices*. Academic Press, London, 2nd ed., 1985.

[24] J. B. Lawrie and I. D. Abrahams. *A brief historical perspective of the Wiener–Hopf technique*. Journal of Engineering Mathematics, vol. 59(4): pp. 351–358, 2007.

[25] J. B. Lawrie, I. D. Abrahams, and C. M. Linton. *Acoustic radiation from two opposed semi-infinite coaxial waveguides. I: overlapping edges*. Wave Motion, vol. 18: pp. 121–142, 1993.

[26] N. N. Lebedev. *Special Functions & their Applications*. Dover Publications, New York, 1972.

[27] Y. Li and C. C. Mei. *Bragg scattering by a line array of small cylinders in a waveguide. Part 1. Linear aspects*. Journal of Fluid Mechanics, vol. 583: pp. 161–187, 2007.

[28] Y. Li and C. C. Mei. *Multiple resonant scattering of water waves by a two-dimensional array of vertical cylinders: Linear aspects*. Physical Review E, vol. 76: p. 016302 (23 pages), 2007.

[29] C. M. Linton. *The Green's function for the two–dimensional Helmholtz equation in periodic domains*. Journal of Engineering Mathematics, vol. 33(4): pp. 377–401, 1998.

[30] C. M. Linton. *Lattice sums for the Helmholtz equation*. SIAM Review, vol. 52(4): pp. 630–674, 2010.

[31] C. M. Linton and D. V. Evans. *The interaction of waves with arrays of vertical circular cylinders*. Journal of Fluid Mechanics, vol. 215: pp. 549–569, 1990.

[32] C. M. Linton and D. V. Evans. *The interaction of waves with a row of circular cylinders*. Journal of Fluid Mechanics, vol. 251: pp. 687–708, 1993.

[33] C. M. Linton and P. A. Martin. *Semi-infinite arrays of isotropic point scatterers. A unified approach*. SIAM Journal on Applied Mathematics, vol. 64(3): pp. 1035–1056, 2004.

[34] C. M. Linton and P. McIver. *Handbook of Mathematical Techniques for Wave/Structure Interactions*. Chapman Hall/CRC, 2001.

[35] C. M. Linton, R. Porter, and I. Thompson. *Scattering by a semi-infinite periodic array and the excitation of surface waves*. SIAM Journal on Applied Mathematics, vol. 67(5): pp. 1233–1258, 2007.

[36] P. A. Martin. *Integral-equation methods for multiple-scattering problems I. Acoustics*. The Quarterly Journal of Mechanics & Applied Mathematics, vol. 38(1): pp. 105–118, 1985.

[37] P. A. Martin. *Multiple Scattering. Interaction of Time-Harmonic Waves with N Obstacles*. Cambridge University Press, 2006.

[38] P. McIver. *Approximations to wave propagation through doubly-periodic arrays of scatterers*. Waves in Random and Complex Media, vol. 17(4): pp. 439–453, 2007.

[39] R. C. McPhedran, N. A. Nicorovici, L. G. Botten, and K. A. Grubits. *Lattice sums for gratings and arrays*. Journal of Mathematical Physics, vol. 41(11): pp. 7808–7816, 2000.

[40] A. B. Movchan, N. V. Movchan, and R. C. McPhedran. *Bloch–Floquet bending waves in perforated thin plates*. Proceedings of the Royal Society A, vol. 463(2086): pp. 2505–2518, 2007.

[41] A. B. Movchan, N. V. Movchan, and C. G. Poulton. *Asymptotic Models of Fields in Dilute and Densely Packed Composites*. Imperial College Press, 2002.

[42] L. S. Mulholland and M. A. Heckl. *Multi-directional sound wave propagation through a tube bundle*. Journal of Sound and Vibration, vol. 176(3): pp. 337–398, 1994.

[43] N. A. Nicorovici, R. C. McPhedran, and L. C. Botten. *Photonic band gaps for arrays of perfectly conducting cylinders*. Physical Review E, vol. 52: pp. 1135–1145, 1995.

[44] B. Noble. *Methods Based on the Wiener-Hopf Technique for the Solution of Partial Differential Equations*. Chelsea Publishing Company, New York, 2nd ed., 1988.

[45] C. G. Poulton, R. C. McPhedran, N. A. Nicorovici, L. C. Botten, and A. B. Movchan. *Asymptotics of photonic band structures for doubly-periodic arrays*. Proceedings of the IUTAM Symposium on Mechanical and Electromagnetic Waves in Structured Media, held in Sydney, Australia, 18–22 January 1999, pp. 227–238, 1999.

[46] C. G. Poulton, A. B. Movchan, R. C. McPhedran, N. A. Nicorovici, and Y. A. Antipov. *Eigenvalue problems for doubly periodic elastic structures and phononic band gaps*. Proceedings of the Royal Society A, vol. 456: pp. 2543–2559, 2000.

[47] L. Rayleigh. *On the influence of obstacle arranged in rectangular order upon the properties of a medium*. Philosophical Magazine, vol. 34: pp. 481–502, 1892.

[48] B. W. Roos. *Analytic Functions in Physics and Engineering*. John Wiley & Sons, 1969.

[49] R. V. Row. *Theoretical and experimental study of electromagnetic scattering by two identical conducting cylinders*. Journal of Applied Physics, vol. 26(6): pp. 666–675, 1955.

[50] D. Sarason. *Notes on Complex Function Theory*. Hindustan Book Agency, 1994.

[51] I. Thompson and C. M. Linton. *On the excitation of a closely spaced array by a line source*. IMA Journal of Applied Mathematics, vol. 72(4): pp. 476–497, 2007.

[52] I. Thompson and C. M. Linton. *An interaction theory for scattering by defects in arrays*. SIAM Journal on Applied Mathematics, vol. 68(6): pp. 1783–1806, 2008.

[53] I. Thompson, C. M. Linton, and R. Porter. *A new approximation method for scattering by long finite arrays*. The Quarterly Journal of Mechanics & Applied Mathematics, vol. 61(3): pp. 333–352, 2008.

[54] E. C. Titchmarsh. *The Theory of Functions*. Oxford University Press, 2nd ed., 1939.

[55] V. Twersky. *Multiple Scattering of Radiation by an Arbitrary Configuration of Parallel Cylinders*. Journal of the Acoustical Society of America, vol. 24(1): pp. 42–46, 1952.

[56] V. Twersky. *Elementary function representations of Schlömilch series*. Archive for Rational Mechanics and Analysis, vol. 8(1): pp. 323–332, 1961.

[57] V. Twersky. *On scattering of waves by the infinite grating of circular cylinders*. IEEE Transactions on Antennas and Propagation, vol. 10: pp. 737–765, 1962.

[58] N. Tymis and I. Thompson. *Low frequency scattering by a semi-infinite lattice of cylinders*. The Quarterly Journal of Mechanics & Applied Mathematics, vol. 64(2): pp. 171–195, 2011.

[59] B. H. Veitch and I. D. Abrahams. *On the commutative factorization of $n \times n$ matrix Wiener–Hopf kernels with distinct eigenvalues*. Proceedings of the Royal Society A, vol. 463: pp. 613–639, 2007.

[60] G. N. Watson. *A Treatise on the Theory of Bessel Functions*. Cambridge University Press, 2nd ed., 1944.

[61] N. Wiener and E. Hopf. *Über eine Klasse singulärer Integralgleichungen*. S. B. Preuss Akad. Wiss., vol. 31: pp. 696–706, 1931.

[62] C. H. Wilcox. *Scattering Theory for Diffraction Gratings*. Springer-Verlag, New York, 1984.

[63] M. C. M. Wright. *Lecture Notes on the Mathematics of Acoustics*. Imperial College Press, 2005.

[64] A. D. Wunsch. *Complex Variables with Applications*. Addison-Wesley, 1999.

[65] V. V. Zalipaev, A. B. Movchan, C. Poulton, and R. C. McPhedran. *Elastic waves and homogenization in oblique periodic structures*. Proceedings of the Royal Society A, vol. 458(2024): pp. 1887–1912, 2002.

[66] F. Záviška. *Über die Beugung elektromagnetischer Wellen an parallelen, unendlich langen Kreiszylindern*. Annalen der Physik, vol. 345(5): pp. 1023–1056, 1913.